Werkstofftechnik

UNIVERSITÄT SIEGEN

Christopher Probst

Microfluidic Tools for Single Cell Analysis

Schriftenreihe der Arbeitsgruppe
des Lehrstuhls für Oberflächen- und Werkstofftechnologie
im Institut für Werkstofftechnik

Herausgeber: Prof. Dr. rer. nat. habil. Xin Jiang

Band 12

Christopher Probst

Microfluidic Tools for Single Cell Analysis

Schriftenreihe der Arbeitsgruppe des Lehrstuhls für Oberflächen- und Werkstofftechnologie im Institut für Werkstofftechnik

Impressum
Prof. Dr. rer. nat. habil. Xin Jiang
Lehrstuhl für Oberflächen- und Werkstofftechnologie
Institut für Werkstofftechnik
Universität Siegen
57076 Siegen
ISSN: 2194-0096
Dissertation, Universität Siegen, 2016

Microfluidic Tools for Single Cell Analysis

Von der Naturwissenschaftlich-Technischen Fakultät der Universität Siegen

zur Erlangung des Grades eines Doktors
der Ingenieurwissenschaften genehmigte

Dissertation

von:	Dipl.-Ing. (FH) Christopher Probst
aus:	Jülich, Deutschland
eingereicht am:	12. Dezember 2014
mündliche Prüfung am:	01. Februar 2016
Referent:	Prof. Dr. rer. nat. habil. Xin Jiang
Korreferent:	Prof. Dr. rer. nat. WolfgangWiechert

Dedication

I dedicate this work to my loving parents and family.

Danksagung

Ich möchte mich an erster Stelle bei Herrn Prof. Dr. Wolfgang Wiechert des Instituts für Bio- und Geowissenschaften 1 (IBG-1) Biotechnologie, bedanken für das in mich gesetzte Vertrauen die Promotion trotz einer Vielzahl an Auflagen zu meistern. Darüber hinaus möchte ich mich bedanken für Herrn Wiecherts Unterstützung in allen wissenschaftlichen Fragestellungen während der Promotion. Großer Dank geht an Herr Prof. Dr. Rainer Lohe des Instituts für Konstruktion der Universität Siegen, für die ursprüngliche Übernahme der Erstkorrektur und die Hilfestellung bei der Eröffnung des Promotionsverfahrens. Einen ganz besonderen Dank möchte ich an Herrn Prof. Dr. Xin Jiang des Lehrstuhls für Oberflächen- und Werkstofftechnologie der Universität Siegen aussprechen, der sich trotz der wenig verbliebenen Zeit für die Übernahme der Erstkorrektur bereit erklärt hatte, sowie die Hilfe bei allen meinen Anliegen die eine Einreichung dieser Arbeit erst ermöglicht haben.

Juniorprof. Dr. Dietrich Kohlheyer möchte ich für die nun mehr als vierjährige ausgezeichnete Betreuung und gemeinsame Zusammenarbeit danken, sowie die Möglichkeit an einen interdisziplinären Forschungsthema zu arbeiten. Darüber hinaus möchte ich mich für großartige Hilfestellungen bei der Verfassung der Vielzahl an Publikationen im Rahmen meiner Doktorarbeit bedanken.

Diese Dissertation und die enthaltenen Publikationen wären nicht möglich gewesen ohne der Hilfe und Mitarbeit vieler Personen des IBG-1. An erster Stelle danke ich meiner Arbeitsgruppe „Microscale Bioengineering“ - Alexander Grünberger, Agnes-Müller Schröer, Nadja Braun, Christian Sachs und Christina Krämer. Im Besonderen möchte ich Alexander Grünberger danken als Freund und Kollege, mit dessen wunderbaren Zusammenarbeit und Unterstützung erst vieles ermöglichte, Agnes-Müller Schröer für ihre jahrelange biologische Expertise und Nadja Braun für die Fertigung der vielen mikrofluidischen Systemen. Darüber hinaus möchte ich auch den von mir betreuten Studenten danken - Christian Freier, Camille Gautier, Julio Arreola, Ximin Chen, Yefta Sudetja und Philipp Frank – für ihre ausgezeichnete Arbeit und Beitrag zu dieser Arbeit. Ich möchte ebenso den vielen Projektpartnern danken – Dr. Eric von Lieres, Dr. Katharina Nöh, Juniorprof. Dr. Julia Frunzke, Dr. Thomas Drepper, Dr. Anita Loeschcke, Dennis Binder, Regina Mahr, Stefan Helfrich, Birgit Stute, Karin Bokelmann und Charaf Eddine Azzouzi.

Ich danke allen Mitarbeitern der Infrastruktur des IBG-1 sowie der Helmholtz Nanoelectronic Facility die mir bei der Umsetzung vieler Projekte Tatkräftig zur Seite gestanden haben. Ich möchte mich auch bei den Mitarbeitern des Lehrstuhls für Strömungsmechanik sowie Oberflächen- und Werkstofftechnologie der Universität Siegen bedanken, die es mir ermöglicht haben im Rahmen meines Promotionsstudiums an einer Vielzahl von Veranstaltungen teilzunehmen.

Eidesstattliche Erklärung

Hiermit erkläre ich an Eides statt, dass ich die vorliegende Dissertation ohne unzulässige Hilfe Dritter und ohne Benutzung anderer, nicht angegebener Hilfsmittel angefertigt habe. Die aus anderen Quellen direkt oder indirekt übernommenen Daten und Konzepte sind unter Angabe der Quelle gekennzeichnet. Die Arbeit wurde bisher weder im In- noch im Ausland in gleicher oder ähnlicher Form einer anderen Prüfungsbehörde vorgelegt. Es wurden keine Dienste eines Promotionsvermittlers oder einer ähnlichen Organisation in Anspruch genommen.

_____ _____

Ort, Datum Christopher W. Probst

Summary

Industrial biotechnology plays an important role in the production of fine chemicals, pharmaceuticals and biofuels. Microorganisms are used to convert sustainable resources, e.g. sugars, into high value products. Yet, in recent years it turned out that genetically identical populations can differ phenotypically. The cause of this heterogeneity is manifold and has been related to microgradients in large scaled bioreactors and the stochasticity in gene expression as well as metabolic pathways. Single cell analysis focuses on unravelling the underlying mechanisms of population based heterogeneity. Here, conventional methods such as flow cytometry and high resolution time-lapse microscopy have been applied intensively for many years. Yet, these methods do not offer the temporal and spatial resolution needed for the investigation the complex processes in cells.

Microfluidics has become a promising new tool for studying bacteria populations at the single cell level with reduced reagents consumption and stable environmental conditions through fast exchange of heat and mass. For achieving a better understanding of the underlying processes in microbial population heterogeneity, new tools were integrated into microfluidic devices, such as cell trapping and cultivation as well as the sampling of single cells.

In order to study solely single bacteria cells with a high temporal and spatial resolution, a new microfluidic device was established as described in Publication I, allowing the immobilization of single *Escherichia coli* cells in micron scaled barrier structures (Figure 1a). Hence, cell growth can be monitored without the interference of descending cells, which are constantly removed by the media flow holding the cell inside the trap.

High-throughput analysis of small bacterial microcolonies of up to 500 cells was realized as shown in Publication II by integrating hundreds of shallow growth chambers into microfluidic channels, restricting the growth of single cells to a monolayer (Figure 1b). Mass-transport inside monolayer growth chambers solely relies on diffusion reducing shear forces to a minimum. Hence, growth of single cells in monolayer growth chambers can be followed at a high-resolution. Furthermore, by using automated image analysis cell lineages can be reconstructed and analyzed in high-throughput manner.

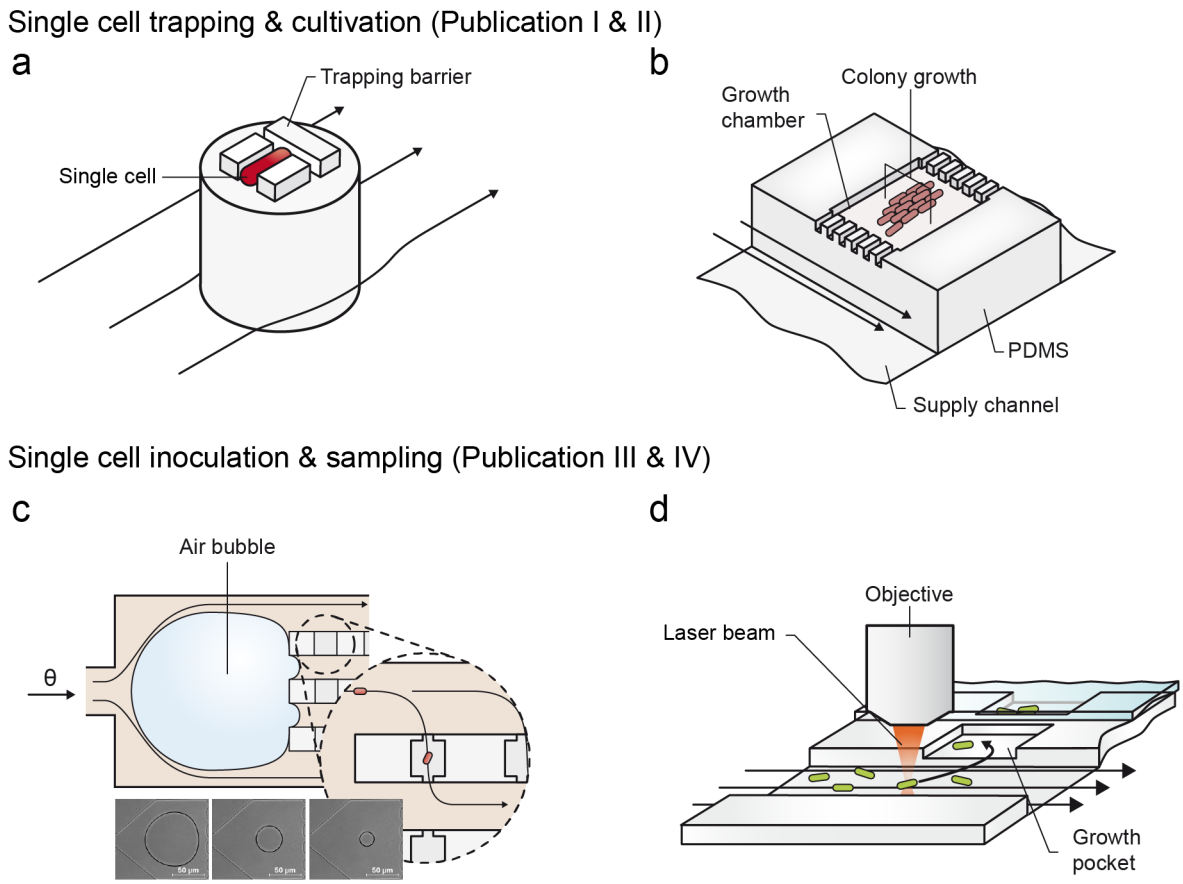

Figure 1: Microfluidic tools developed in this thesis for the analysis of single cells. (a) Trapping and cultivation of single bacteria cells in micron scaled barrier structures. (b) High-throughput investigation of small microcolonies in monolayer growth chambers. (c) Efficient loading process for the inoculation of single cells into monolayer growth chambers. (d) Sampling of single cells from microcolonies in microfluidic growth pockets, applying optical tweezers.

A novel loading procedure was developed, to guarantee isogenic (clonal) starting conditions in microfluidic monolayer growth chambers - one bacteria cell per chamber (Publication III). Here, an artificially introduced air bubble is applied to temporally distort the flow profile, leading to convective flow inside the monolayer growth chambers as depicted in Figure 1c. Subsequently, single cells get stuck inside the shallow chambers. After the air bubble is removed mass-transport inside the growth chambers is solely dominated by diffusion again. In this study, the process of air bubble based cell loading as well as loading efficiency was characterized and optimal growth condition after cell loading could shown.

High-throughput cultivation and analysis of small microbial colonies in monolayer growth chambers not allowed for retrieving single cells of interest for further analysis on or outside the microfluidic device. Publication IV introduced a new concept by integrating high-throughput microfluidic single-cell analysis and optical tweezers for sampling single cells from small microcolonies. Optical tweezers apply

a highly focused infrared laser beam in order to trap and manipulate micron sized objects and cells with the force of light only. It was shown that single cells of *Escherichia coli* could be dragged in and out of shallow growth pockets illustrated in Figure 1d. Characterization of the possible influences due to infrared laser irradiation were carried out and the obtained result showed that short exposure times < 1 min did not influence growth. In a first proof-of-principle experiment it could be demonstrated that an individual cell could be removed from a microcolony and relocated into an empty growth pocket.

Zusammenfassung

Die industrielle Biotechnologie spielt eine wichtige Rolle bei der Herstellung von Feinchemikalien, pharmazeutischen Produkten und Biokraftstoffen. Hierzu werden Mikroorganismen verwendet welche nachhaltige Ressourcen, z. B. verschiedene Zucker, in hochwertige Produkte umwandeln. Es hat sich in den vergangenen Jahren herausgestellt, dass sich genetisch identische Populationen phänotypisch unterscheiden können. Der Grund für diese Heterogenität ist vielseitig und kann auf kleinste Gradienten in großvolumigen Bioreaktoren und die Stochastizität der Genexpression sowie der Stoffwechselwege zurückgeführt werden. Die Analyse von einzelnen Zellen konzentriert sich auf die Entschlüsselung der Mechanismen welche zu der Heterogenität in Population führen. Hierzu, werden konventionelle Methoden wie die Durchflusszytometrie und der hochauflösenden Mikroskopie bereits seit mehreren Jahren erfolgreich eingesetzt. Diese Methoden bieten trotzdem nicht die benötige räumliche und zeitliche Auflösung für die Untersuchung der komplexen Prozesse in Zellen.

Mikrofluidik ist eine vielversprechende neue Technologie für die Untersuchung von bakteriellen Populationen auf der Ebene von einzelnen Zellen. Diese Technik zeichnet sich insbesondere aus durch einen geringen Verbrauch von Reagenzien sowie stabile Umweltbedingungen, durch einen schnellen Masse- und Wärmeaustausch. Um ein besseres Verständnis der komplexen Prozesse in Bakterien Populationen zu gewinnen, wurden im Laufe dieser Dissertation verschiedene Werkzeuge in mikrofluidischen Systemen integriert. Darunter zählen das Immobilisieren und Kultivieren von einzelnen Zellen oder kleinen Zellverbänden sowie auch die Probenahme von einzelnen Zellen.

Um einzelne Bakterien Zellen mit einer hohen zeitlichen und räumlichen Auflösung zu untersuchen wurde ein neues mikrofluidisches System entwickelt welches im Abschnitt „Publication I" vorgestellt wird. Das beschriebene System ermöglicht die Immobilisierung einzelner Zellen der Spezies *Escherichia coli* in Mikrometer großen Auffangstrukturen. Hierdurch kann das Wachstum einer einzelnen Zelle verfolgt werden ohne möglichen Einfluss der durch die Zellteilung entstehenden Nachkommen. Diese werden durch den konstant Strom an Medium entfernt, welcher auch die ursprüngliche Zelle in der Auffangstruktur hält (Figure 1a).

Die Analyse von kleinen Bakterien Populationen bis über 500 Zellen im Hochdurchsatz, wird im Abschnitt „Publication II" diskutiert. Hierzu wurden mehre hunderte Wachstumskammern mit einer Höhe von 1 µm in mikrofluidischen Kanälen integriert, welche das Wachstum von Bakterien in eine Ebene zwingt (Figure 1b). Der Stofftransport in einzelnen Wachstumskammern basiert ausschließlich auf Diffusion, wodurch etwaige Scherkräfte auf ein Minimum reduziert werden. Hierdurch kann das Wachstum von einzelnen Zellen mit einer hohen Auflösung verfolgt werden. Zusätzlich, mit Unterstützung von automatischer Bildauswertung, wird die Rekonstruierung und Untersuchung der Abstammung der Zellen zueinander im Hochdurchsatz ermöglicht.

Um einen genetisch identischen Ausgangspunkt zu garantieren – eine Zelle pro Wachstumskammer – wurde eine neue Methode zur Füllung von Wachstumskammern entwickelt (Abschnitt „Publication III“). Hierzu wurde eine Luftblase in das System gegeben, welche eine Änderung des Flussprofiles erlaubt. Dadurch wird es kurzeitig möglich einen konvektiven Fluss in der Wachstumskammer einzuleiten wie es in Figure 1c zu sehen ist. Zellen die mit dem konvektiven Fluss eingespült werden, bleiben dann unter Umständen in den Wachstumskammern hängen. Nach dem die Luftblase aus dem System ausgetragen wurde, findet der Stofftransport in den Wachstumskammern wieder ausschließlich durch Diffusion statt. In einer ersten Studie wurde das Verfahren sowie die Effizienz der Luftblasen basierten Beladung von Wachstumskammern untersucht. Es konnte weiter festgestellt werden dass dieser Beladungsvorgang keinen Einfluss auf das Wachstum der Zellen nimmt.

Trotz der in dieser Arbeit entwickelten Methode zur Hochdurchsatz Kultivierung und Analyse von Bakterien Populationen in mikrofluidischen Wachstumskammern, war es bisher nicht möglich Proben aus einzelnen Wachstumskammern zu nehmen. In Abschnitt „Publication IV“ wird hierzu die Vereinigung von mikrofluidischer Hochdursatz Einzelzellanalyse und optischer Pinzette vorgestellt. Die optische Pinzette verwendet einen stark gebündelten infraroten Laserstrahl um kleinste Objekte sowie Zellen mit ausschließlich der Kraft des Lichtes zu manipulieren. Es konnte gezeigt werden das einzelne Zellen des Spezies *Escherichia coli* aus und in die Wachstumskammern überführt werden konnten, wie es in Figure 1d dargestellt ist. Die Charakterisierung möglicher negativer Folgen der Bestrahlung mit infrarotem Laserlicht ergab, dass eine kurzzeitig Verwendung der optischen Pinzette von weniger als einer Minute kein Einfluss auf das Wachstum der Zellen nahm. In einem ersten Experiment konnte darüber hinaus gezeigt werden, dass eine einzelne Zelle von einer Population separiert und aus der Wachstumskammer in eine noch nicht befüllte überführt werden konnte.

Table of Contents

List of Publications

2016

Joachim Köpff†, Christian Sachs†, Alexander Grünberger, **Christopher Probst**, Dietrich Kohlheyer, Wolfgang Wiechert, Katharina Nöh and Marco Oldiges: *Growth of filamentous bacteria on single-cell level.* In submission.

Peter M. Kusen, Georg Wandrey, **Christopher Probst**, Martina Holz, Sonja Meyer zu Berstenhorst, Dietrich Kohlheyer, Jochen Büchs and Jörg Pietruszka: *Optogenetic Regulation of Complex Gene Expression in Yeast using Photo-Labile Caged Methionine*. ACS Synthetic Biology. Under review.

Dennis Binder†, **Christopher Probst**†, Alexander Grünberger†, Anita Loeschcke, Karl-Erich Jaeger, Dietrich Kohlheyer and Thomas Drepper: *Comparative microfluidic analysis of E. coli expression systems.* PLOS ONE. Under review.

2015

Dennis Binder, **Christopher Probst**, Claus Bier Anita Loeschke and Alexander Grünberger: *Lichtgesteurte Genexpression auf Einzelzellebene*. Biospektrum, (2015). (**Link**)

Stefan Helfrich, Charaf Azzouzi, **Christopher Probst**, Alexander Grünberger, Wolfgang Wiechert, Dietrich Kohlheyer and Katharina Nöh: *Vizardous Interactive Analysis of Microbial Populations with Single Cell Resolution*, Bioinformatics, (2015). (**Link**).

Alexander Grünberger†, **Christopher Probst**†, Stefan Helfrich, Arun Nanda, Birgit Stute, Karin Bokelmann, Charaf Eddine Azzouzi, Eric von Lieres, Katharina Nöh, Wolfgang Wiechert, Julia Frunzke and Dietrich Kohlheyer: *Spatiotemporal Microbial Single-Cell Analysis Using a High-Throughput Microfluidics Cultivation Platform*, Cytometry Part A, (2015). (**Link**).

Christian Dusny†, Alexander Grünberger†, **Christopher Probst**, Wolfgang Wiechert, Dietrich Kohlheyer and Andreas Schmid: *Evaluating the technical bias of microcultivation environments on single cell physiology in Corynebacterium*, Lab on a Chip, (2015). 15(8), p. 1822-34. (**Link**).

2014

Christopher Probst†, Alexander Grünberger†, Nadja Braun, Stefan Helfrich, Katharina Nöh, Wolfgang Wiechert, Dietrich Kohlheyer: *Rapid inoculation of single bacteria into parallel picoliter fermentation chambers*. Analytical Methods, (2014). 7(1),p. 91-98. (**Link**).

Dennis Binder, Alexander Grünberger, Anita Loeschcke, **Christopher Probst**, Claus Bier, Jörg Pietruszka, Wolfgang Wiechert, Dietrich Kohlheyer, Karl-Erich Jaeger, Thomas Drepper: *Light-responsive control of bacterial gene expression: precise triggering of the lac promoter activity using photocaged IPTG.* Integrative Biology 6, 755-765 (2014). (**Link**).

2013

Christopher Probst, Alexander Grünberger, Wolfgang Wiechert, Dietrich Kohlheyer: *Polydimethylsiloxane (PDMS) Sub-Micron Traps for Single-Cell Analysis of Bacteria.* Micromachines 4, 357-369 (2013). (**Link**).

Christopher Probst, Alexander Grünberger, Wolfgang Wiechert, Dietrich Kohlheyer: *Microfluidic growth chambers with optical tweezers for full spatial single-cell control and analysis of evolving microbes*. Journal of microbiological methods 95, 470–476 (2013). (**Link**).

Alexander Gruenberger, **Christopher Probst**, Antonia Heyer, Wolfgang Wiechert, Julia Frunzke, Dietrich Kohlheyer: *Microfluidic Picoliter Bioreactor for Microbial Single-cell Analysis: Fabrication, System Setup, and Operation*. Journal of Visualized Experiments 82, e50560 (2013). (**Link**).

2012

Alexander Grünberger, Nicole Paczia, **Christopher Probst**, Georg Schendzielorz, Lothar Eggeling, Stephan Noack, Wolfgang Wiechert, Dietrich Kohlheyer: *A disposable picolitre bioreactor for cultivation and investigation of industrially relevant bacteria on the single cell level*. Lab on a Chip 12, 2060-2068 (2012). (**Link**).

† These authors contributed equally to this work

List of Conference Proceedings

2015

Christopher Probst, Christian Freier, Regina Mahr, Alexander Grünberger, Stefan Helfrich, Wolfgang Wiechert, Katharina Nöh, Julia Frunzke and Dietrich Kohlheyer, *Closing the gap between microfluidic single-cell analysis and bioprocess development for microorganisms*, Proceedings of the 19th International Conference on Miniaturized Systems for Chemistry and Life Science, 25th-29th October 2015, Gyeongju, Korea.

2014

Alexander Grünberger, **Christopher Probst**, Stefan Helfrich, Julia Frunzke, Stephan Noack, Katharina Nöh, Wolfgang Wiechert and Dietrich Kohlheyer, *Microfluidic Single-Cell Analysis Platform for Biotechnological Process Development*, Proceedings of the 18th International Conference on Miniaturized Systems for Chemistry and Life Science, 26th-30th October 2014, San Antonio, USA. (**Link**).

Alexander Grünberger, Sophie Weber, **Christopher Probst**, Wolfgang Wiechert, Dietrich Kohlheyer: *Optimizing Growth Performance of Corynebacterium glutamicum at the Single-Cell Level. Chemie Ingenieur Technik* 86 (9), 1414 (2014). (**Link**).

Alexander Grünberger, **Christopher Probst**, Wolfgang Wiechert, Dietrich Kohlheyer: *High-Throughput Growth Rate Determination of Bacteria Microcolonies on Single Cell Level*. *Chemie Ingenieur Technik* 84 (8), 1336–1337 (2012). (**Link**).

2013

Alexander Grünberger, Katja Schmitz, **Christopher Probst**, Stephan Noack, Wolfgang Wiechert and Dietrich Kohlheyer, *Simple microfluidics for complex organisms: A microfluidic chip system for growth and morphogenesis studies of filamentous fungi,* Proceedings of the 17th International Conference on Miniaturized Systems for Chemistry and Life Science**,** 27th-31th October 2013, Freiburg, Germany, ISBN 978-0-9798064-6-9. (**Link**).

2012

Alexander Grünberger, **Christopher Probst**, Wolfgang Wiechert, Dietrich Kohlheyer: *Femtoliter Growth Channels: Bacteria Long-Term Growth Patterns Analysis on Single Cell Level*. *Chemie Ingenieur Technik* 84 (8), 1407 (2012). (**Link**).

Christopher Probst, Alexander Grünberger, Dietrich Kohlheyer, Wolfgang Wiechert: *Phenotypic Sorting and Analysis of Bacteria Production Strains Using Optical Tweezers and Microfluidics*. *Chemie Ingenieur Technik* 84 (8), 1344 (2012). (**Link**).

Alexander Grünberger, **Christopher Probst**, Wolfgang Wiechert, Dietrich Kohlheyer: *Femtoliter Growth Channels: Bacteria Long-Term Growth Patterns Analysis on Single Cell Level*. Chemie Ingenieur Technik 84(8), 1407 (2012). (**Link**).

List of Conference Proceedings

Christopher Probst, Alexander Grünberger**,** Wolfgang Wiechert, and Dietrich Kohlheyer: *Screening of Escherichia coli on single-cell level by hyphenating microfluidic picoliter fermentation and optical tweezers*, Proc. of 3rd European Conference on Microfluidics, 03th-05th of December 2012, Heidelberg, Germany

Alexander Grünberger, **Christopher Probst**, Stefan Helfrich, Wolfgang Wiechert, Katharina Nöh, Dietrich Kohlheyer: *Industrial Biotechnology meets Microfluidics – Disposable high-throughput single cell analysis device for industrially relevant bacterial strains*. Proc of 3rd European Conference on Microfluidics, 3td December – 5th December 2012, Heidelberg, Germany.

2011

Alexander Grünberger, **Christopher Probst**, Stefan Binder, Roshanak Ziaee, Lothar Eggeling, Wolfgang Wiechert and Dietrich Kohlheyer: *Single Cell Trapping and Analysis for Prokaryotic Production Strains in Sub-µm Fluidic Structures*, Proceedings of the 15th International Conference on Miniaturized Systems for Chemistry and Life Science, 02th-06th October 2011, Seatle, WA, USA. (**Link**).

List of Posters

2015

Christopher Probst, Alexander Grünberger, Dennis Binder, Iska Steffens, Thomas Drepper, Wolfgang Wiechert and Dietrich Kohlheyer: *Optical control of gene expression in bacteria on the single-cell level by caged compounds*. Colloquium: Synthetic Biology Opportunities for Interdisciplinary Research from Biology to Engineering, 24th June 2015, Aachen, Germany.

Ena Zunic, Anna Schechtel, **Christopher Probst**, Alexander Grünberger, Christian Freier, Gerd Seibold, Wolfgang Wiechert and Dietrich Kohlheyer: *Dynamic environmental control in microfluidic devices for single-cell analysis of biological production processes.* Colloquium: Synthetic Biology Opportunities for Interdisciplinary Research from Biology to Engineering, 24th June 2015, Aachen, Germany.

2014

Alexander Grünberger, **Christopher Probst,** Julia Frunzke, Stephan Noack, Wolfgang Wiechert, Dietrich Kohlheyer: *Microfluidic Single-Cell Cultivation: Opportunity for Industrial Bioprocess Development.* EMBL Conference – Microfluidics 2014, 23rd July – 25th July 2014, Heidelberg, Germany.

Sophie Weber, Alexander Grünberger, **Christopher Probst,** Wolfgang Wiechert, Dietrich Kohlheyer: *Optimizing growth performance of Corynebacterium glutamicum at the single-cell level.* ProcessNet-Jahrestagung 2014 und 31. DECHEMA Jahrestagung der Biotechnologen, 29th September – 2nd October 2014, Aachen Germany.

Julio Arreola, **Christopher Probst,** Michael J. Schöning, Dietrich Kohlheyer: *Temperature control in Microfluidics for single-cell Analysis: Characterization and development of thin-film sensors.* Engineering of Functional Interfaces 2014, EnFi 2014, 14th July – 15th July 2014, Jülich, Germany.

Dietrich Kohlheyer, Alexander Grünberger, **Christopher Probst,** Stefan Helfrich, Julia Frunzke, Lothar Eggeling, Katharina Nöh, Stephan Noack, Wolfgang Wiechert: *Single-cell Bioreactors boost Bioprocess Development: New Insights into Cellular Metabolism.* Metabolic Engineering X, 15th June – 19th June 2014, Vancouver, Canada.

2013

Dennis Binder, Alexander Grünberger, Anita Loeschcke, **Christopher Probst**, Jörg Pietruszka, Wolfgang Wiechert, Dietrich Kohlheyer, Karl E. Jaeger, Thomas Drepper: *Characterization of light-triggered gene expression in E. coli with respect to population and single cell response*. New approaches and concepts in microbiology. EMBL Heidelberg, 14th October 2013, Heidelberg, Germany.

Dennis Binder, Alexander Grünberger, Anita Loeschcke, **Christopher Probst**, Jörg Pietruszka, Wolfgang Wiechert, Dietrich Kohlheyer, Karl E. Jaeger, Thomas Drepper: *Characterization of light-triggered gene expression in E. coli with respect to population and single cell response*. Jülicher Biotechday 2013, Forschungszentrum Jülich. 11th October 2013, Jülich Germany.

Dennis Binder, Alexander Grünberger, Anita Loeschcke, **Christopher Probst**, Jörg Pietruszka, Wolfgang Wiechert, Dietrich Kohlheyer, Karl E. Jaeger, Thomas Drepper: *Characterization of light-triggered gene expression in E. coli with respect to population and single cell response*. Symposium on Advanced Imaging in Cell- and Microbiology: Technology and Applications. Forschungszentrum Jülich. 10th October 2013, Jülich, Germany.

List of Posters

Alexander Grünberger, Katja Schmitz, **Christopher Probst,** Stephan Noack, Wolfgang Wiechert, Dietrich Kohlheyer: *Simple microfluidics for complex organisms: A microfluidic chip System for growth and Morphogenesis studies of filamentous fungi.* µTAS 2013, 27th October – 31st October 2013, Freiburg, Germany.

Christopher Probst, Alexander Grünberger, Julia Frunzke, Wolfgang Wiechert, Dietrich Kohlheyer: *Microfluidic cultivation technology and application: analysing single-microbes under perfect environmental control.* EMBL Heidelberg "New Approaches and Concepts in Microbiology", 14th October – 16th October 2013, Heidelberg, Germany.

Christina Krämer, Alexander Grünberger, **Christopher Probst**, Wolfgang Wiechert, Dietrich Kohlheyer: *Continuous Non-Invasive Real-Time Viability Measurement of Bacteria on Single Cell Level in Microfluidic Chip Cultures.* EMBL Heidelberg "New Approaches and Concepts in Microbiology", 14th October – 16th October 2013, Heidelberg, Germany.

Alexander Grünberger, **Christopher Probst,** Wolfgang Wiechert, Dietrich Kohlheyer: *Femtoliter chemostat for long-term bacteria growth and production analysis on single cell level.* 2nd International Conference Implementation of Microreactor Technology in Biotechnology, IMTB 2013, 5th May – 8th May 2013, Cavtat, Croatia.

Johanna Heinrich, Alexander Grünberger, **Christopher Probst,** Wolfgang Wiechert, Dietrich Kohlheyer: *Single cell growth under constant environmental conditions and defined C sources: A case study for Corynebacterium glutamicum.* VAAM-Tagung 2013, 10th March – 13th March 2013, Bremen, Germany.

Johanna Heinrich, Alexander Grünberger, **Christopher Probst,** Wolfgang Wiechert, Dietrich Kohlheyer: *Single cell growth under constant environmental conditions and defined C sources: A case study for Corynebacterium glutamicum*. VAAM-Tagung 2013, 10th March – 13th March 2013, Bremen, Germany.

Alexander Grünberger, **Christopher Probst,** Wolfgang Wiechert, Kohlheyer, Dietrich: *Femtoliter chemostat for long-term bacteria growth and production analysis on single cell level*. Single Cell Analysis Europe 2013, 5th March – 6th March 2013, Barcelona, Spain.

Christopher Probst, Philipp Frank, Alexander Grünberger, Wolfgang Wiechert, Dietrich Kohlheyer: *Time lapse microbial single cell analysis in a micro fabricated batch reactor*. Single Cell Analysis Europe 2013, 5th March – 6th March 2013, Barcelona, Spain.

2012

Alexander Grünberger, Stefan Helfrich, **Christopher Probst**, Katharina Nöh, Wolfgang Wiechert, Dietrich Kohlheyer: *High-Throughput lineage tree investigations of bacteria microcolonies using arrays of monolayer growth chambers*. The 16th International Conference on Miniaturized Systems for Chemistry and Life Sciences, µTAS 2012, 28th October – 1st November 2012, Okinawa, Japan.

Alexander Grünberger, Stefan Helfrich, **Christopher Probst**, Katharina Nöh, Wolfgang Wiechert, Dietrich Kohlheyer: *Industrial Biotechnology meets Microfluidics - Disposable high-throughput single cell analysis device for industrially relevant bacterial strains.* 3rd European Conference on Microfluidics µFlu 2012, 3rd December – 5th December 2012, Heidelberg, Germany.

2011

Alexander Grünberger, **Christopher Probst**, Wolfgang Wiechert, Dietrich Kohlheyer: *Single Cell Trapping and Analysis for Prokaryotic Production Strains in Sub -µm Fluidic Structures,* NanoBioTech-Montreux 2011**,** 14th-16th November 2011, Montreux, Switzerland

Alexander Grünberger, **Christopher Probst**, Wolfgang Wiechert, Dietrich Kohlheyer: *Single Cell Trapping and Analysis for Prokaryotic Production Strains in Sub -µm Fluidic Structures,* 15th International Conference on Miniaturized Systems for Chemistry and Life Science (µTAS)**,** 02th-06th October 2011, Seattle (WA), USA

List of Patents

Dietrich Kohlheyer, Alexander Grünberger, **Christopher Probst**, *Vorrichtung und Verfahren zur Einzelzellanalyse von Mikroorganismen*, patent number, 102014007424.

List of Abbreviations

Abbreviation	Explanation
BMBF	Bundesministerium für Bildung und Forschung, Federal Ministriy of Education and Research
C. acetobutylicum	*Clostridium acetobutylicum*
C. glutamicum	*Corynebacterium glutamicum*
DAF-FM	4,5-diaminofluorescein 4-amino-5-methylamino-20,70-difluorofluorescein
DNA	Deoxyribonucleic acid
DO	Dissolved oxygen
E. coli	*Escherichia coli*
e.g.	Exempli gratia
et al.	et alii
FACS	Fluorescent activated cell sorter
FC	Flow cytometry
MFY	Macrolex Fluorescent Yellow
nDEP	Negative dielectrophoresis
OT	Optical tweezers
PCB	Printed circuit board
PDMS	Poly(dimethylsiloxane)
PtOEP	Platinum octaethylporphyrin
PtOEPK	Platinum(II) octaethylporphine ketone
PtTFPP	Platinum(II)-5,10,15,20-tetrakis-(2,3,4,5,6-pentafluorphenyl)-porphyrin
RNA	Ribonucleic acid
RTDP	Ruthenium tris (2,20 - bipyridil) dichloride hexahydrate
SU-8	Brand name of negative photoresist
UV	Ultraviolet

Table 1: List of Abbreviations.

List of Symbols

Symbol	Description	Unit
ΔP	Pressure drop	Pa
D	Coefficient of diffusion	$m^2\ s^{-1}$
d	Channel length	m
h	Channel height	m
L	Characteristic channel length	m
p	Pressure	Pa
Q	Volumetric flow rate	$m^3\ s^{-1}$
R	Radius	m
Re	Reynolds number	-
R_h	Hydraulic resistance	
t	Time	s
w	Channel width	m
ρ	Density	$kg\ m^{-3}$
μ	Dynamic viscosity	Pa s
A	Cross-section fluid channel	m^2
φ	Mean flow-rate	nl/min
w_f	Fluid channel width	µm
w_v	Control channel width	µm

Table 2: List of Symbols.

List of Figures

List of Tables

1 Industrial biotechnology

Industrial biotechnology employs microorganisms for the production of chemicals, pharmaceuticals, biofuels and amino acids. Industrial biotechnology makes out 10.2 % of the overall biotechnology sector in Germany with an annual turnover of 2.86 billion Euros in 2013, according to a recent survey conducted by the Federal Ministry of Education and Research (BMBF) [1]. In a recent effort by the BMBF, a national research strategy was initiated promoting a production landscape towards a bio-sustainable economy[2]. Hence, there is strong demand in further improving existing bio-based production processes and finding new ways to in making use of sustainable substrates. Nevertheless, the production greatly depends on the used organism, which output can vary due to the stochastic nature of the processes itself, converting a substrate into a desired product.

Assuming clonal populations, optimal bioreactor control and mixing, uniform cell behavior during growth might be expected. However, it has emerged in recent years that clonal bacterial populations can be physiologically heterogeneous [3] (Figure 2). Hence there is strong demand to gain knowledge on population heterogeneity and the impact on industrial-scaled production.

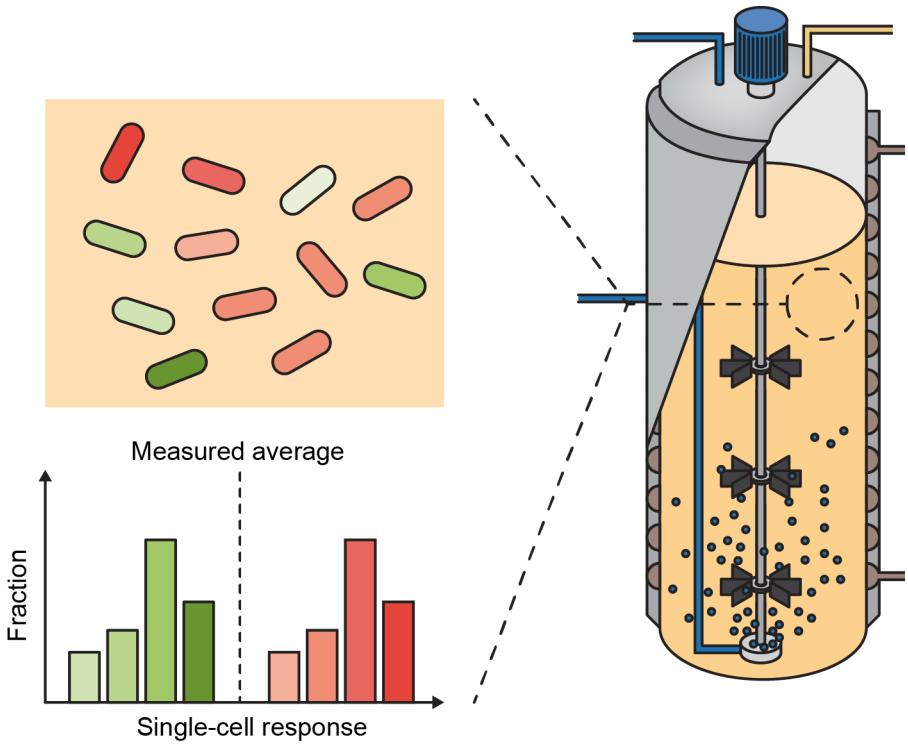

Figure 2: Looking closer into a large scaled production process by single-cell analysis, reveals a heterogeneous nature of bacterial populations.

2 Population heterogeneity

Microbial population in industrial bioreactors are clonal, but “it is becoming apparent that isogenic microbial populations contain substantial cell-to-cell differences in physiological parameters such as growth rate, resistance to stress and regulatory circuit output” [4]. The origin of population heterogeneity is manifold: microgradients in large-scale bioreactors [3], stochastic nature of gene expression [5] and metabolic pathways[3] as well as effects related to aging[6].

Heterogeneity in bacterial populations can manifest in various ways, such as persister cells, which can be observed in harsh environments after the use of antibiotics. The phenomenon has already been observed over half a century ago [7], resulting in a tolerance of few cells in a clonal population to the treatment with an antibiotic. In contrast to resistance which is inherited genetically, decadences of persister cells are once more vulnerable to antibiotics. Persistence in bacteria has been recognized as possible cause of chronic diseases in human and a complete understanding of the underlying mechanisms is still missing [8].

Formation of filamentous cells, indicated by a drastic increase in cell size without the occurrence of cell division, in an otherwise regular sized population was found as a strategy to evade the immune system of an infected host [9].

3 Single cell analysis

In the wake of gaining a better understanding of the underlying mechanisms of population heterogeneity, a variety of established methods have been applied. Flow cytometry (FC) has become an important tool for analyzing and sorting populations, based upon a fluorescent signal [10]. Fluorescent activated cell sorting (FACS) instruments consecutively pass cells in a stream of liquid towards a laser beam for irradiation as depicted in Figure 3a. Afterwards, the liquid is separated into individual droplets containing a single cell. Based upon the retrieved fluorescence signal, droplets can be sorted into different containers by applying an electrical charge. FACS is capable of analyzing and sorting up to 80,000 cells per second [11]. Yet, FACS is only a snapshot analysis which does not allow to investigate time depended processes.

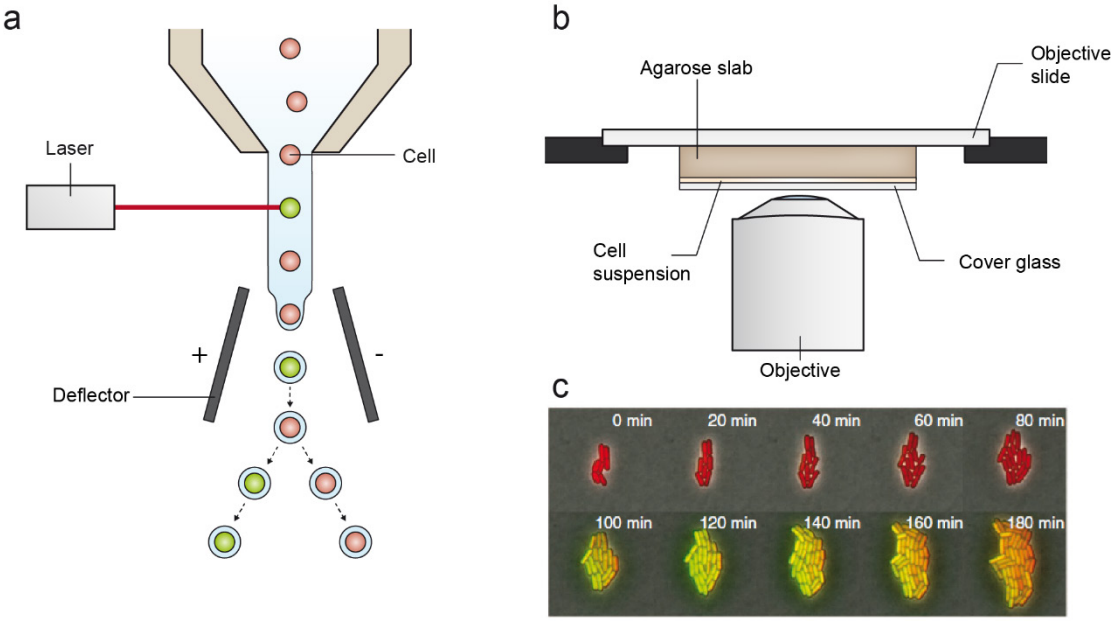

Figure 3: Overview of conventional single cell analysis methods. (a) Principle of FACS, adapted from [12]. (b) High-resolution microscopy (agarose slabs). (c) Observation of single cell growth and fluorescence on agarose slabs, modified from [13].

Microscopy based analysis of population heterogeneity related phenomena in bacteria has been performed by Elowitz and co-workers [14]. Single cells were immobilized on a substrate made from agarose (agar agar) and cultivation media. Consequently, a small amount of cell suspension was pipetted onto it and fixated with a cover glass [13]. Hence, cells are forced in one focal plane allowing high-resolution imaging and analysis of growth, morphology and fluorescence expression over time. Still, throughput is strongly limited and environmental conditions are not stable since molecules can diffuse freely through agarose. Hence, there is a strong demand for new methods that allow investigating single cells in high-throughput manner and with a high resolution.

4 Microfluidics

Microfluidics can be defined as the science and technology to manipulate small volumes of fluids (10^{-9} to 10^{-18} liters) inside channels with dimensions of tens to hundreds of micrometers. Microfluidic systems possess entirely laminar flow, viscous forces become dominant and mixing occurs by diffusion solely.

Microfluidics has advanced to a promising new tool to study microorganisms on the single-cell level by reduced reagent consumption and stable environmental conditions through fast exchange of heat and mass.

4.1 Theory

In this chapter, the fundamental physical principles are introduced to describe the flow in microfluidic devices as well as the mixing capabilities of different species by solely diffusive processes.

4.1.1 Convective mass transport

Flow in microfluidic channels is considered to be strictly laminar due to the small length scales, (Figure 4a) whereas flow is turbulent in macro scaled systems (Figure 4b).

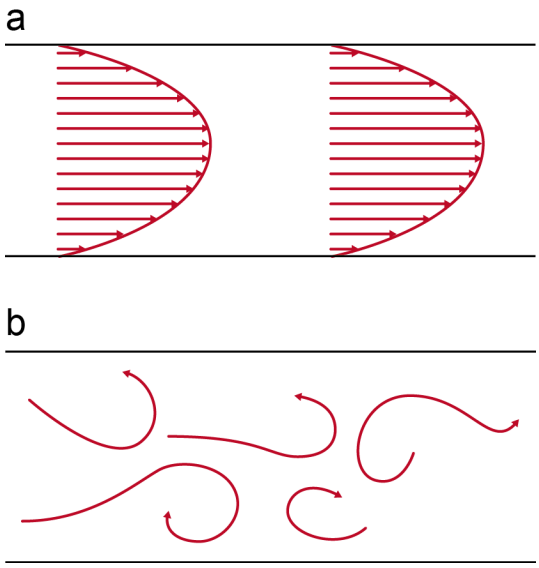

Figure 4: (a) Laminar flow (b) Turbulent flow.

Both flow regimes can be discriminated using the dimensionless Reynolds number as defined in Equation 1:

$$\mathrm{Re} = \frac{\rho u d}{\mu} \qquad \text{Equation 1}$$

where ρ refers to the fluid density, d to the channel length, u to the velocity and μ to the dynamic viscosity.

Laminar flows are characterized by low Reynolds numbers (Re < 2000), whereas in microfluidics Re < 1 is typical. Calculations of flows in microfluidics can be made using the Navier-Stokes equation for a Newtonian fluid driven by a pressure gradient:

$$\rho \frac{\partial \vec{u}}{dt} + \rho \vec{u} \nabla \vec{u} = -\nabla p + \mu \nabla^2 \vec{u} \qquad \text{Equation 2}$$

where $\vec{u}$ refers to the velocity, p to the pressure, ρ to the fluid density, and μ to the dynamic viscosity. The Navier-Stokes equation can be simplified when the fluid is incompressible, Newtonian, isotropic, with temperature independent viscosity and flowing through a constant cross-section (Equation 3).

$$0 = -\frac{\partial p}{\partial x} + \mu \left(\frac{\partial^2 u_x}{\partial y^2} + \frac{\partial^2 u_x}{\partial z^2} \right)$$

Equation 3

$$0 = \frac{\partial p}{\partial y} = \frac{\partial p}{\partial z}$$

Considering a channel with a circular cross-section, we obtain an equation for the parabolic flow (Equation 4).

$$u_x(R) = -\frac{1}{4\mu} \frac{dp}{dx} (r_0{}^2 - R^2) \qquad \text{Equation 4}$$

where $u_x(R)$ is the velocity profile along x for a given radius R (Figure 5).

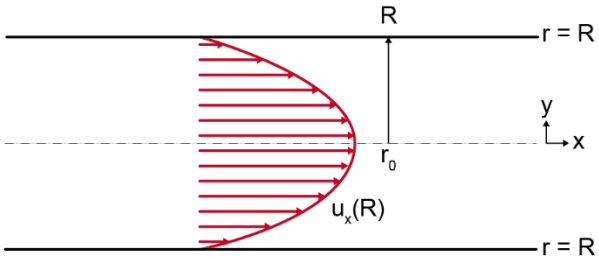

Figure 5: Parabolic velocity profile $u_x(R)$ in a channel with a circular cross-section, direction of flow from left to right.

By further simplifications, the Poiseuille equation can be obtained as described in Equation 5 for a microfluidic channel with a rectangular cross-section. Q represents the volumetric flow rate, w the channel width, h the channel height and L the characteristic length of the channel. The volumetric flow

rate Q, can additionally be described by the relation of the pressure drop ΔP and the hydraulic resistance R_h, which depends on the channel geometry (w, h, L) and the viscosity.

$$\Delta P = \frac{12\mu L}{wh^3} Q \qquad \frac{\Delta P}{R_h} = Q$$

Equation 5

4.1.2 Diffusive mass transport

Laminar flow in microfluidics enables mixing by diffusion only. Considering two adjacent liquid streams in a microfluidic channel (Figure 6), mixing only occurs at the boundary phases over length of the channel.

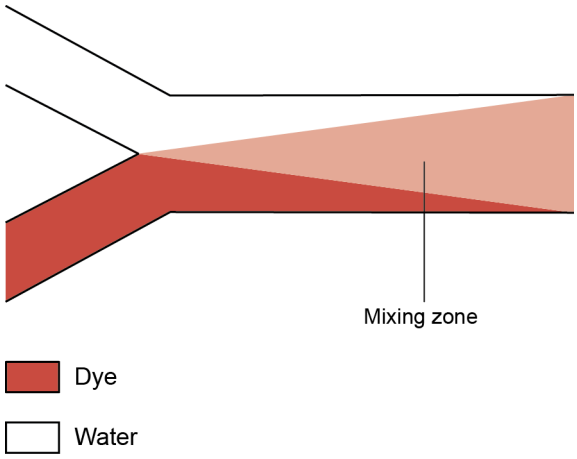

Figure 6: Diffusive mixing of dye and water along a channel at the boundary phase.

Fick's second law can be used to describe changes of the concentration profile by diffusion (Equation 6):

$$\frac{\partial C_i}{\partial t} = D\frac{\partial^2 C_i}{\partial x^2} \qquad \text{Equation 6}$$

where D refers to the diffusion coefficient for the change of concentration over time along the x axis. For simple cases the concentration profile can be expressed by Equation 7, where the diffusion length $2\sqrt{Dt}$ can be derived from:

$$C(x,t) = C(0)\mathrm{erfc}\left(\frac{x}{2\sqrt{Dt}}\right) \qquad \text{Equation 7}$$

4.2 Fabrication of microfluidic devices

Microfluidic devices have been fabricated from a variety of materials, such as glass, PDMS [15], thermoplastics, paper [16] and wax [17] as shown in Table 3. Still, PDMS represents the widest spread material in a broad range of applications.

Microfluidic PDMS devices are fabricated by replicating structures from a master mold [18]. Master molds are commonly fabricated by means of photolithography, with a minimal feature size of below 10 nm [19], as depicted in Figure 7. First, a silicon wafer is cleaned and spin-coated with a photoresist, commonly SU-8 (Figure 7a,b). Excessive solvents are removed from the photoresist prior patterning. Patterns in the photoresist are created by a photomask placed on top and exposure to UV light (365 nm) (Figure 7c). Photomasks are fabricated using an electron beam writer, achieving resolutions below 10 nm [19]. After exposure to UV light, exposed photoresists parts are developed in a developer solution (Figure 7d). In a final step, developed micro structures are hard baked. PDMS is poured over the master mold and cured (Figure 7e). Afterwards, the cured PDMS is irreversible bonded to a glass substrate, by activating both in an oxygen plasma (Figure 7f).

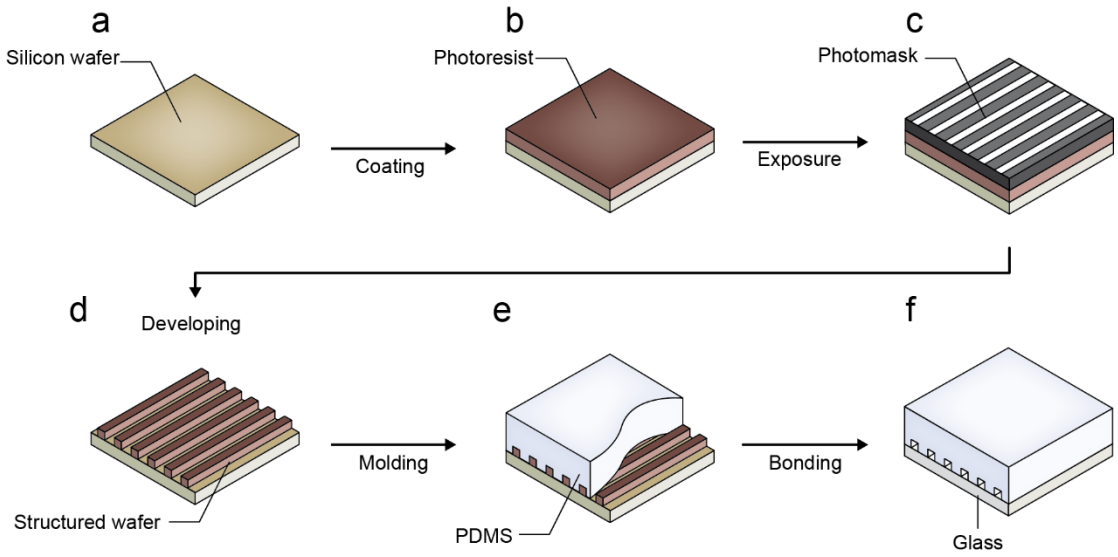

Figure 7: Essential fabrication steps of microfluidic replica molding adapted from [18]: (a) cleaned silicon wafer, (b) coating of photoresist, (c) exposure, (d) developing, (e) molding and (f) bonding.

The described fabrication steps, however, need to be carried out in a clean room facility, which is cost-intensive and requires skilled personal. Many alternatives have been developed, offering a "cleanroom-free" alternative to the fabrication of master molds.

Table 3 presents an overview of the different alternative fabrication methods that have been established. The described methods greatly differ in the size of the smallest feature, e.g. a channel, that can be created ranging from 10 µm [20, 21] up to 200 µm [22].

Photolithographic methods that do not necessarily require a cleanroom, such as the fabrication of printed circuits boards (PCB) have been derived as well for creating master molds [23–26]. Here, copper plated substrates covered with a photoresist are patterned, developed and etched to retrieve micron sized structures. Patterns are as well created using a photomask and exposing the photoresist to UV light. Yet, photomasks are rather printed using a laser toner printer [24] instead of using an electron beam writer, achieving resolutions in a range of below 100 µm [25]. The process of patterning, developing and etching can be repeated by laminating another layer of photoresist onto the substrate. The photoresist used in the fabrication of PCBs, are referred to as dry film photoresist. The photoresist is coated onto a flexible foil and can be laminated onto a substrate using heat and a roller. Stephan and co-workers [27] directly applied dry film resists for fabricating multilayered master molds and created features ranging from a size of 20 µm – 130 µm [27], depending on the resolution of the photomask.

Alternatively to the use of dry film photoresists, Yue and co-workers [28] proposed solder resists, commonly applied in the fabrication of PCBs to hinder solder to come in contact with unwanted areas. Screen printing was applied to homogeneously spread the resin like solder resist over a desired substrate. Hence, resolutions of 50 µm [28] could be reached.

Micromachining of metals (brass, aluminum) [20] achieves the highest resolutions with a minimal feature size of below 10 µm [20, 21], in contrast to conventional photolithography. Still, milling leaves grooves in the material, which might be undesired[20].

Tan and co-workers [29] suggested the use of toner printing machines to rapidly fabricate structures on foil using tools available in every office. Hence, channels with a minimal width of 50 µm and height of 8 µm – 14 µm could be printed, depending on the resolution of the printer. Further, Nguyen and co-workers [30] reported the usage of shrinkable thermoplastic foil patterned by toner printing and shrank by 95% using heat, achieving minimal features smaller than 100 µm.

Wax as an alternative printing material for master molds was realized by Kaigala *et al.* [31] and Li *et al.* [32] using different approaches. Kaigala and co-workers made use of a commercially available wax printing machine, in contrast to Li and co-works which constructed a wax droplet dispensing system. Both methods achieved a resolution of 200 µm [31, 32].

Cutting of micron sized channels in plastics using either a laser [33] or grafts cutters [22] (xurography) was applied to fabricate microfluidic master molds. Laser cutting can achieve resolutions ranging from 90 µm – 100 µm [33] depending of the beam size, in contrast to grafts cutter with a minimal resolution of 20 µm – 200 µm [22].

3D printing of master molds was first introduced as an alternative way of fabrication by Mc Donald and co-workers in 2002 [15], but seemed not feasible due to the high prices for 3D printing machines back then. Today, the availability of high-precession desktop 3D printers below 3,000 US$ [34], offers

the possibility to fabricate microfluidic molds with resolutions smaller than 50 µm and printing times in the range of minutes [34]. Additional, 3D printing allows the fabrication of arbitrary shapes, which are not possible to achieve with conventional photolithographic methods.

Despite the different methods described for the fabrication of master molds, PDMS can also be directly patterned by means of laser ablation. First described by Liu and co-workers [35] in 2009, a pulsed CO_2 laser is used to create channels with a possible minimal resolution of 50 µm in few minutes.

Table 3: Overview of different fabrication methods of microfluidic devices for PDMS, thermoplastics, paper, glass and wax.

Material	Method		Min. feature size	Advantages	Ref
PDMS	Replica molding	SU8 resist	10 nm	high resolutions	[19]
		3D printing	50 µm	fast, inexpensive, arbitrary shapes	[15, 34]
		Micromachining	< 10 µm	fast, large scale production	[20, 21]
		Wax printing	200 µm	fast	[31, 32]
		Toner printing	50 µm	fast, inexpensive	[29, 36]
		Printed circuit boards	100 µm	fast, multiple layers	[23–26]
		Graft cutting (xurography)	20 - 200 µm	fast, multiple layers	[22]
		Laser ablation	90 – 100 µm	fast	[33]
		Screen printing	50 µm	multiple layers	[28]
		Dry film resists	20 µm – 130 µm	inexpensive, multiple layers	[27]
		Shrink-film	< 100 µm	fast	[30]
	Laser engraving		50 µm	fast	[35, 37, 38]
Thermoplastics	Embossing		< 10 µm	fast, large scale production	
	Injection molding			fast, large scale production	
	3D Printing		50 µm	fast, inexpensive, arbitrary shapes	[39]
	Graft cutting (Xurography)		20 - 200 µm	fast, multiple layers	[22, 40]
	Wax printing/Etching			multiple layers	[41]
	Dry film resists		20 µm – 130 µm	fast, inexpensive, multiple layers	[42–45]
	Laser engraving		50 µm	fast, multiple layers	[37]

Paper	Wax printing		inexpensive, multiple layers, degradable	[16]
	Laser ablation	< 50 nm	fast	[46, 47]
Wax		25 µm	fast	[17, 48]

5 Microfluidic single cell analysis

Microfluidic single cell analysis methods can be divided in two main approaches [49]: I) analysis of whole cells (growth, morphology, fluorescence) and II) analysis of cell lysate (DNA, RNA, proteins, metabolites) as depicted in Figure 8.

Analysis of cell lysate has been achieved either with contents (RNA, DNA, enzymes, proteins, metabolites) of cells released prior to microfluidic chip experiments or by various methods (chemical, electrical, physical and optical) [49] inside the device (Figure 8a). In contrast, analysis of "whole" cells focuses on exposing a single cell or small populations to certain external stimuli and observing the resulting behavior (Figure 8b). External stimuli can be changes of the environment (temperature, pH and nutrients) as well as exposure to mechanical forces [50] or changing light conditions [51]. Observation of the cell behavior after external stimulus allows analyze cell growth, morphology and signal of genetically encoded fluorescent sensors.

In this thesis, focus in the publications is given on the various methods that have been established to immobilize and analysis single "whole" cells in microfluidic devices.

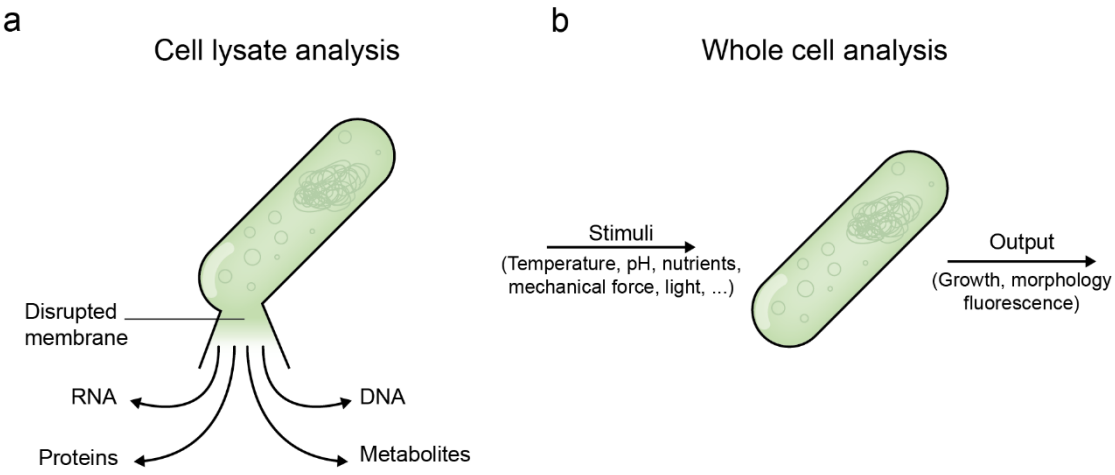

Figure 8: Categories of microfluidic single cell analysis: (a) cell lysate analysis, (b) whole cell analysis.

5.1 Single cell trapping in microfluidics

Immobilization of living organisms inside microfluidic devices requires different aspects to be taken into account, such as size and shape as depicted in Figure 9. Microfluidic single cell analysis covers a vast variety of different species, which differ greatly in size - starting from below a micron in case of bacteria [52] up to 100 µm for mammalian cells [53]. Further, the shape of a cell can be an important factor for immobilization, as it can be either more round shaped (mammalian, yeast) or rod-shaped as bacteria.

Various principles for trapping single cells of different organism have been established over, which can be separated into two different categories: I) non-surface contact and II) surface contact, and are described in more detail in the following.

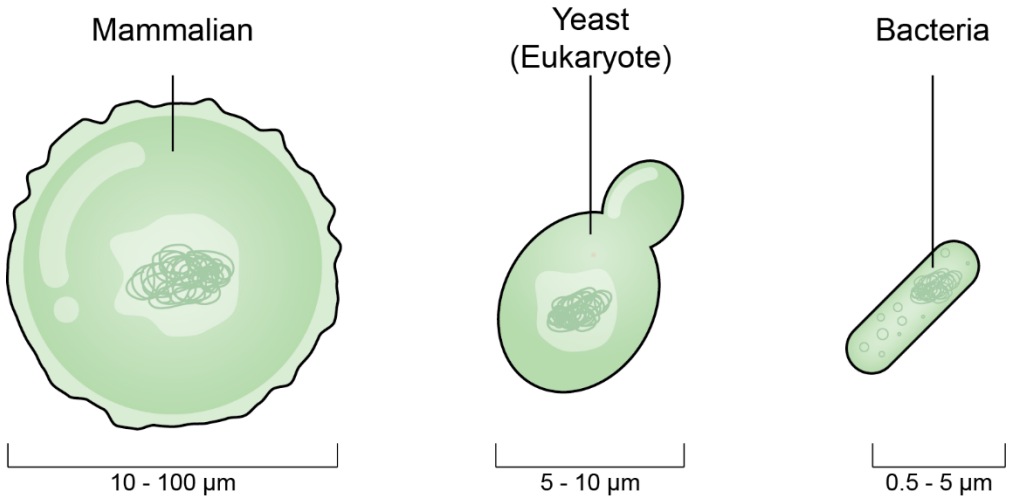

Figure 9: Different organisms (mammalian [53], yeast [52] and bacteria [52]) that have been investigated by microfluidic single cell analysis.

5.1.1 Non-surface contact single-cell trapping

Non-surface contact trapping was realized by making use of various physical principles such as dielectrophoresis [54], optics [55], magnetism, acoustics [56],[57], hydrodynamics and droplets [58, 59]. Figure 10 shows an overview of exemplary methods, representing one of the mentioned physical principles each.

Negative dielectrophoresis (nDEP) makes use of the dielectric characteristic of an object/cell, where a force is generated by applying an electrical field to the object/cell. Fritzsch and co-workers [54] presented a devices applying nDEP for manipulating as well as trapping and cultivating various microorganisms inside a cage, made of four individual controllable electrodes (Figure 10a). Still, throughput is limited to only a small number of trapping and cultivation sites (N = 2) per device. Further, possible heating effects caused by nDEP have to be compensated during cultivation.

Optical tweezers (OT) use a highly focused laser beam to entrap micro sized objects by the force of light only. First applications of using OT for the trapping and cultivation of microorganisms such as *Escherichia coli*, have been shown already over 20 years ago by Ashkin and co-workers [60]. Integration of OT into a microfluidic device was successfully demonstrated by Eriksson and co-workers [61], which used a spatial light modulator to create several focused laser spots to construct an array of trapped yeast cells (Figure 10b). OT setups often apply lasers with a wavelength of 1064 nm [62], which is speculated to be the cause for heating the water in and around a trapped cell, as well as the formation of oxygen radicals [62]. Probst and co-workers showed that by using OT solely for trapping and manipulation of cells for short periods of time (< 1 min), in combination with surface contact based trapping, the growth of *Escherichia coli* [62] was not influenced.

Robert and co-workers [63] introduced the concept of magnetic tweezers for single cell analysis, by inserting iron nanoparticles in cells and by applying an external magnetic field, to manipulate individual cells (Figure 10c). High-throughput sorting was realized based on the different amount of iron nanoparticles the cells had been taken up. Few studies have continued the use of magnetic tweezers[64] and less is known about the possible toxicity by the nanoparticles.

Acoustic waves generated on the surface of a piezoelectric material combined with a microfluidic channel (Figure 10d), where used by Ding and co-workers to manipulate particles as well as cells of *Caenorhabditis elegans* [56]. Acoustic trapping allows for manipulating small scaled objects without having to consider any particular shape or electrical, magnetic and optical characteristics [56].

Microdroplets with a volume of pL to nL can be created and analyzed (> 10 kHz) in a high-throughput manner inside microfluidic channels from two unmixable phases, an aqueous and oil one (Figure 10e). Single cells can be encapsulated in droplets in combination with various reagents for screening applications [59],[58],[65],[66],[67].

Tanyeri and co-workers[68] realized stable trapping of particles, solely by hydrodynamic forces, in a junction of two orthogonal arranged channels as depicted in Figure 10f. First confinement and cultivation of *E. coli* was recently reported, which allowed to observe growth over multiple generations (N = 5) [69].

Detailed comparison of the various non-surface contact based trapping principles regarding used organisms, throughput, limitations/biocompatibility, ease of fabrication and complexity of the setup are shown in Table 4.

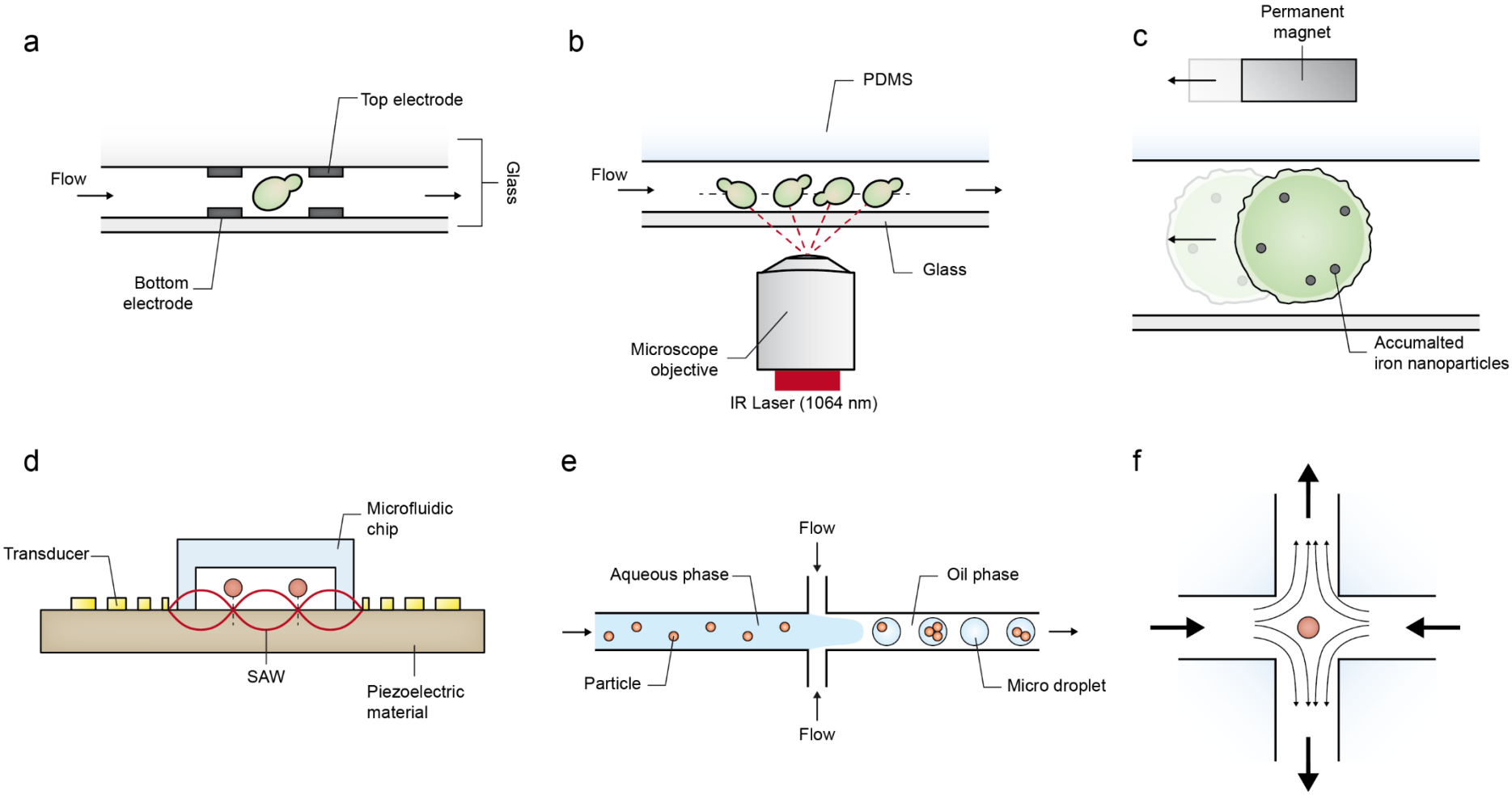

Figure 10: Overview non-surface contact based methods: (a) nDEP, (b) optical tweezers, (c) magnetic tweezers, adapted from [68]; (d) standing acoustic waves (acoustic tweezers), adapted from [56], (e) droplets adapted from, (f) hydrodynamic trap (flow focusing).

	Organisms	Throughput	Limitations/Bio-compabiliby	Additional fabrication steps	Experimental setup	Ref.
Electrical	Mammalian, Yeast, Bacteria	Limited amount of electrical cages can be integrated in one device	Compensation of electrical heating necessary.	Electrodes have to be integrated.	Complex setup to drive and control electrodes.	[54]
Optical	Yeast, Bacteria	Multiple trapping spots can be created, but requires a more complex experimental setup.	Heating and creation of oxygen radicals.	no	Realisation of a single optical trap is possible with standard research microscopes.	[55, 61, 62, 70–72]
Acoustic	Mammalian	Multiple trapping spots can be realized and controlled individual	No influences reported.	Transducer and piezoelectric material necessary.	Complex setup to control and manipulate acoustic waves.	[56, 57],[73]
Magnetic	Mammalian	Yes	Magnetic particles have to be integrated into the cells, might having toxic side-effects.	no	External/internal magnet needed.	[63],[74],[64]
Hydrodynamic	Bacteria	Limited capabilities for trapping multiple cells inside a device.	Possible influence on cells by shear forces.	no	Precise control of flow streams necessary to keep cell trapped.	[68],[69]
Droplets	Mammalian, Yeast, Bacteria	Creation and analysis at high frequencies of up to 10 kHz (REF)	Limited supply of nutrients.	no	no	[58, 59, 66, 75][65] [67]

Table 4: Comparison of non-surface contact based single cell trapping principles regarding type of organism, throughput, limitations, ease of fabrication and complexity of experimental setup.

5.1.2 Surface contact single cell trapping mechanisms

Surface contact methods for separating single cells from a bulk solution have been used in a broad variety of. In order to cope with the varying requirements for different applications several concepts haven been realized in microfluidic devices - microwells, fluid resistance trapping, sieve structures, growth grooves, growth chambers and hybrid devices. An illustration of the different trapping mechanisms is shown in Figure 11.

Microwells (Figure 11a) represent a simple method regarding the ease of fabrication and filling procedure to immobilize single cells. Hundreds of micron sized wells can be incorporated in a microfluidic device tailored to the specific size and shape of an organism Figure 11a. Microwells are eventually filled by flushing a suspension of cells over it. Applications related to the use of microwells have facilitated a wide range of different organisms – mammalian [76–78], plants [79], yeast [80] and bacteria [81–86].

Tan and co-workers [87] developed a trapping mechanisms relying on the difference of hydraulic resistance only. Figure 11b illustrates the original design by Tan and co-workers [87] with a straight channel consisting of an array of multiple trapping cavities. Each trapping cavity is connected by a bypass-channel either on the top or bottom of the main channel. Blockage of a trapping cavity by a particle immediately changes the hydraulic resistance and directs flow to the bypass channel. Further improvements by Kobel and co-workers [88] achieved higher efficiency in trapping and showed the possibility to confine and analysis individual mammalian cells.

Arrays of barrier structures inside a channel, acting as a sieve, to confine single cells have shown to be a simple and efficient way to immobilize single cells of various organisms. As shown in Figure 11c, flow can go around and underneath the trapping structures as long no cells is stuck. After a cell is hold back, flow can merely go around while pushing the cell against the barrier, holding it in place. First shown by Di Carlo and co-workers [89, 90] in 2006 to entrap individual mammalian cells, further variations of this principle followed enabling the trapping and analysis of algae [51, 91], yeast [92, 93] and bacteria [94–96].

The phenomenon of persistence in bacteria due to antibiotic treatment has been observed over many decades [7], but a complete understanding is still missing [8]. Balaban and co-workers [97] presented a microfluidic PDMS device consisting of several small growth grooves fitting exactly the size of single cells of *E. coli* as depicted in Figure 11d. This allowed screening for persister cells, which make out only a very small fraction of a population, for analysis. Wang and co-workers [98] reported a similar device for studying the possibility of ageing in *E. coli*. In contrast to the original concept, growth grooves consisted of only a single inlet with a

"mother" cell located at the end. Hence, consequent division of multiple "mother" cells could be observed over many generations. Moffitt and co-workers proposed also the use of a different material like agarose, which is permeable to small molecules, for studying effects like auxotrophy [99]. Further applications have made use of the two concepts to study single cells [100],[101–103].

Investigation of small populations of few hundred cells under constant environmental conditions in microfluidic devices can be realized in micron sized growth chambers, as illustrated in Figure 11e. Growth chambers were applied to investigate small populations of mammalian, yeast and bacteria cells. The different concepts can be separated with respect to the resolutions that are achievable to directly observe the growth, morphology and expression of fluorescence in single cells. Groisman *et al.* [104]and others have presented simple microfluidic growth chambers, however, investigation of individual cells are not possible since cells are allowed to grow freely in a 3D volume. High-resolution analysis was realized by confining cells in shallow growth chambers, restricting growth to a monolayer. Hence, individual cells in a small population can be monitored and tracked allowing reconstructing of lineages over multiple generations. Dénervaud and co-workers [105] reported a microfluidic devices consisting of multiple growth chambers for cultivating and analyzing of over 1,000 different yeast strains under constant conditions. Cultivation of bacteria in monolayer growth chambers was presented by Prindle and co-workers [106] for studying the chemical communication (quorum sensing) of bacterial cells in a population. Multiple variations of this concept were applied to study small populations of bacteria [62, 107].

Braschler and co-workers [108] developed a microfluidic device that allows the immobilization of single cells in a hydrogel (Figure 11f). Hydrogels bare the advantage to be solidified either chemically or by heat and vice versa. Hence, single cells can be trapped and released dynamically. Hydrogels in microfluidics haven been applied for various studies on mammalian [109–113], yeast [108] and bacteria cells [114].

Detailed comparison of the various surface contact based trapping principles regarding the number of trapped cells, type of organism, material of the microfluidic device, application as well as the possibility to reconstruct lineages are shown in Table 5.

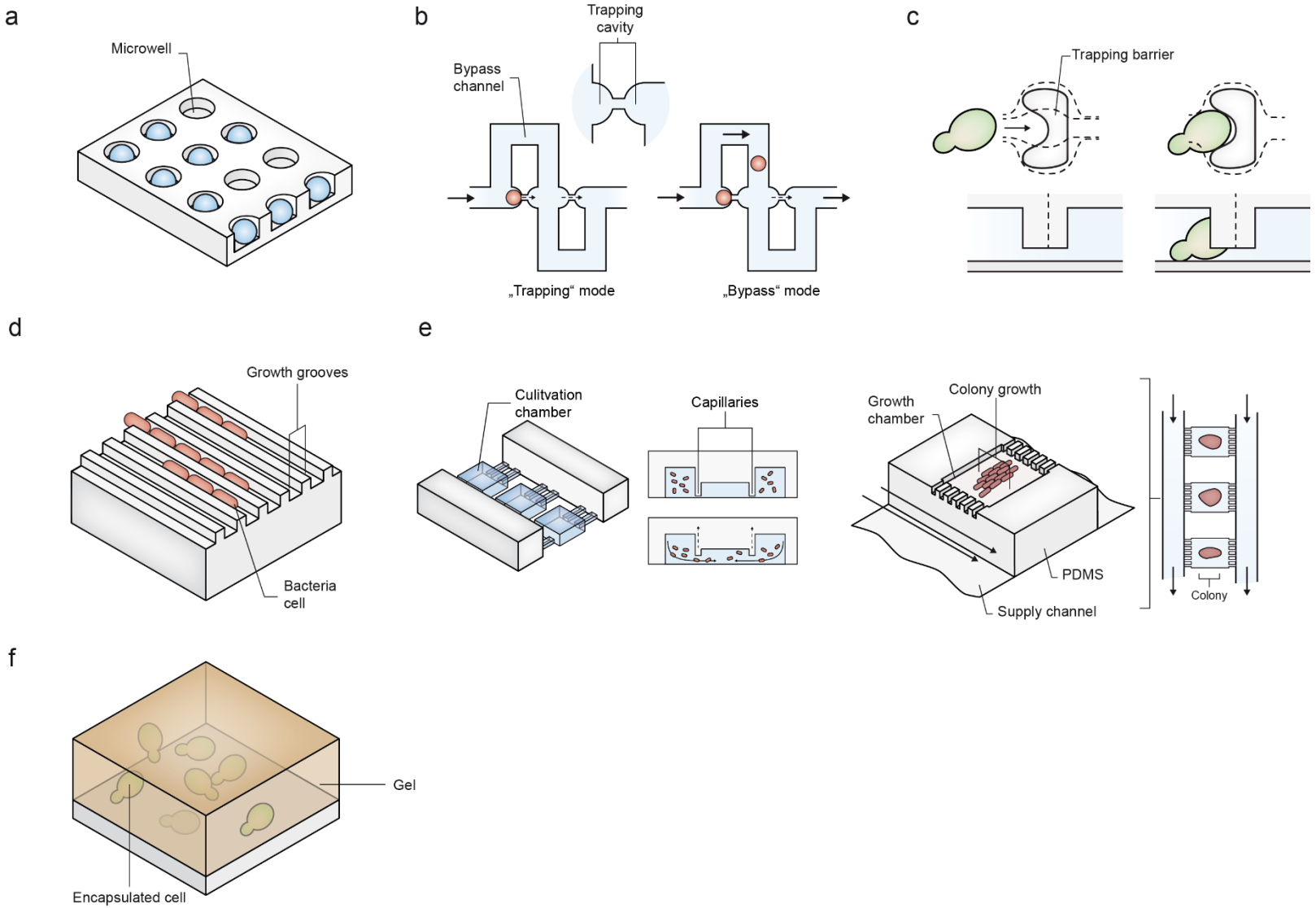

Figure 11: Overview of surface contact based single trapping methods: (a) microwells, (b) fluid resistance trapping, (c) sieve structures, (d) growth grooves, (e) growth chambers, (f) gel encapsulation.

Table 5: Overview of surface contact based trapping mechanisms for single cell analysis regarding the number of immobilized cells, cell type, material of the microfluidic device and the different fields of application.

Type	No. of cells	Organism	Material	Application	Ref
Growth chambers	microcolony	Bacteria[104, 106, 107, 115–124], Yeast[105, 125–130], Mammalian[131–138]	PDMS	co-cultivation[120–122], quorum sensing[106, 123]	[104–107, 115–125, 127–135, 137–141]
Growth grooves	few	Bacteria[98–103, 142–146], Mammalian [147]	PDMS, Agarose[99]	cell growth[144–146, 148], antibiotic persistence[97], aging[149]	[98–103, 142–146, 148]
Sieve structures	single cells	Yeast[92, 93], Bacteria[94–96], Mammalian[150–156], Algae[51, 91]	PDMS, PMMA [91]	aging[93], cell growth[51, 92, 94], cell fusion[154], immunoassy[95]	[51, 89, 91–96, 150–160]
Fluid resistance trapping	single cells, microcolony[161]	Mammalian[50, 88, 162–166], Yeast[167]	PDMS	co-cultivation[162], tissue stiffness [50], study of embryogenesis[165], cell growth[167]	[50, 88, 162–167]
Microwells	single cells/ microcolony	Mammalian[76–78], Bacteria[81–86, 168], Plant[79], Yeast [80]	PDMS, Agarose[169]	cell growth[78, 86], immunology [170, 171], western blotting[169], co-cultivation[85], quorum sensing[168]	[76–80, 82–86, 168, 169, 171–182]
Hydrogel encapsulation	single cells/ microcolony	Yeast[108] ,Mammalian [109–113], Bacteria [114]	-	cell growth[108, 110–113], quorum sensing[114]	[108–114, 183]

Publications

In this thesis, various microfluidic tools have been developed for the successful cultivation and analysis of single bacteria cells in microfluidic devices, they are subject of following publications.

Publication I, a method is presented for immobilizing, cultivating and analyzing single bacteria cells in microfluidic devices. Trapping and cultivation of single “mother” cells was realized by arrays of micron sized barrier structures arranged in the flow of a microfluidic channel. Proof-of-principle investigation of growth was carried out to verify homogenous proliferation of cells.

Publication II, introduces a microfluidic device for cultivating and analyzing microcolonies of bacteria in a high-throughput manner. Single cells are confined in shallow cultivation chambers forcing growth to a monolayer. Hence, high-resolution microscopy and automated image analysis allows reconstruction of cell lineages over multiple generations and several microcolonies. Hence, screening for rare cellular events in small population was achieved.

Publication III features a novel method for simplifying the filling process of single cells in microfluidic PDMS devices containing growth chambers. Artificial introduced air bubbles were used to temporarily distort the flow profile in microfluidic channels, allowing to fill solely diffusion based growth chambers in a fast and simple manner. Characterization of the filling producer as well as possible influences on the cell growth was investigated.

Publication IV illustrates a new approach in retrieving single cells from small microcolonies inside microfluidic cultivation chambers. Optical Tweezers (OT) were integrated into a microscopy setup allowing the filling and removal of individual cells from a cultivation chamber. Validations of the possible harmful effects caused by the OT irradiated laser light have shown that small time scales in cell manipulation (< 1 min) due not influence cell growth. First proof-of-principle experiments were conducted showing the removal of cells of interest from a growth chamber and relocation in an uninhabited one.

6 Publication I - Polydimethylsiloxane (PDMS) Sub-Micron Traps for Single-Cell Analysis of Bacteria

Christopher Probst, Alexander Grünberger, Wolfgang Wiechert, Dietrich Kohlheyer
Micromachines **4**, 357-369 (2013).
DOI:10.3390/mi4040357

6.1 Abstract

Microfluidics has become an essential tool in single-cell analysis assays for gaining more accurate insights into cell behavior. Various microfluidics methods have been introduced facilitating single-cell analysis of a broad range of cell types. However, the study of prokaryotic cells such as Escherichia coli and others still faces the challenge of achieving proper single-cell immobilization simply due to their small size and often fast growth rates. Recently, new approaches were presented to investigate bacteria growing in monolayers and single-cell tracks under environmental control. This allows for high-resolution time-lapse observation of cell proliferation, cell morphology and fluorescence-coupled bioreporters. Inside microcolonies, interactions between nearby cells are likely and may cause interference during perturbation studies. In this paper, we present a microfluidic device containing hundred sub-micron sized trapping barrier structures for single *E. coli* cells. Descendant cells are rapidly washed away as well as components secreted by growing cells. Experiments show excellent growth rates, indicating high cell viability. Analyses of elongation and growth rates as well as morphology were successfully performed. This device will find application in prokaryotic single-cell studies under constant environment where by-product interference is undesired.

6.2 Introduction

Single-cell analysis is a promising field for researchers from various disciplines as it holds potential for unraveling the intrinsic mechanisms of life with high accuracy. Investigations are performed on a single-cell basis rather than using typical bulk and average based measurements, which may mask conspicuous phenomena on the single-cell level. Therefore, microfluidics has become an essential part of the study of living microorganisms at small scale with spatial and temporal resolution, which would not be possible with conventional cytometric methods such as fluorescent activated cell sorting (FACS) and coulter counter.

Single-cell analysis is a promising field for researchers from various disciplines as it holds potential for unraveling the intrinsic mechanisms of life with high accuracy. Investigations are performed on a single-cell basis rather than using typical bulk and average based measurements, which may mask conspicuous phenomena on the single-cell level. Therefore, microfluidics has become an essential part of the study of living microorganisms at small scale with spatial and temporal resolution, which would not be possible with conventional cytometric methods such as fluorescent activated cell sorting (FACS) and coulter counter.

Microfluidic single-cell analysis assays can be divided into two main categories, namely studying either the whole cell (growth [184], morphology [107], or fluorescent bioreporters [185, 186]) or its lysate (genome, transcriptome, proteome and metabolome) [49]. Emerging technologies such as genetically encoded bioreporters have extended the toolbox for noninvasive whole-cell single-cell analysis and have been applied to measure metabolic states such as intercellular pH [187] and product formation [185].

Recently, two main microfluidic cultivation principles for single cells were exploited, namely:

(i) the cultivation of single mother cells growing into discrete isogenic microcolonies [104, 106, 107] and

(ii) arrays of physically separated individual cells and cell tracks [89, 154].

In microcolonies, individual cells may be exposed to extracellular stimuli from neighboring cells, for example due to secreted metabolites or environmental gradients within the microcolony [99]. However, when performing perturbation studies to analyze single-cell responses, avoiding such community effects becomes essential.

Various physical principles have been applied to immobilize individual cells by means of, for example, single droplets [59, 188], acoustic waves [56], electrophoretic forces [54, 189–193], optical tweezers [194] or mechanical objects and structures [195]. Most of these single-cell

trapping methods require laborious setups and may impact on the entrapped cells through temperature gradients or the formation of oxygen radicals [196], for example.

Alternatively, mechanical barriers and trapping structures inducing hydrodynamic forces on the cell enable the fast and reliable immobilization of hundreds of cells in parallel [89]. Single cells were entrapped in arrays of cup-shaped barrier structures with the openings facing towards the flow direction. Simultaneous cell pairing and the fusion of large arrays of cells were realized in [154] using the same passive cell-trapping approach. Instead of barrier structures, single cells can also be immobilized using rejoined gaps, where a meander-shaped channel is interconnected at multiple points by narrow junctions along its length [88]. The difference in the hydraulic resistance of the channels forces single cells into the narrow channels, where they become entrapped. The immobilization realized by both approaches is a statistical process and does not allow for a specific cell to be taken out of the flow or released again. More active control over the immobilization was achieved by applying negative pressure in order to pull cells into narrow channels arranged along the channel walls [197–200]. Throughput is typically decreased by better spatial control over the single cells. Despite the many advantages of these methods, all of them share the same limitation concerning cell size and shape. Previous work was carried out mainly with large mammalian cells or spherical eukaryotic cells such as yeast. Efforts have been made to apply identical concepts for immobilizing bacteria, for example *Escherichia coli*. Obviously, their small size (10 times smaller than yeast) and typically rod-shaped morphology make it difficult to immobilize them precisely [96]. Most concepts lack the possibility of removing the surplus of daughter cells once a single mother cell divides, leading to larger colonies after cell division. As microbial growth is often faster than eukaryotic cell growth, a reliable microbial single-cell analysis system necessitates the continuous removal of daughter cells.

To enable long-term analysis, the so-called “mother machine” was utilized to immobilize and cultivate hundreds of *E. coli* mother cells in narrow dead-end channels with a height of 1 µm [98]. At the end of each channel, the proliferating mother cell was observed over several hours as well as multiple generations of its descendants before cells were pushed out of the channel and flushed away. The mother machine concept is well suited for cell aging studies as the old pole mother cell remains at a fixed position. However, accumulation of secreted products inside the dead-end channels and concentration gradients might still cause cell–cell heterogeneity in more complex assays. A similar approach was reported by [99, 100] in which parallel growth channels with two openings facing the media supply streams were used to cultivate single cells. As single cells grew towards both openings of the tracks, the device was

not suited for cell aging studies. In contrast, a balanced culture was maintained over multiple generations. Instead of PDMS, [99] applied porous agarose as chip material to allow diffusion between each of the growth channels. Indeed, this was proven through the successful co-cultivation of two dependent *E. coli* auxotrophs that can complement the amino acid deficiencies of one another [99]. Due to the agarose material, concentration gradients may lead to inhomogeneous cultivation conditions. Inoculation of mother cells was achieved by simply pipetting a cell suspension onto the bottom glass slide of the device, before placing the agarose perfusion chip with incorporated growth channels on top of it. Instead, [100] applied PDMS as chip material, not facilitating diffusion between the growth channels. However, cell–cell interactions and accumulation of secreted products may occur inside the densely packed growth channels. In [100], device cell seeding was achieved by an imbalance of the two media volume flows inside the main channels actively pushing the mother cells into the tracks.

This article outlines the fabrication and characterization of sub-micron sized single-cell traps for the cultivation and analysis of individual bacteria located inside a continuous media flow. High-resolution electron-beam-written photolithography masks were utilized to fabricate SU-8 molds with 300–400 nm structural resolution with the approximate size of typical bacteria and smaller. Polydimethylsiloxane (PDMS) replication was performed to fabricate single-use chip devices, thereby replicating the sub-micron SU-8 trapping structures well. *E. coli* MG1655 cells were immobilized simply by flow inside the single-cell traps, cultivated, and observed by time-lapse microscopy over several hours. Division times at 20 min demonstrated excellent cell viability. Due to the fast media flow towards and around the traps, side products secreted by the cells were rapidly washed away without affecting any other cells further downstream. Supporting flow profile analysis was performed using computational fluidic dynamics. The present system will be used for single-bacteria perturbation studies.

6.3 Experimental

6.3.1 Soft Lithography

A video-based description of a comparable fabrication method can be found in [201]. Microfluidic master molds were fabricated using the negative photoresist SU-8 (MicroChem, Newton, MA, USA). Prior to resist deposition, a 4-inch silicon wafer was cleaned with piranha solution followed by hydrofluoric acid and rinsed with DI water. After dry spinning, the substrate was dehydrated for 20 min at 200 °C. For the first layer of photoresist, a mixture of two different SU-8 photoresists was used to achieve the designated height of 1 µm. The photoresists SU-8 2000.5 and SU-8 2010 were mixed in a ratio of 24:88, with a total weight of 60 g. This mixture was spin-coated onto the substrate at 500 rpm with an acceleration of 100 rpm/s for 10 s and at 2000 rpm with an acceleration of 300 rpm/s for 30 s. Soft bake was performed at 65 °C for 90 s, at 95 °C for 90 s and at 65 °C for 60 s. Afterwards, the substrate was exposed (7 mW/cm²) for 3 s using a mask aligner (MA-6, SUSS MicroTec, Garching, Germany) and an electron-beam-written chromium dark-field mask. Post-exposure bake was carried out at 65 °C for 60 s and 95 °C for 60 s. Unexposed parts of the photoresist were dissolved by immersing the substrate in developer solution (mr-DEV 600, micro resist technology GmbH, Berlin, Germany) for 60 s, then again in fresh developer solution for 40 s, and dipping it in isopropanol for 20 s. Developed substrates were dried and hard-baked for 10 min at 150 °C.

The second layer was coated with the negative photoresist SU-8 2010 at 500 rpm with an acceleration of 100 rpm/s for 10 s and 4000 rpm with an acceleration of 300 rpm/s for 30 s. After the deposition, the substrate was baked at 65 °C for 15 min and at 95 °C for 60 min. The photoresist was exposed (7 mW/cm²) for 12 s using a mask aligner (MA-6, SUSS MicroTec, Garching, Germany) and an electron-beam-written chromium dark-field mask. Post-exposure bake was carried out at 65 °C for 5 min and at 95 °C for 3 min. The development was carried out as described for the first layer. Finally, the structures were hard-baked for 6 h at 150 °C.

PDMS replicas were fabricated by pouring a 10:1 mixture of PDMS (Sylgard 184, Dow Corning, Midland, MI, USA) onto the wafer and baking it at 80 °C for 90 min. Next, the PDMS slab was peeled off the wafer and cut into separate chips. The chips were washed in n-pentane for 90 min to remove monomer residue and then transferred to an acetone bath for 90 min to remove the n-pentane. The chips were dried overnight. Prior to the experiments, each chip was thoroughly cleaned with acetone, isopropanol and, after drying, with scotch tape to remove any dust particles that may have clung to it. For high-resolution microscopy, a cleaned

chip was bonded onto a 170 µm thin glass cover slip using an oxygen plasma generator (Diener electronic GmbH, Ebhausen, Germany).

6.3.2 Sample Preparation

E. coli (MG1655) was pre-cultured in 20 mL of fresh LB medium in 100 mL shake flasks and cultivated at 37 °C and 150 rpm overnight. 25 µL of the overnight culture was transferred to 20 mL of fresh LB and grown until an optical density (OD 600, BioPhotometer plus, Eppendorf AG, Hamburg, Germany) of 1 was reached. Afterwards, 100 µL of the main culture was diluted in 900 µL of fresh LB medium prior to inoculation into the microfluidic device.

6.3.3 Experimental Procedure

E. coli cells were inoculated into single-cell trapping arrays and cultivated for 4 h. Cells were entrapped by infusing the cell suspension through the main channel until the traps were filled with single cells. Afterwards, the main channel was continuously flushed with fresh growth medium (200 nL/min) to remove excessive cells and ensure constant environmental conditions. Cells were grown at 37 °C using an in-house developed incubator mounted to a motorized microscope (Ti Eclipse, Nikon, Tokyo, Japan). Time-lapse images of immobilized cells were taken at 5 min intervals and analyzed using the commercially available software suit NIS-Elements.

6.4 Results and Discussion

6.4.1 Trap Layout and Geometry

Due to the typical size of *E. coli* (500 nm diameter and 2 µm length), the various concepts for the immobilization of single eukaryotic cells that have been demonstrated in other studies do not work properly for *E. coli*. However, [89] laid the foundation for microfluidic barrier trapping structures. In a first approach, we miniaturized the existing concepts for barrier structures down to the size of single *E. coli*. Our microfluidic device incorporates two key elements, namely:

(i) the main channels for cell suspension and growth media supply, with a height of 10 µm (Figure 12a), and

(ii) the cultivation area containing barrier structures for cell entrapment with a height between 800 nm and 1 µm, as depicted in Figure 12b.

A cell suspension was flushed through the main channel to inject single bacteria into the traps. The barrier structures developed by [89] allowed fluid flow to pass over the structures between PDMS and glass. This principle was not possible in our approach as bacteria tend to grow into narrow gaps [117]. Initial experiments with this newly developed single-cell trapping method revealed that clogging occurred through unspecific adhesion of the cells during the filling process as well as during cultivation (Figure 12c). Cells became trapped before reaching the gap of the trapping region or adhered to the glass slide inside the 1 µm channel. This shows that systems which were initially developed for eukaryotic cells cannot simply be scaled down to match conditions for single-bacteria analysis. In particular, the handling of different shapes and the removal of daughter cells that appear have to be considered. In a second approach, the trapping region was improved by reducing the plateau area to minimize clogging and unspecific adhesion, enabling cells to flow by without getting stuck (Figure 13a). Nevertheless, further experiments showed that this alteration did not prevent the adhesion of cells outside of the barrier structures. Finally, the trapping region was reduced to a round pillar with a height of 9 µm and a diameter of 17 µm (Figure 13b). This change allowed the successful immobilization of single *E. coli* cells without undesirable adhesion during the filling process and during cell growth. After division, daughter cells were immediately removed from the trapping region and washed away with the media stream.

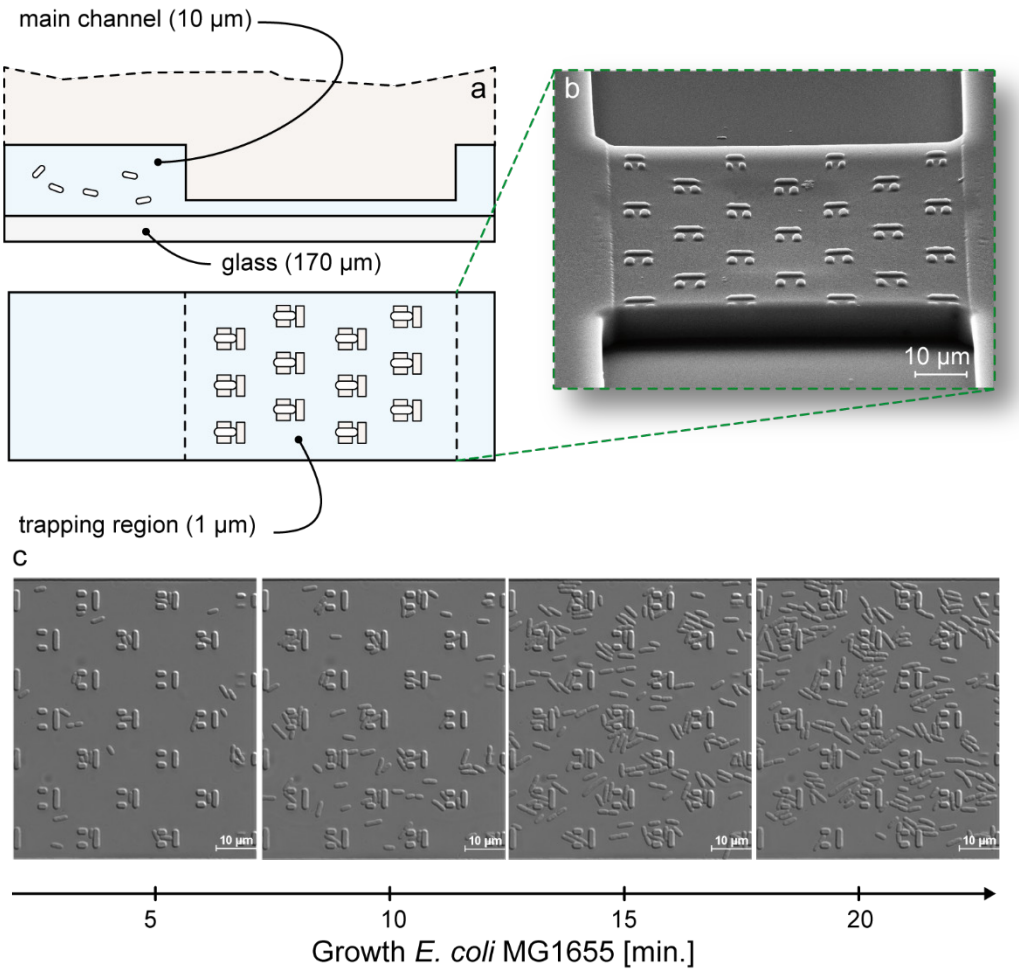

Figure 12: (a) Immobilization of single bacteria into a trapping array. (b) SEM images of trapping region containing several trapping structures for the immobilization of single bacteria. (c) Unspecific adhesion of *E. coli* leading to crowded growth in first single-cell trapping concept.

Single-cell studies presented in this paper were carried out using two types of barrier structures as depicted in Figure 14. The first design allows one cell at a time to be immobilized (Figure 14a) inside a 1.5 µm wide gap formed by three rectangular barriers with a width of 2 µm and a height of 1 µm. The second design allows two cells to be trapped simultaneously, increasing the throughput compared to the first structure, which allows single-cell trapping only. The gap between the barrier structures is 1 µm in width and 1 µm in length. The constriction at the end of each gap is 500 nm in width (Figure 14b). In contrast to previously published single-bacteria analysis devices by [98–100], our system facilitates fast and efficient inoculation by simply injecting the cell suspension.

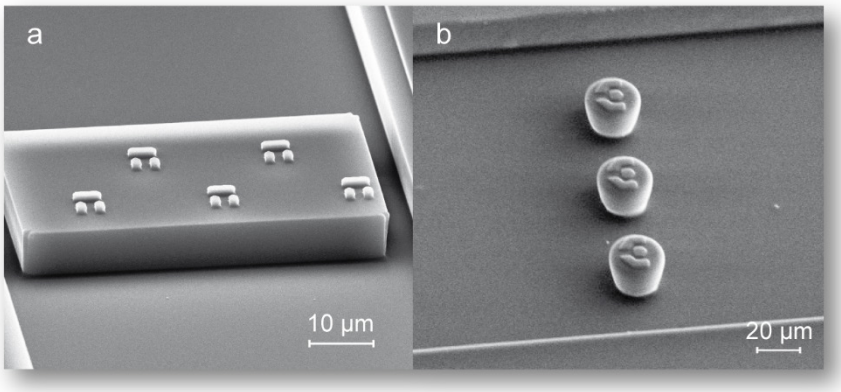

Figure 13: (a) SEM image of single-cell trapping structures with partially reduced trapping area. (b) SEM image of final trapping structure.

In fact, within a few seconds of perfusion, a good number of traps were inoculated, each with a single cell. The current proof-of concept chip contained 45 single traps and 42 double traps resulting in a loading capacity of individual 129 bacteria. As shown in Figure 14b, 60% of the single-traps and 87% of the double-traps were occupied within 20 s. Experiments showed that despite the small dimensions between the barrier structures of design (a), *E. coli* was still able to grow through the barrier structure. Better results were achieved with design (b), where the additional constriction of 500 nm at the end of each gap restricted growth to the front inlet direction.

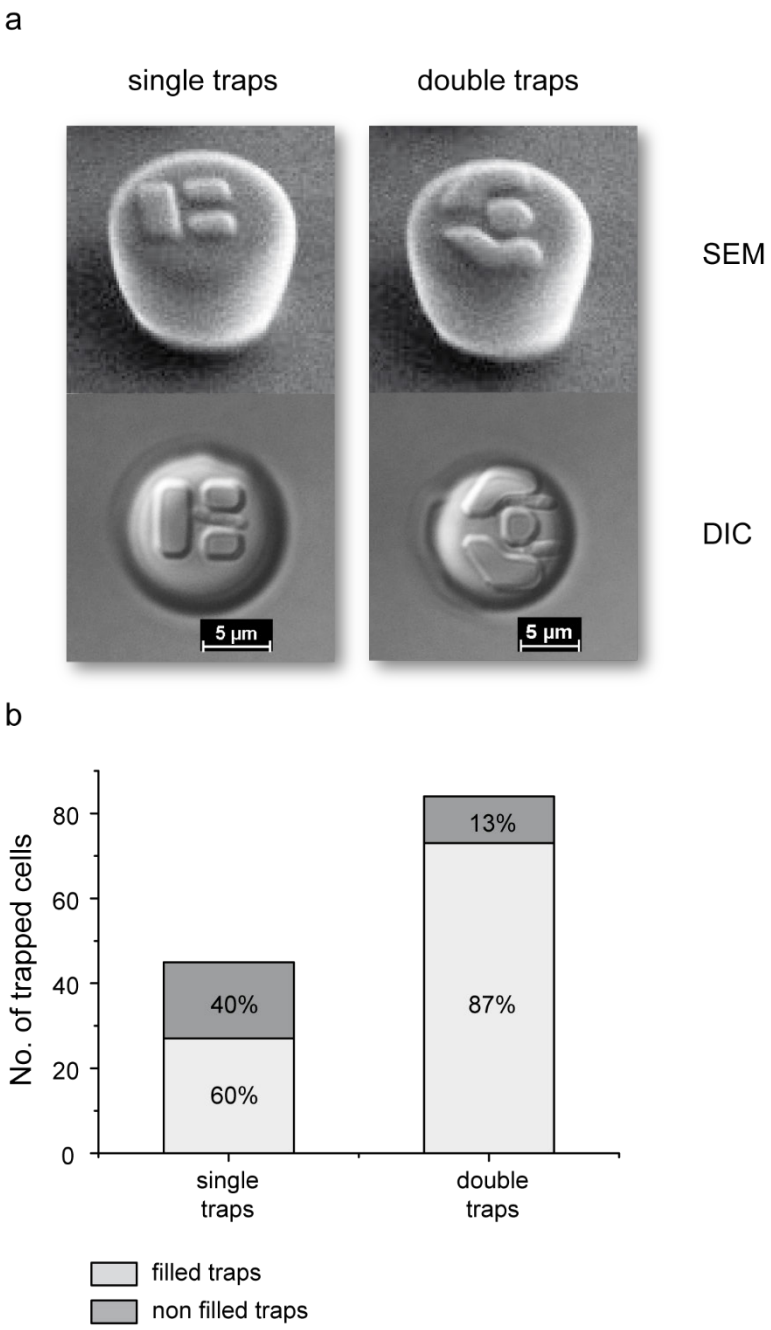

Figure 14: (a) Sub-micron single-cell trapping structures used for the successful immobilization and cultivation of *E. coli*. (b) Comparison of the number of trapped cells in single and double cell traps. After flushing the device with the cell suspension for a couple of seconds, 60% of the single traps and 87% of double traps were filled.

6.4.2 Numerical Simulation

Numerical simulations were conducted using COMSOL Multiphysics to analyze the fluid flow inside and around the single-cell trapping structures. Figure 15a shows the model geometry used in all simulations with a total length of 100 µm, width of 100 µm and height of 10 µm. The inlet boundary was defined to have a volumetric velocity of 16.67 x 10^{-12} m^3/s, corresponding to a flow rate of 1000 nL/min in our system, which equals the flow rate used for cell inoculation during experiments. The outlet boundary was set to a gauge pressure of 0 Pa. All other surfaces of the geometry were defined as walls with a no-slip condition. Reduction of the channel height (1 µm) near the trapping structure led to a drastic 1000 fold increase in the hydraulic resistance and much lower velocity inside the traps (Figure 15c) compared to the neighboring regions of the channel with an overall height of 10 µm (Figure 15b). Once a single cell is trapped, the flow is forced to diverge and flow around the trapping structure instead of flowing through the structure, and cannot trap any additional cells. This guarantees that only one cell at a time is trapped. Due to the reduced area of the shallow space surrounding the trapping structure, no additional cells can be caught in front. Furthermore, due to a higher convective flow around the trapping structure, by-products and surplus cells are washed away continuously, maintaining constant conditions over time.

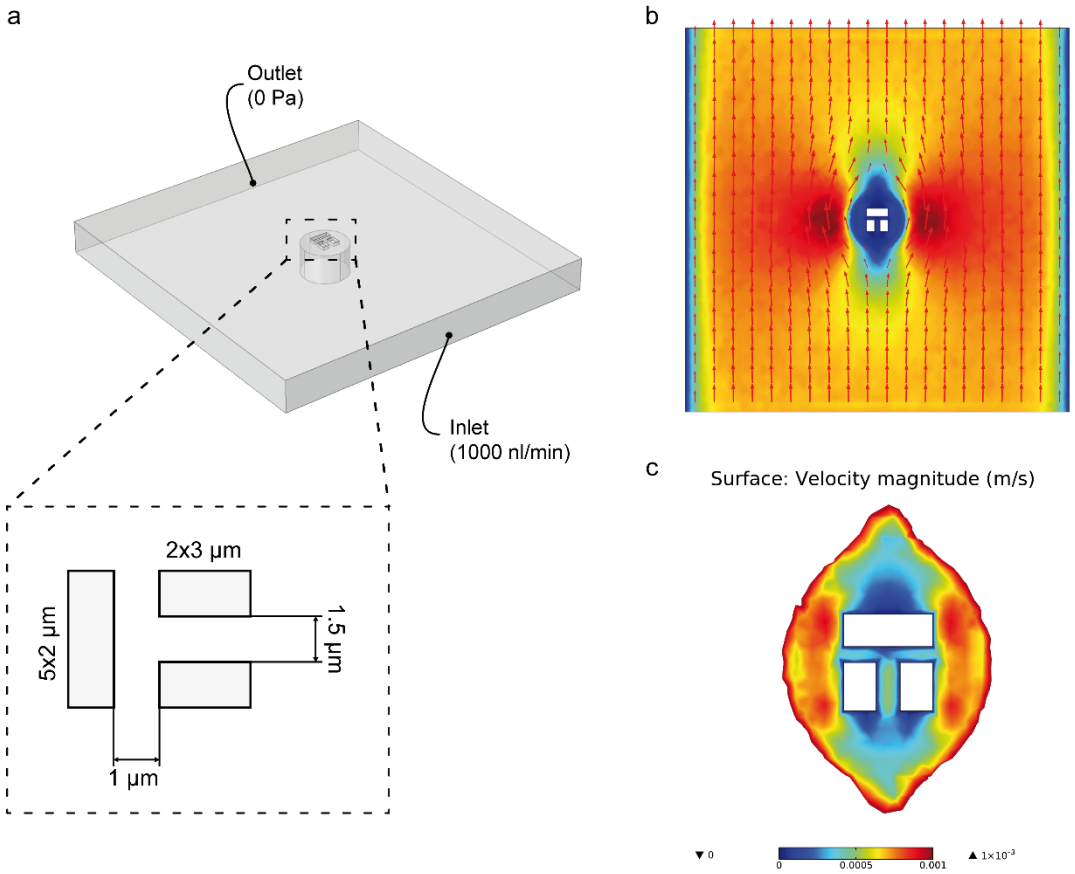

Figure 15: (a) Geometry used for numerical simulation with an inlet flow rate of 1000 nL/min, outlet gauge pressure 0 Pa and walls defined as no-slip walls. (b) Flow profile and velocity distribution along the whole microfluidic channel. (c) Distribution of flow velocity in the shallow region surrounding the trapping structure.

6.4.3 Single Cell Cultivation

Growth and morphology are key viability indicators in microbiology [202]. Single-cell growth assays analyzing division time and morphology were used in the present approach to validate our device. As shown in Figure 16a, we measured the cell length from one individual *E. coli* over 300 min cultivation by manually analyzing recorded time-lapse images. Division times as well as cell elongation rates were obtained. For analysis, a linear curve was fitted to the cell length over each generation period as illustrated in Figure 16. The slope of each fit represents the respective elongation rate, as shown in Figure 16.

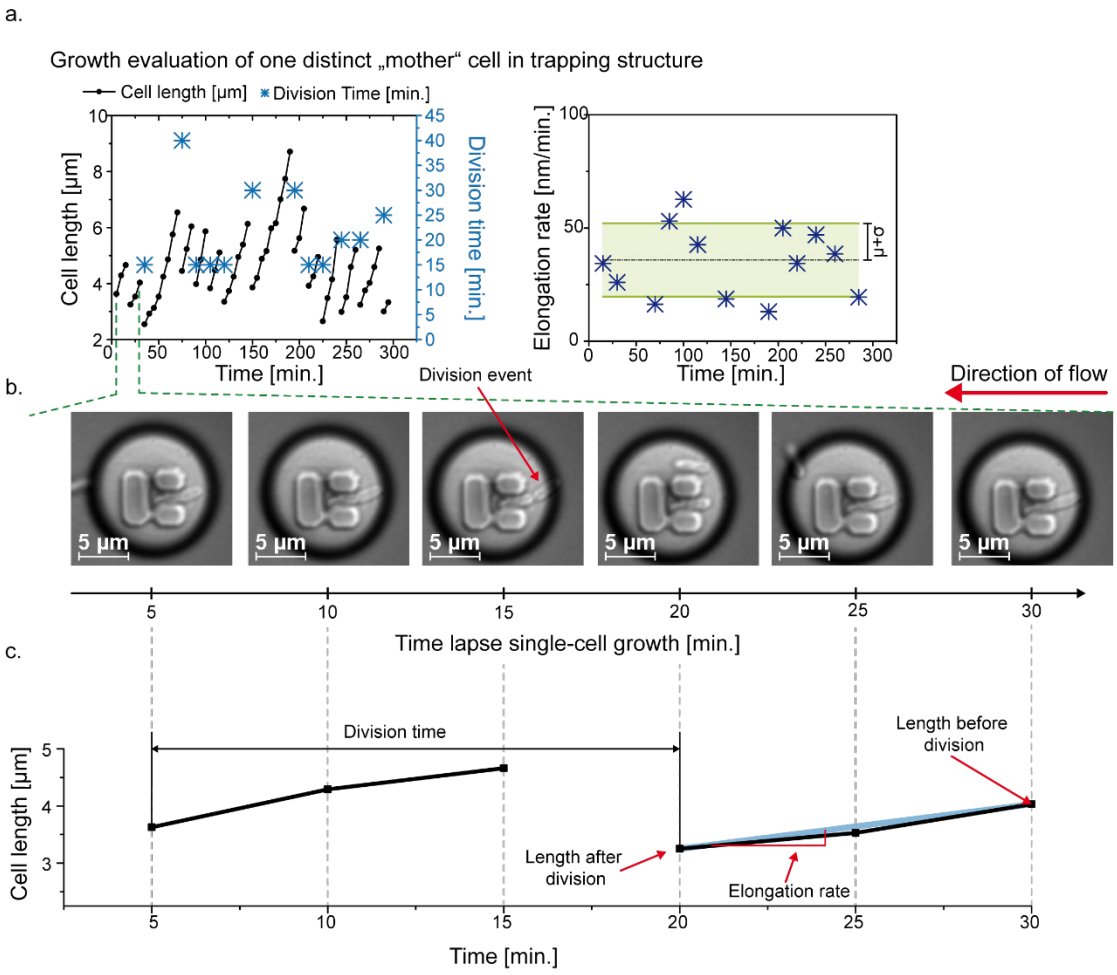

Figure 16: (a, b) Single-cell traces (cell length, division time and elongation rate) of one distinct *E. coli* mother cell. (c) Time-lapse image series showing the successful removal of a “daughter” cell from the trap during cultivation. (d) Cell length over the 30 min of cultivation describing the determination of the division time as well as the elongation rate.

By averaging the division time of single cells in multiple single-cell trapping arrays (Figure 16b), we derived a 20 min division time of *E. coli*, which corresponds well to previously reported results [98, 99]. Division times were derived by manual image analysis, as depicted Figure 16c,d. The time-lapse image in which both cells were apparently separated by a visible

septum, was considered as the division end. Obviously, the higher the image frequency during time-lapse microscopy, the more accurate the division time could be evaluated. In our experiments, we found the time-lapse imaging frequency of 5 min as a reasonable compromise between total throughput and accuracy of analysis. The mean division time and standard deviation were calculated over at least 9 generations from five traps, respectively Figure 17a). Longer division times can be explained by the appearance of filaments, a well-known phenomenon in many microbial organisms often induced by cell stress [9].

Filamentation leads to much longer cells and delays the division event. However, by evaluating cell length before (L_{Before}) and after (L_{After}) division, we observed an almost Gaussian distribution (Figure 17b). Filamentation only occurred in a few instances and was mainly observed directly after the seeding of the single-cell trapping structures. After the first division, the filamentous cells reverted to normal growth behavior with an average L_{Before} = 5 µm and L_{After} = 3 µm. The Gaussian distribution was validated by using the Kolmogorov-Smirnov test (goodness of fit). As it can be seen in Figure 17b, for a significance level of a = 0.05 and a critical value d = 0.174 (n = 61) it was found that D_{after} = 0.094 (p-value = 0.643) and D_{before} = 0.085 (p-value = 0.781). Since both values are smaller than the critical value d, we concluded that they are evenly distributed. Thus, we can presume that our newly developed method is suitable for the cultivation and analysis of single-cells such as *E. coli*.

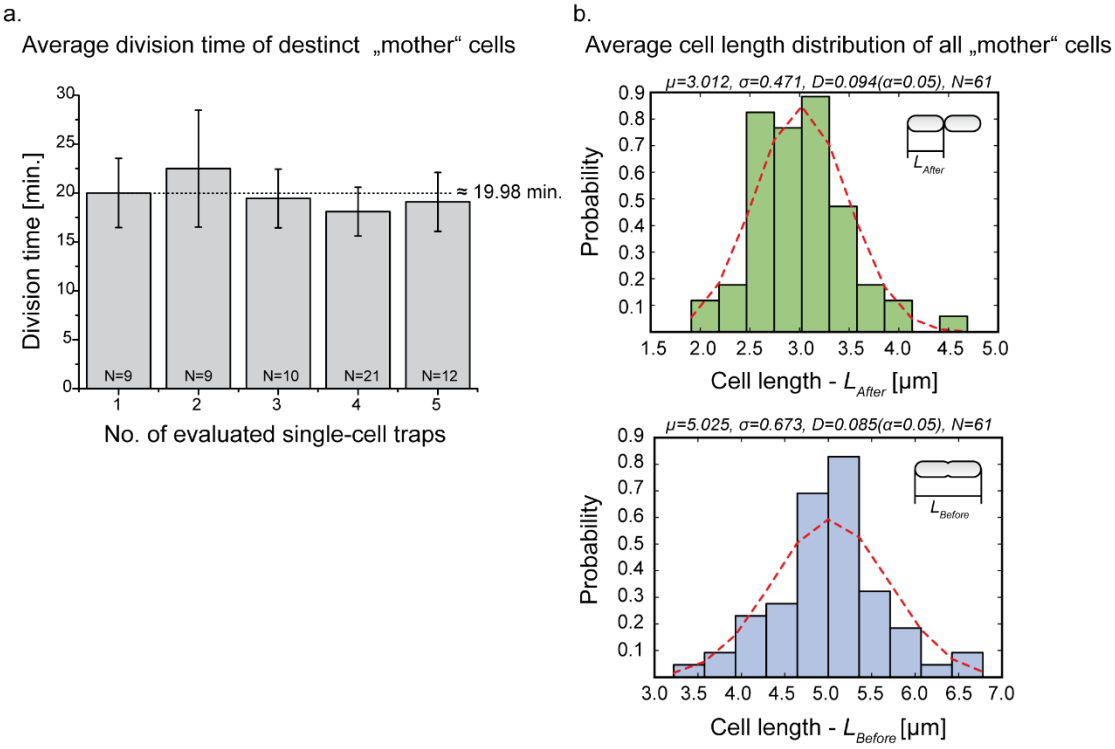

Figure 17: (a) Average division time of 20 min derived from 5 single-cell trapping structures over the whole cultivation period of 300 min. (b) Average cell length distribution before (L_{Before} ≈ 5 µm) and after (L_{After} ≈ 3 µm) division of all analyzed traps, showing a nearly Gaussian distribution.

6.5 Conclusions

Microfluidics has emerged as a powerful tool in single-cell analysis, with a wide spectrum of different applications. However, many microfluidic systems for single whole-cell analysis are restricted by the size of the organisms (mammalian cells or eukaryotic cells such as yeast) that can be cultivated. In the present article, we presented a microfluidic device containing sub-micron sized single-cell traps for the immobilization and cultivation of individual bacteria, successfully demonstrated with *E. coli*. Furthermore, a simple loading procedure was established in which simply the cell suspension is perfused through the media supply channel filling the traps with a good efficiency and reproducibility within a few seconds. Barrier structures with sub-micron sized channel geometry allowed for the trapping of single rod-shaped *E. coli*. The layout ensured that neighboring cells and by-products were continuously removed by a fast media flow maintaining constant conditions. We cultivated *E. coli* cells over several hours showing constant division times and typically rod-shaped morphology, indicating good viability. Our findings form the basis for further single-bacteria analysis under constant environmental conditions without neighboring cells affecting each other. In future

applications, our device is going to be applied for analyzing extracellular and intracellular responses of single bacteria due to short term fluctuations in pH, temperature, carbon sources and others. This will be achieved, e.g., by the application of genetically encoded fluorescence sensors [185, 186]. The layout can be applied to many other types of typically rod-shaped bacteria of similar size.

7 Publication II - Spatiotemporal microbial single-cell analysis using a high-throughput microfluidics cultivation platform

Alexander Grünberger†, Christopher Probst†, Stefan Helfrich, Arun Nanda, Birgit Stute, Wolfgang Wiechert, Eric von Lieres, Katharina Nöh, Julia Frunzke and Dietrich Kohlheyer*
Cytometry A, (2015).

7.1 Abstract

Cell-to-cell heterogeneity typically evolves due to a manifold of biological and environmental factors and special phenotypes are often relevant for the fate of the whole population but challenging to detect during conventional analysis. We demonstrate a microfluidic single-cell cultivation platform that incorporates several hundred growth chambers, in which isogenic bacteria microcolonies growing in cell monolayers are tracked by automated time-lapse microscopy with spatiotemporal resolution. The device was not explicitly developed for a specific organism, but has a very generic configuration suitable for various different microbial organisms. In the present study we analyzed *Corynebacterium glutamicum* microcolonies, thereby generating complete lineage trees and detailed single-cell data on division behavior and morphology in order to demonstrate the platform's overall capabilities. Furthermore, the occurrence of spontaneously induced stress in individual *C. glutamicum* cells was investigated by analyzing strains with genetically encoded reporter systems and optically visualizing SOS response. The experiments revealed spontaneous SOS induction in the absence of any external trigger comparable to results obtained by flow cytometry analyzing cell samples from conventional shake flask cultivation. Our microfluidic setup delivers detailed single-cell data with spatial and temporal resolution; complementary information to conventional flow cytometry results.

7.2 Introduction

While unraveling and understanding population heterogeneity, high throughput is of utmost importance to derive statistically reliable data, since many cellular phenomena occur with a very low probability per time unit. These rare events and population heterogeneity may be highly dynamic and often have evolved allowing isogenic populations, for example, by division of labor and bet-hedging strategies, to cope with more complex and dynamic environments. In bet-hedging strategies, a very small phenotypic subpopulation can be essential for the fate of the total population in particular under fluctuating environmental conditions. In division of labor strategies, specialized phenotypic subpopulations can have severe impact on the populations overall performance, for example with respect to growth or infection. To correctly understand this cellular heterogeneity, spatial and temporal resolution at the single-cell level, ideally during controlled perturbation studies, has gained much attention in the last few years (1,2). Therefore, simple agarose pad approaches have been frequently used to investigate single-cell growth (3,4) and single-cell lag phase behavior (5). In addition to agarose pads with limited environmental control (6,7), matured and user-friendly microbial single-cell culture and analysis systems are not yet available as standard analytics. However, progress in the field of microfluidics is promising (1,8,9).

Microfluidic single-cell devices in which single cells and colonies can be cultivated over long time periods under well-defined environmental conditions have been developed (8-11). Inside microstructures, individual cells can then be monitored by automated time-lapse microscopy (12-14), allowing new insights into single-cell physiology, behavior and lineage which are typically obscured by conventional bulk technologies.

By high-density large scale integration, microfluidic devices with improved throughput have been reported, for example, for single-cell analysis of various yeast strains (15) and bacteria (16,17). The latter and similar devices often operate with very special cultivation geometries that do not harbor the whole isogenic microcolony but only a fraction, thereby providing incomplete lineage information. Moreover, many of these devices were applied for the cultivation of one specific organism only, thus limiting a wide application range.

Over the last few years, we have developed a microbial single-cell cultivation technology with a strong focus on practical applicability and versatility. The present report describes a disposable, microfluidic cultivation device for the analysis of isogenic microbial microcolonies under well-controlled environmental conditions. Its beneficial and practical usability as a generic high-throughput microbial single-cell analysis tool is presented. Its functionality is

demonstrated by analyzing the model organism and industrially applied bacterium *Corynebacterium glutamicum*. Detailed single-cell data and analysis plots of *C. glutamicum* are shown to highlight the broad analysis capability, rather than interpreting the biological phenomena in detail. In addition, the identification of single SOS (rec A) expressing cells is demonstrated utilizing an fluorescent reporter to transform an intracellular signal into a detectable readout.

In comparison to many previously published single-cell cultivation systems, our platform combines several unique technological features and fulfills the following important characteristics:

- single use,
- full microcolony growth providing complete lineage information,
- single-cell resolution since cellular growth is geometrically restricted to monolayers,
- spatial as well as temporal resolution due to image-based time-lapse microscopy,
- high throughput (>100,000 cells/cultivation),
- excellent micro-environmental control by continuous media perfusion,
- cell growth under mainly diffusive mass transport with negligible convection and
- applicable to various bacteria (In the present study we cultivated *Corynebacterium glutamicum.* Experimental data on Escherichia coli and Gluconobacter oxydans will be published elsewhere.).

7.3 Materials and Methods

7.3.1 Device fabrication and setup

Polydimethylsiloxane (PDMS) microfabrication was carried out to manufacture single-use microfluidic devices with integrated 10 µm high supply channels and cultivation chambers with a height of 1 µm. A 100 mm silicon wafer was spin-coated separately with two layers of SU-8 photoresist, processed by photolithography. Profilometer measurements were performed regularly to validate SU-8 structure heights during wafer fabrication. This silicon wafer served as a reusable mold during subsequent PDMS casting. Thermally cured and separated PDMS chips were treated with oxygen plasma and permanently bonded to 170 µm thick glass slides just before the experiments. Manually punched inlets and outlets were connected with tubing (Tygon S-54-HL, ID = 0.25 mm, OD = 0.76 mm, VWR International) via dispensing needles (dispensing tips, ID = 0.2 mm, OD = 0.42 mm, Nordson EFD). SU-8 and PDMS fabrication is common to date and a very detailed fabrication protocol can be found elsewhere (18,19).

7.3.2 Flow characterization

Microscopic flow profile characterization was performed by infusing fluorescently labeled microspheres with diameters of 200 nm (yellow-green fluorescent 505⁄515 nm; catalogue number: F8811) and of 1 µm (blue fluorescent 350⁄440 nm; catalogue number: F8815, Molecular Probes, Invitrogen). 1 µm spheres were utilized to visualize the cell inoculation and trapping process. 200 nm spheres were used to emulate diffusive mass transport during cultivation conditions. Prior to microsphere injection, all microfluidic channels were primed with a 0.1 % BSA solution (buffer: dH_2O, pH = 7.0) at 700 nl/min for 60 minutes to minimize unspecific microspheres adhesion. All microsphere suspensions (2 % solids) were diluted 1:1000 in 0.1 % BSA solution. The exposure time during fluorescence microscopy was 10 s to capture complete flow trajectories. Further details can be found in the time-lapse imaging section.

7.3.3 Bacterial strains and pre-cultivation

C. glutamicum ATCC 13032 was used for general cultivation experiments. *C. glutamicum/*pJC1-P_{recA}-*e2-crimson* was used when screening for spontaneously induced SOS. Here, an e2-crimson protein is co-expressed with recA resulting in fluorescent cells when recA is induced. Detailed information on the construction of *C. glutamicum/*pJC1-P_{recA}-*e2-crimson* is given in (20).

CGXII was used as standard mineral medium for *C. glutamicum* cultivations consisting of (per liter): 20 g $(NH_4)_2SO_4$, 5 g urea, 1 g K_2HPO_4, 1 g KH_2PO_4, 0.25 g $MgSO_4 \cdot 7H_2O$, 42 g 3-morpholinopropanesulfonic acid (MOPS), 10 mg $CaCl_2$, 10 mg $FeSO_4 \cdot 7H_2O$, 10 mg $MnSO_4 \cdot H_2O$, 1 mg $ZnSO_4 \cdot 7H_2O$, 0.2 mg $CuSO_4$, 0.02 mg $NiCl_2 \cdot 6H_2O$, 0.2 mg biotin, and 0.03 mg of protocatechuic acid. The medium was adjusted to pH 7 and 4 % glucose (w/v) was added as a carbon source. All chemicals were purchased from Carl Roth and Sigma Aldrich. The medium was autoclaved and sterile-filtered (0.22 µm pore size) to prevent clogging of the microfluidic channels by particles and cell agglomerates.

Cells were pre-cultured as 20 mL cultures in 100 mL baffled Erlenmeyer flasks on a rotary shaker at 120 rpm orbital shaking at 30 °C. A first pre-culture in BHI (Brain-heart infusion, Becton Dickinson, USA) complex medium was inoculated into a second pre-culture in CGXII mineral medium, which was finally inoculated at OD_{600} = 0.05 into CGXII mineral medium, the main culture.

7.3.4 Microfluidic cultivation

Fluid flow into the microfluidic chip was controlled with a 4-fold NeMESYS syringe pump (Cetoni GmbH, Germany). A detailed setup protocol can be found in (18,19). Prior to microfluidic cultivation, the microfluidic chip was purged with fresh and sterile-filtered CGXII medium at 400 nl/min for 10 min.

Afterwards, the chip was infused with bacterial suspension for single-cell inoculation as described in full detail recently (21). Bacterial suspensions were withdrawn from the main culture at the exponential growth phase (OD_{600} between 0.5 and 1). As soon as sufficient single cells were inoculated into the microfluidic cultivation chambers, solely CGXII medium was infused at 400 nl/min throughout the entire cultivation.

7.3.5 Time-lapse imaging

Experiments were carried out using an inverted time-lapse live cell microscope (Nikon TI-Eclipse, Nikon Instruments, Germany) equipped with a 100x oil immersion objective (CFI Plan Apo Lambda DM 100X, NA 1.45, Nikon Instruments, Germany) and a temperature incubator (PeCon GmbH, Germany). Phase contrast and fluorescence time-lapse images of growing microcolonies were captured every 10–20 minutes using an ANDOR LUCA R DL604 CCD camera. Fluorescence images were recorded with an exposure time of 200 ms using a 300 watt Xenon light source (Lamda DG-4, Sutter Instruments, USA) at maximum intensity and

appropriate optical filters (excitation: HQ 600/37, dichroic: DM630, emission: HQ 675/67; AHF Analysentechnik AG, Germany).

7.3.6 Image analysis and data visualization

Time-lapse movies of monolayer growth chambers were analyzed using a custom, specialized workflow implemented as an ImageJ/Fiji plugin (22). Cell identification was performed using a segmentation procedure tailored to detect individual rod-shaped cells in crowded populations. Detected cells were subsequently tracked throughout all image sequences using an adapted single particle tracking approach as implemented in TrackMate (23). This image analysis approach allowed the extraction of measurable quantities of individual cells, for example, cell number, cell area, mean single cell fluorescence, as well as derived quantities, for example the growth rate. All data sets were subsequently processed using the analysis and visualization software 'Vizardous' (24). Vizardous assists the user with analysis and interpretation tasks for single-cell data in an interactive, configurable and visual way by augmenting lineage trees with time-resolved cellular characteristics.

For detailed growth rate analysis (Figure 20 and 21), specific chambers were selected that contained only 1 or 2 cells at the beginning of the experiment. For SOS-response studies (Figure 24), all inoculated chambers were considered for analysis.

To determine growth rates of isogenic microcolonies (Figure 21), the number of cells in each colony was counted up to a colony size of approximately 130 cells. The maximum growth rate μ_{max} [1/h] was then estimated from the plot Ln(Cell number) vs. time by fitting an exponential function to the cell number increase applying the method of least squares (25), as depicted in the insert in Figure 4a.

The analysis of spontaneously induced SOS expression in cells (Figure 23 and 24b) was performed as follows: First, the contour of each cell was determined. Second, the mean fluorescence intensity of the cell was determined. Third, spontaneously induced cells were determined from fluorescence vs. cell area plots. Spontaneously induced *C. glutamicum* cells exhibiting a 5-fold higher mean fluorescence than non-induced cells were classified as SOS positive (SOS+). Results of microfluidic high-throughput screening experiments (Figure 24c) were obtained by determining the total fluorescence intensity of fluorescing cells. Non-fluorescing cells were not further analyzed. The average final cell number of 750 cells per cultivation chamber was applied to derive the percentage of SOS+ cells.

7.3.7 Flow cytometry (FC)

FC was performed on an Aria II (Becton Dickinson, San Jose, USA) flow cytometer with 633 nm excitation by a red solid-state laser. E2-Crimson fluorescence was detected using a 660/20 nm band-pass filter. About 100,000 cells were analyzed to determine SOS response at different time points. Cells with a fluorescence output 12- to 18-fold higher than the average were counted as SOS+ cells (Publication II - Supplement 3). The different gating during FC and MGC analysis are related to technical differences of the optical systems. For FC measurements (FACSaria II, BD), the PMT voltage was adjusted to obtain a good dynamic range of the fluorescent signal. During MGC cultivation the fold change of SOS positive cells was significantly lower. However, the stop of cellular growth and changes in morphology observed via time-lapse imaging are in agreement with an induction of the SOS response.

7.3.8 Computational fluid dynamics

Computational fluid dynamics (CFD)-based analysis was performed using COMSOL multiphysics (Comsol Multiphysics GmbH, Germany) with the model geometry shown in Figure 18d. The underlying mesh is described in more detail in Publication II - Supplement 1. The incompressible stationary flow was modeled by the Navier-Stokes equation (Equation 8 & Equation 9):

$$\rho(\vec{u}\cdot\nabla)\vec{u} = \nabla[-pI + \mu(\nabla\vec{u} + (\nabla\vec{u})^T)] \qquad \text{Equation 8}$$

$$\rho\nabla\cdot\vec{u} = 0 \qquad \text{Equation 9}$$

with $\vec{u}$ the velocity, p the pressure, I the identity matrix, $(\nabla\vec{u})^T$ the transpose of $\nabla\vec{u}$, μ = 0.0012 Pa s the dynamic viscosity of a 4 % glucose-water solution (w/v); ρ = 1016.5 kgm^{-3} the fluid density of a 4 % glucose-water (w/v) solution. The velocity at the two supply channel inlets was 0.002 ms^{-1} which corresponds to a volumetric flow rate of 40 nL min^{-1}. On chip a total flow rate of 400 nL min^{-1} is equally distributed among 10 supply channels.

The transport of glucose (dc/dt) was described by the time dependent convection-diffusion equation (Equation 10):

$$\frac{\partial c}{\partial t} = -\vec{u}\,\nabla c + \nabla\cdot(D\,\nabla c) \qquad \text{Equation 10}$$

with *c* the molecule concentration of glucose, D = $0.67 \cdot 10^{-9} m^2 s^{-1}$ the diffusion coefficient of glucose and $\vec{u}$ the velocity field given by the solved Navier Stokes equation. The starting concentration of the glucose solution was 244 mol/m^3.

7.4 Results

7.4.1 Device layout and principle

The present microfluidic system is intended for high-throughput single-cell cultivation and analysis of growing isogenic microcolonies. The device consists of a PDMS glass chip with the approximate size of a postage stamp (20 mm x 15 mm x 3 mm) (length x width x height) with incorporated microfluidic channels (Figure 18a). The chip has one inlet channel that supplies medium, incorporates 400 monolayer growth chambers (MGC) (2x4 arrays of 50 MGCs) and has a single outlet channel (Figure 18c). Each MGC (40 µm x 40 µm x 1 µm) can accommodate a single microcolony of approximately 750 individual bacteria (Figure 18d). The uniform height of 1 µm restricts microcolony growth to a defined cell monolayer (Figure 18e). MGCs are arranged between two tenfold deeper supply channels (10 µm x 30 µm) (height x width) with laterally interconnected micrometer sized connecting channels (19 µm x 2 µm x 1 µm) (length x width x height) as depicted in Figure 18c-d.

Throughout standard cultivation, medium is fed continuously at nearly identical flow rates into each supply channel and thus negligible pressure difference occurs across the MGC perpendicular to the flow. However, during the primary inoculation phase, the volume flow rates in the parallel supply channels are unequal, resulting in a perpendicular pressure difference and thus fluid convection supporting direct cell transport into the MGC.

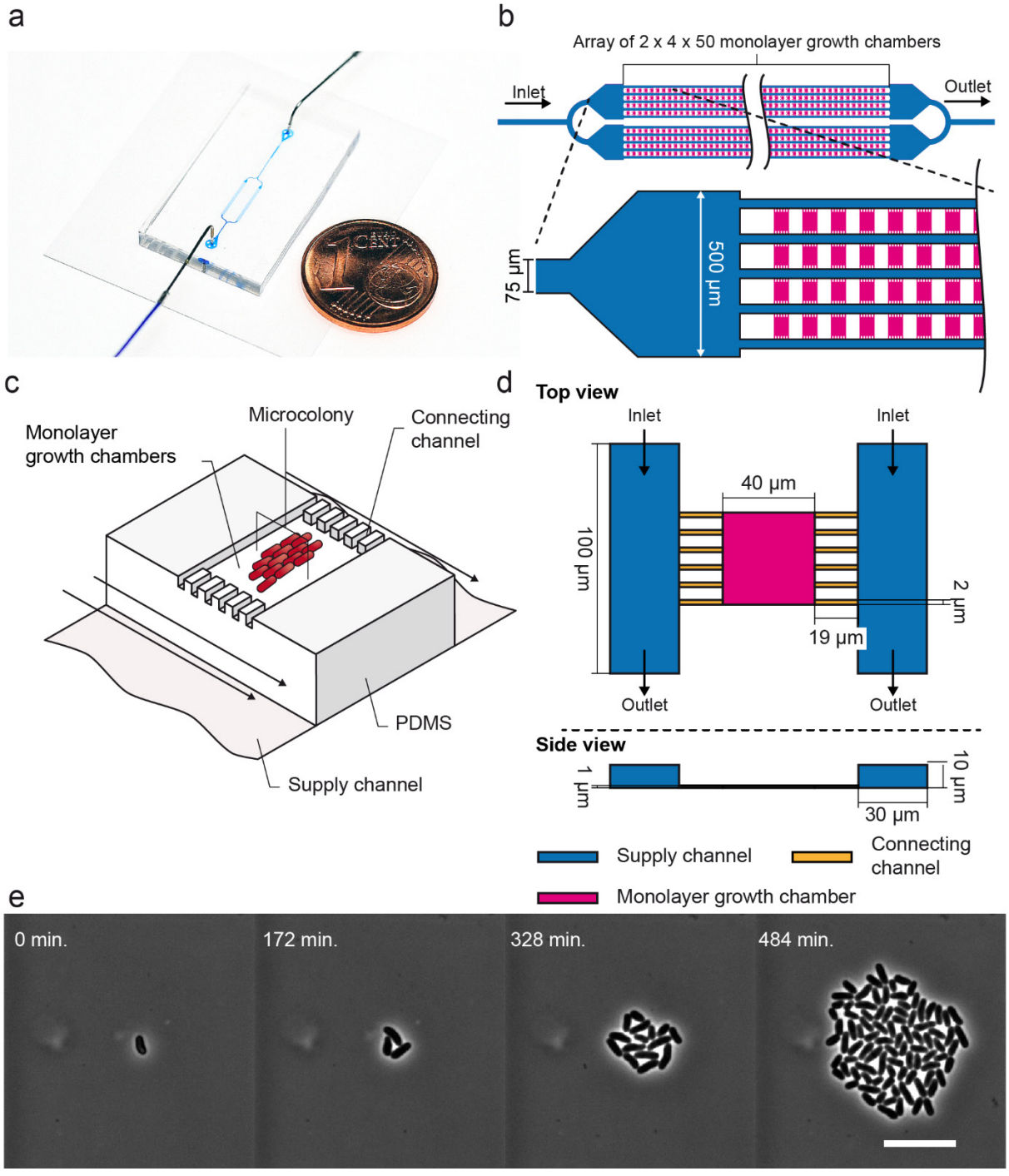

Figure 18: (a) Microfluidic PDMS glass device for high-throughput single-cell cultivation and analysis. (b) 2D CAD design of microfluidic channels with arrays of MGC arranged in parallel (c) 3D dimensional illustration of a single MGC highlighting the different depths of the channels. (d) Geometry of the MGC used for the CFD simulations. (e) Growing microcolonies of up to 750 cells can be observed for several hours depending on the organism and media used; here *C. glutamicum* (scale bar 10 µm).

7.4.2 Flow tracer analysis

To optically visualize laminar stream lines and diffusive mass transport conditions, the microfluidic chip was characterized experimentally using fluorescent microspheres. 1 µm microspheres with a comparable diameter to that of typical bacteria cells were infused into the fully wetted chip to visualize the cell trapping process. As shown, few 1 µm microspheres were randomly trapped and remained inside the MGC throughout the course of the experiment (bright spots in Figure 19a). Our inoculation procedure utilizes a nanoliter sized air bubble entrapped right before each fivefold channel branching (Figure 18b), thereby sealing single channels temporarily modifying the flow conditions (21). This induces pressure differences across the MGCs and convective flow through the cultivation chambers, facilitating active cell transport into the chambers. Within two minutes the air bubble disappears by diffusion through the permeable PDMS and normal flow conditions with balanced flow rates through all supply channels are restored.

Once sufficient cells are trapped in the MGC in a realistic cultivation, the growth phase is initiated by changing the medium from the cell suspension to cultivation medium. During this cultivation phase, both parallel media streams have nearly identical volume flow rates, resulting in diffusive mass transport conditions with negligible convective flow inside the MGCs. This diffusive mass transport was experimentally validated by supplementing the fluid with 200 nm fluorescent microspheres which exhibited diffusive migration only, as indicated by the random fluorescence flow traces (Figure 19a).

7.4.3 Computational fluid dynamics

CFD simulations were performed to gain essential knowledge on flow velocities, mass transport and nutrition supply. For CFD simulations, a flow rate of 40 nl/min per supply channel was configured. This corresponds to a total medium flow rate of 400 nl/min equally distributed between 2 x 5 parallel supply channels (see Figure 18b). The visualized simulations show a homogenous parabolic velocity profile inside the parallel supply channels (Figure 19b). In contrast to this, the flow inside the MGC is negligibly low in the y-direction (Figure 19b) and x-direction (Figure 19c) during cultivation conditions. It has to be noted, that the present CFD simulation geometry does not perfectly match the experimental configuration. On chip (Figure 18b) some supply channels are connected to MGCs at both sides, whereas the simulation was based on a fully symmetrically and single MGC configuration. In reality this little asymmetry might induce inhomogeneous flow rates through the 10 supply channels. In fact, very detailed CFD simulations (not presented in the present manuscript) using the realistic chip geometry

showed slightly inhomogeneous differences, with channel to channel differences as high as 4 % maximum. However, the same simulations revealed that inside the MGCs diffusion was absolutely dominating and no convection could be determined. This can be mainly explained by the low flow rates and the high hydrodynamic resistance difference between the 10 fold deeper supply channel and the shallow MGCs. Furthermore, derived cell growth rates inside the chambers did not show particular phenotypes related to certain MGC locations on chip.

A medium switch was simulated to acquire characteristic nutrition supply rates under potentially changing medium conditions. Within 2 s after the change from no glucose to 244 mol/m³ glucose delivered by the supply flow (Figure 19d), the glucose concentration at the MGC center reached 50 % of its maximum concentration value by diffusive mass transfer (Figure 19e). A homogenous and nearly constant glucose distribution was achieved within 6 s only (Figure 19f).

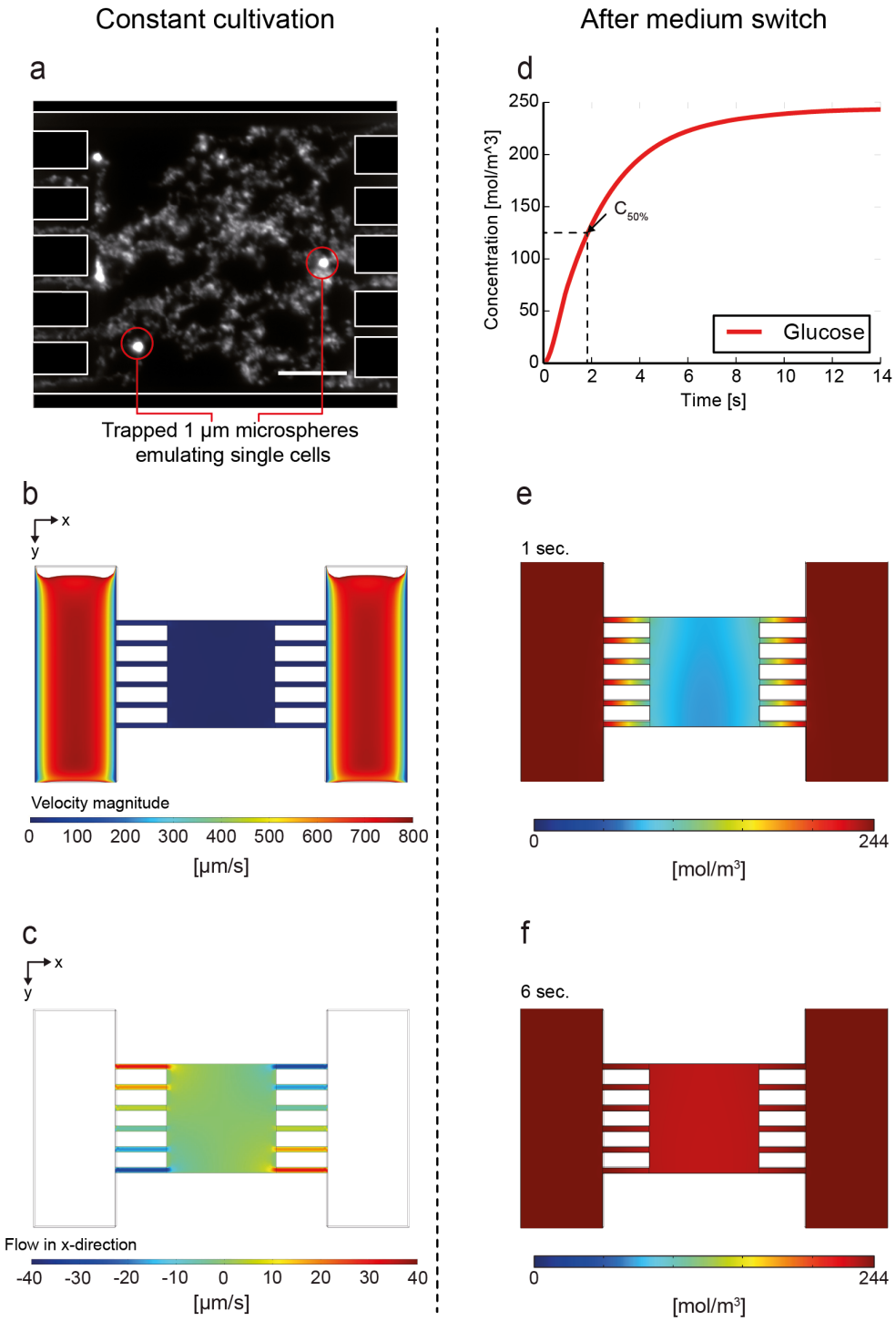

Figure 19: Characterization of fluid flow and concentration profiles inside an MGC: (a) Fluorescence traces of 200 nm microspheres show diffusive migration behavior inside a single MGC during cultivation conditions (scale bar 10 µm). Two 1 µm microspheres were trapped inside the MGC during a cell trapping emulation. (b) CFD simulations revealed laminar parabolic flow inside the supply channels (velocity magnitude). (c) Inside the MGC convective flow is negligible low with the highest velocity inside the connecting channels. (d) Simulations chart of nutrient supply after a sudden medium change from no glucose to 244 mol/m³ glucose in the supply streams. (e+f) Glucose concentration profile during simulations revealed fast medium changes within seconds.

7.4.4 Microbial single-cell analysis of isogenic microcolonies

An exemplary in-depth analysis was performed on two separate *C. glutamicum* ATCC 13032 colonies with single-cell resolution. By cell identification and tracking, lineage trees could be generated as shown in Figure 3 a, b. Furthermore, characteristic single-cell growth and morphological parameters were extracted, in particular, division time distributions (Figure 20c-d), as well as cell length before and after each division event (Figure 20e-f). All distributions showed Gaussian behavior, with few outliners exceeding 3 times the standard deviation. To further support these findings, further analyzes were performed. Length characteristics were derived as illustrated in Figure 20g.

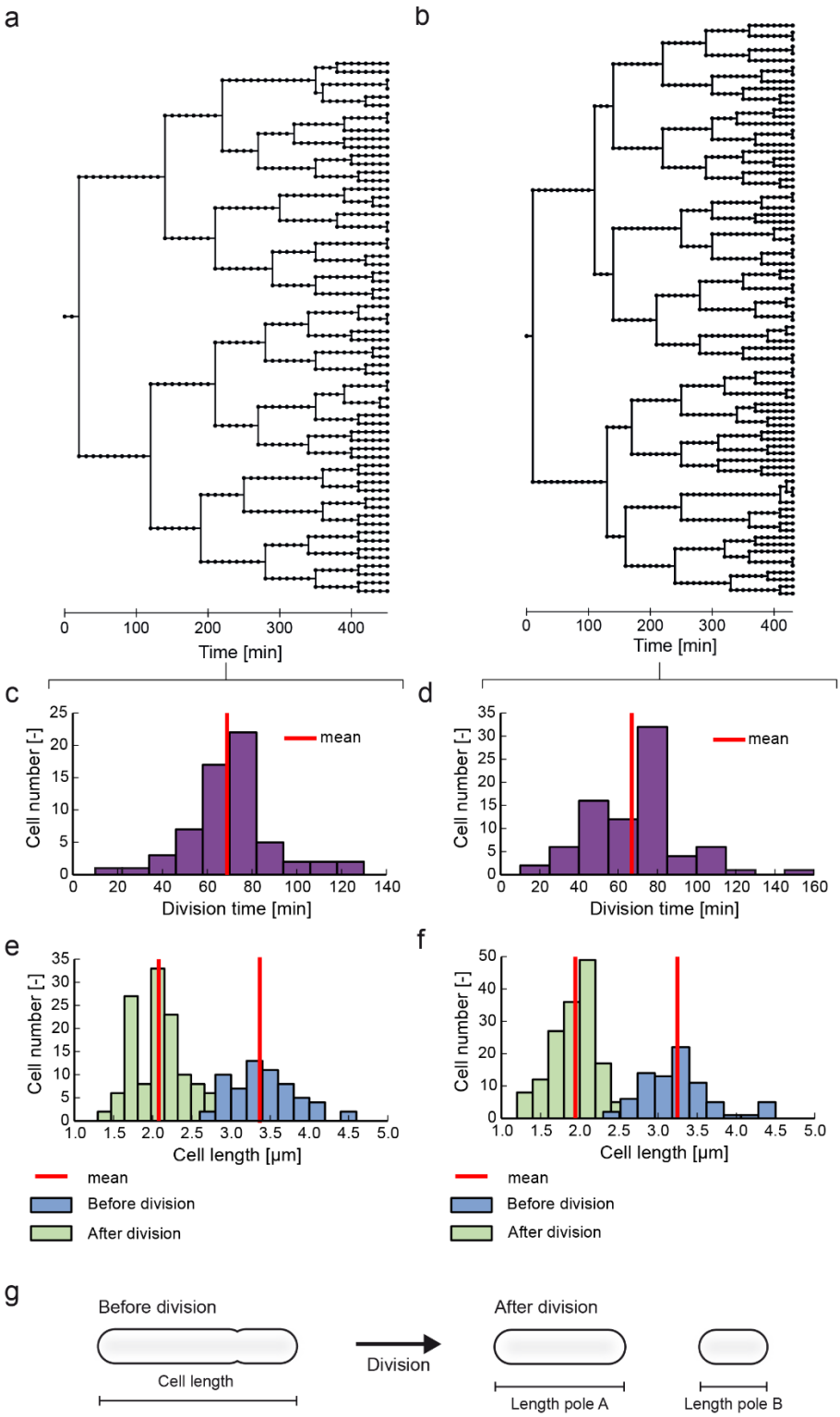

Figure 20: Heterogeneity analysis of two clonal *C. glutamicum* microcolonies: (a, b) Lineage trees showing the overall growth and division behavior. (c, d) Division time distribution for $t_{d,\ average\ c}$ = 68.87 ± 20.56 min and $t_{d,\ average\ d}$ = 66.88 ± 24.06 min. (e, f) Cell length distribution before ($L_{before,\ average\ e}$ = 3.37 ± 0.44 µm, $L_{before,\ average\ f}$ = 3.25 ± 0.46 µm and after division ($L_{after,\ average\ e}$ = 2.08 ± 0.33, $L_{after,\ average\ f}$ = 1.94 ± 0.35 µm) derived from lineage trees. (g) Description of morphology related parameters: Cell length before division; cell length of pole A and pole B after division.

37 colonies containing a total of 4804 cells were further analyzed to gather single-cell data from higher cell numbers and the results are depicted in Figure 21. Based on this data, an average and maximum growth rate of $\mu_{max,mean}$ = 0.64 ± 0.04 1/h (Figure 21a) was calculated based on the exponentially inclining cell number and an average division time of $t_{d,average}$ = 64.81 ± 3.95 min. Furthermore, a length analysis of all single cells was conducted, deriving cell length before and cell length directly after each division event over the entire cultivation period of approximately 7 hours and is shown in Figure 21b.

Utilizing the available spatial and temporal information from time-lapse imaging of 4804 cells, the division time (Figure 21c) and the elongation rate (Figure 21d) were plotted against the cell generations, respectively, to analyze more complex circumstances and dynamics of morphology and division parameters. The cellular division time appears to be fairly stable over several generations while in contrast the single-cell elongation rates [µm/min] increase by approximately 50 % on average during the first 4 generations before reaching a moderately constant value for the following generations.

The relationship between two related daughter cells and their individual division times is plotted in Figure 4 e while individual daughter elongation rates are shown in Figure 21f. No correlation can be found for the two cases; division times and the elongation rates of two related daughters appear to be normally distributed.

Moreover, a correlation analysis was performed to determine if mother cells with long division times (or cell length) have daughter cells with short division times (or cell length) (Figure 21g-h). The results show a strong linear correlation between the mother cell length and daughter cell length (Figure 21g). In contrast, the mother division time does not correlate with the daughter division times but shows a normal distribution (Figure 21h). A detailed division analysis and statistical tests of the corresponding histograms were additionally performed for each of the 37 colonies separately. The results are shown in Table 1.

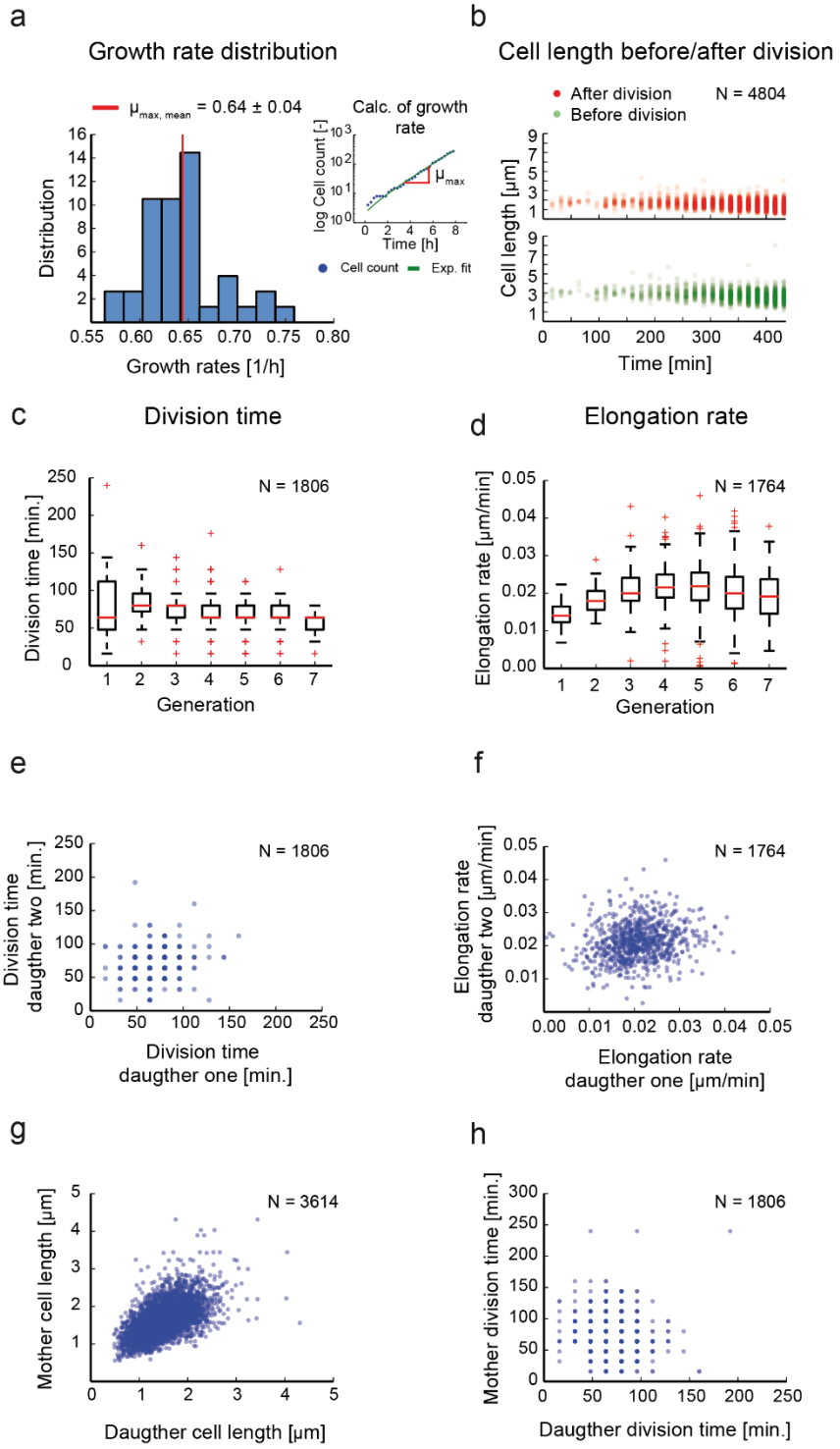

Figure 21: High-throughput single-cell analysis of several microcolonies ($N_{col.}$ = 37) and a total cell number of 4804 cells: (a) Growth rate distribution plot from each analyzed colony with a mean of $\mu_{max,\ mean}$ = 0.64 ± 0.04 [1/h] and an average division time of $t_{d,average}$ = 64.81 ± 3.95 min. (b) Cell length before and after division over the entire cultivation period. (c) Box plot of the division time over the cell generations ($N_{gen.}$ = 7). (d) Box plot of elongation rates over the cell generations ($N_{gen.}$ = 7). (e) Scatter plot of division times of daughter cell one and daughter cell two. (f) Scatter plot of elongation times of daughter cell one and daughter cell two. (g) Scatter plot of the newborn mother cell length vs. cell length of the related next generation daughter cells. (h) Scatter plot of mother cell division time vs. division time of the related next generation daughter cells.

7.4.5 Identifying rare cellular events in C. glutamicum

As evident from Figure 20 and Figure 21, cell length and division behavior (both parameters are directly accessible from phase contrast image data) of *C. glutamicum* varied significantly between individual cells. With our MGC setup, we were able to identify several exceptional outliers and rare events, namely (Figure 22): a) asynchronous division resulting in two daughter cells of uneven length, b) cellular filamentation, c) deformed cells, d) branched cells and e) dormant cells. These rare events typically appeared with very low probability per time unit.

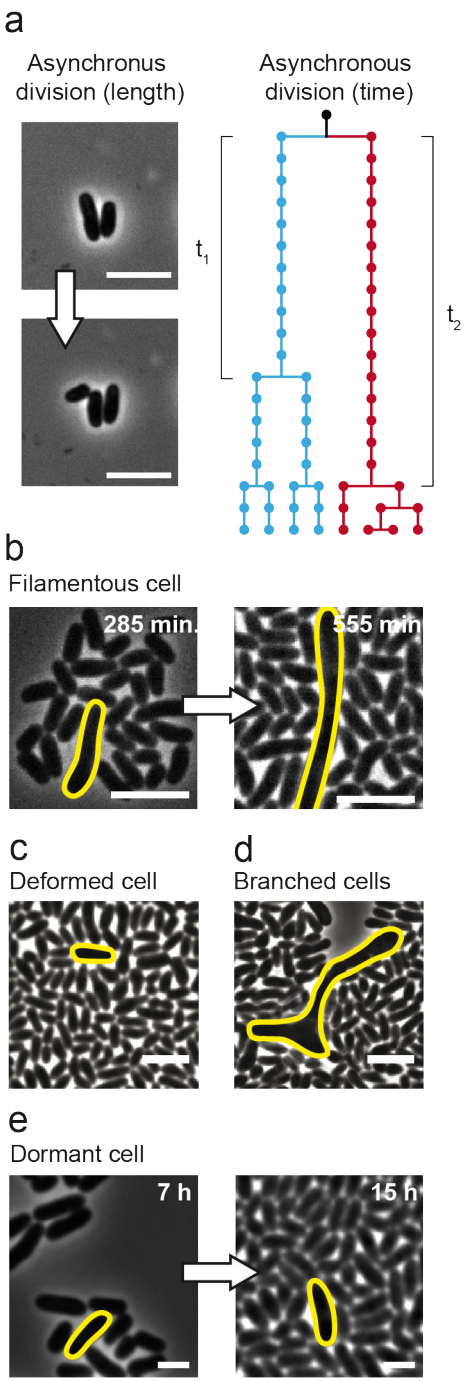

Figure 22: Overview of rare events during *C. glutamicum* cultivation in MGC: (a) Asynchronous division resulting in different cell lengths and division times (scale bar 5 µm), (b) filamentous cell growth (scale bar 5 µm), (c) deformed (scale bar 5 µm), (d) branched cells (scale bar 5 µm), and (e) dormant cells (scale bar 2.5 µm).

7.4.6 Dynamics of spontaneously induced SOS in single C. glutamicum cells

In addition to screening for more obvious phenotypes with unusual division behavior and morphology, our technology was used to screen for individual cells undergoing cellular SOS response, which is not directly detectable by phase contrast microscopy. Thus, a genetically encoded reporter system which is able to perceive a cell's response to DNA damage was used (further denoted as "SOS reporter"). In response to DNA damage, RecA binds ssDNA, catalyzes the autoproteolytic cleavage of the repressor LexA and thus leads to its own activation (20) (further denoted as "SOS+ cells"). The cellular SOS response is then transformed into an optically detectable readout – an intracellular fluorescence signal. Hence, the SOS reporter gives a visual output for the transcription of the gene encoding the single-strand binding protein RecA. For detailed information and characterization of the used strain, the reader is referred to Nanda et al. (20).

During microfluidic cultivation of *C. glutamicum*/pJC1-P_{recA}-*e2-crimson* under identical cultivation conditions as previously reported, phase contrast microscopy images again revealed few rare morphologically deformed and filamentous phenotypes. Figure 23a shows a time-lapse image sequence of an isogenic *C. glutamicum*/pJC1-P_{recA}-*e2-crimson* colony in which an individual cell stopped cellular division but continued elongating for several hours, while all other cells grew normally as expected (Figure 23b). At the same time, only this specific elongated cell exhibited a constantly increasing SOS reporter fluorescence for several hours. The dynamics of the specific SOS event are visualized in the corresponding cell size (measured here using the projected cell area) and single-cell mean fluorescence vs. time chart (Figure 23c).

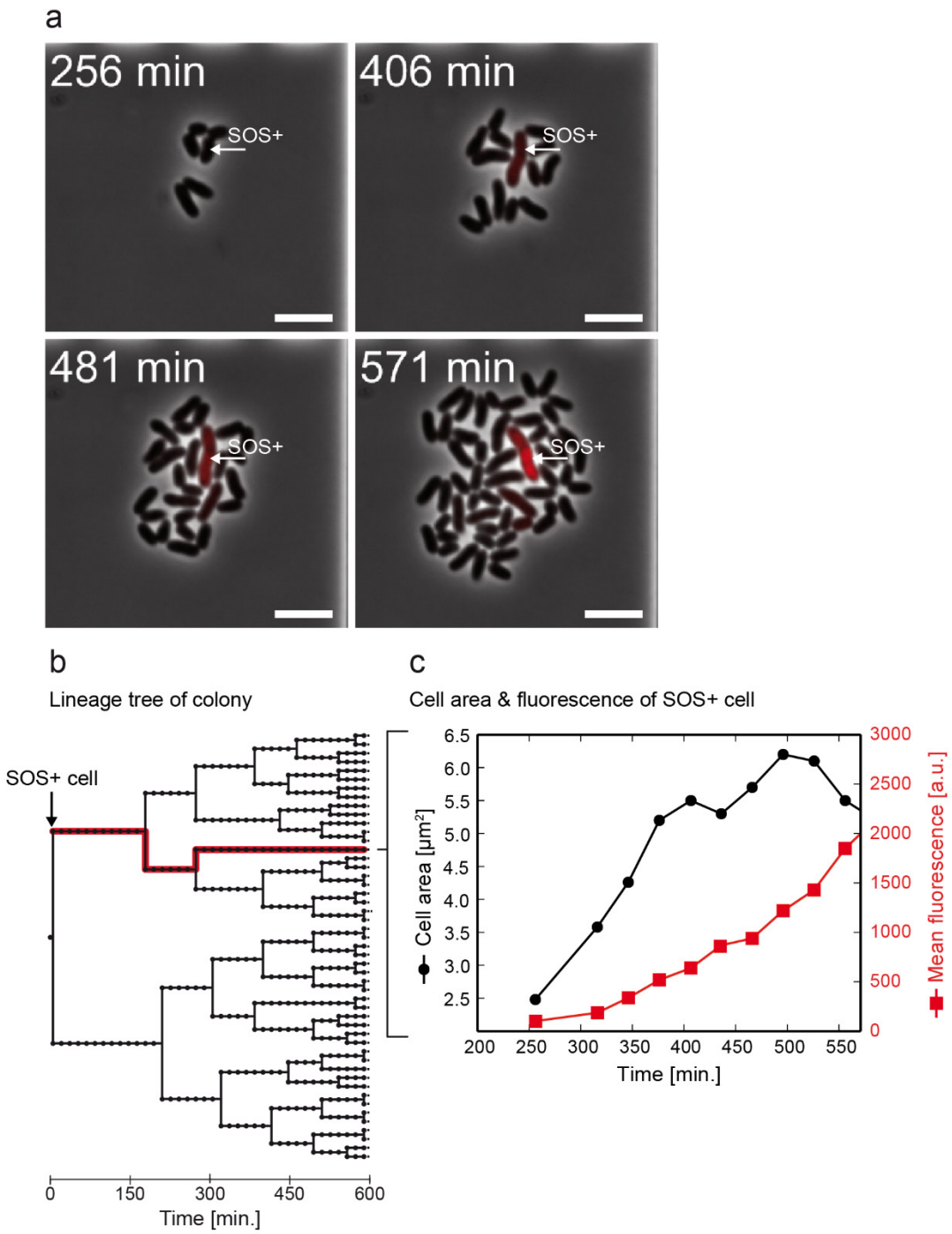

Figure 23: Dynamic SOS response of *C. glutamicum* (scale bars 5 µm): (a) *C. glutamicum* colony containing one single cell exhibiting spontaneously induced SOS response during cultivation; (b) corresponding lineage tree showing the homogeneous growth, except one cell that stops growing; (c) corresponding mean fluorescence and cell area vs. time illustrating cellular dynamics.

7.4.7 High-throughput screening of SOS+ cells

Instead of analyzing all available 3055 time-lapse images separately recorded during 12 hours of *C. glutamicum*/pJC1-P_{recA}-*e2-crimson* cultivation, only the final still images of each microcolony were screened for spontaneously induced SOS+ cells in the following analysis. Three exemplary clonal microcolonies from the identical microfluidic cultivation are shown in Figure 24a. The corresponding scatter plots are given in Figure 24b. In more detail: MGC microcolony I (N_{MGCI_cells} = 858) contained no SOS+ cell (0 %), MGC microcolony II (N_{MGCII_cells} = 870) contained two SOS+ cells (0.26 %) and MGC microcolony III (N_{MGCIII_cells} = 707) contained 25 SOS+ cells (3.53 %) as shown by the parallel lines drawn at 5-fold higher threshold fluorescence than the fitted dashed line in the fluorescence vs. area plots for the entire population. Clearly, the number of SOS+ cells directly depends on the selected gating, as shown in more detail in Publication II - Supplement 2.

Overall, the complete screening on all MGC microcolonies (N_{MGC_COLONY} = 318) revealed that between 0.07 % and 0.49 % of all cells ($N_{total\_cells} \approx 318 \times 750 = 238.500$) were SOS+ (Figure 24c and Publication II - Supplement 2). Our findings are in good agreement with results obtained by offline FC analysis after conventional shaking flask cultivations of *C. glutamicum*/pJC1-P_{recA}-*e2-crimson* (Figure 24d) in which the percentage of SOS+ cells was between 0.05 % and 1.25 % ($N_{total}=10^6$) (20). This value highly depends on the gating and number of cells analyzed, as illustrated in more detail in Publication II - Supplement 3.

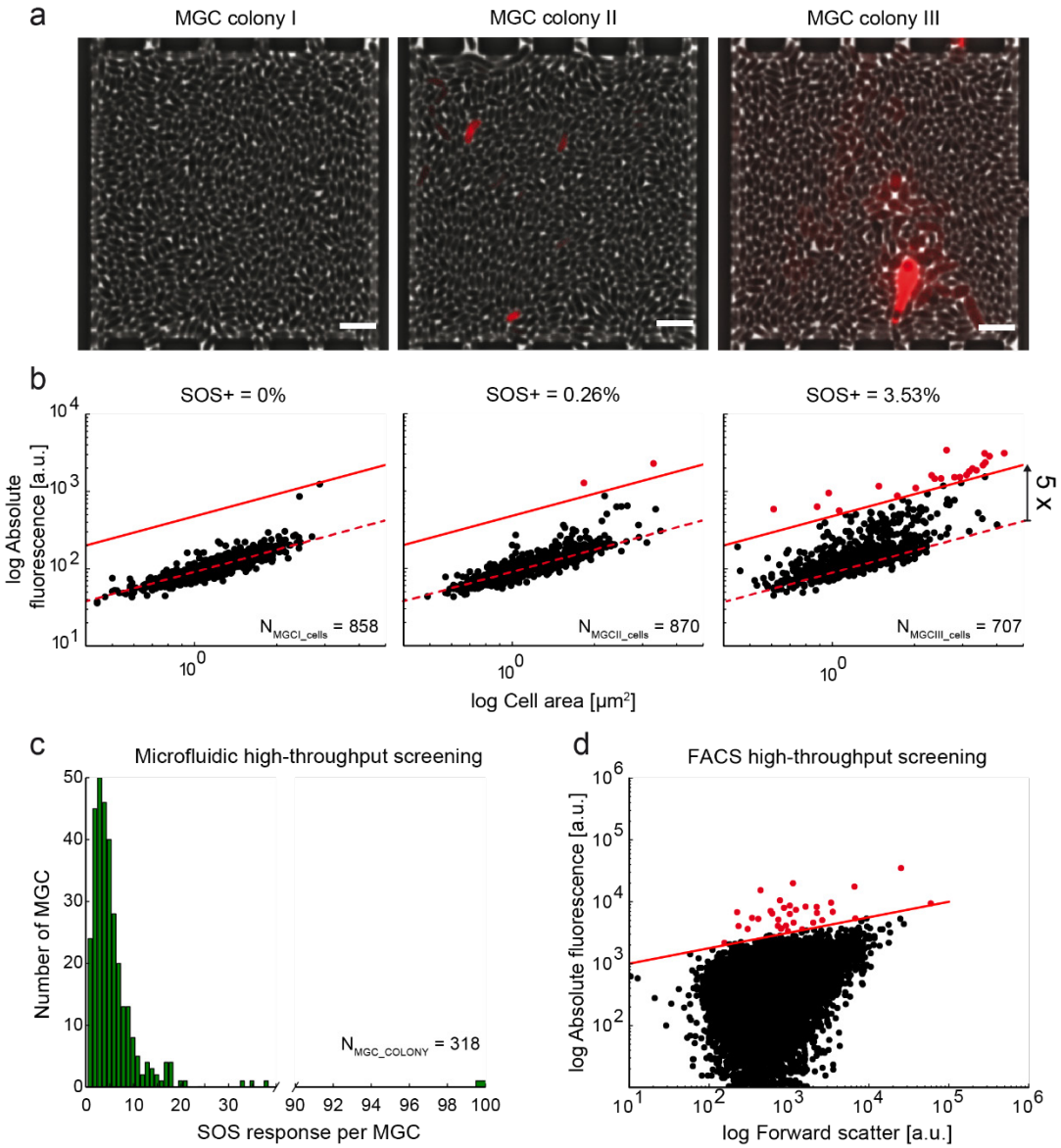

Figure 24: SOS response (SOS+) quantification during microfluidic single-cell cultivation: (a) images of three final clonal colonies (scale bar 25 µm); (b) corresponding total fluorescence vs. cell area scatter plots; dashed line corresponds to the background fluorescence, parallel straight line corresponds to the 5-fold higher fluorescence threshold; (c) distribution of SOS+ cells over 318 separate MGC microcolonies in total; (d) for comparison, scatter plot derived from flow FC and shaking flask cultivations.

7.5 Discussion

Currently, most of the single-cell results are derived from FC and time-lapse microscopy. During live cell microscopy, cells are often cultivated on simple agarose pads (6) to observe growing microcolonies over time and extract specific cellular parameters from subsequent off-line image analysis. In addition to the required automated time-lapse microscopy, agarose pads are simple enough that they can be prepared in practically any microbiology lab. However, agarose pads very quickly reach their experimental limitations, since there is nearly no method of controlling the micro-environment during the course of the experiment.

When single cells have to be cultivated for longer time periods over many generations inside well-controllable environments, there is practically no alternative to microfluidic single-cell cultivation technology. This becomes even more evident when single-cell cultivation inside dynamic environments is desired. Unfortunately, microfluidics technology is not generally available in most laboratories, since advanced fabrication facilities and expert knowledge are required to build tailor-made devices. Successfully applied systems fulfilling the demands of a microbiologist, especially applicability as well as simplicity, are typically developed by highly interdisciplinary project consortia. In the present work, we used a fairly simple microfluidic platform technology for various applications and strains in microbial single-cell analysis.

The presented chip incorporates several hundred MGCs inside a single device. The high degree of parallelization enables the generation of statistically reliable information, a prerequisite for investigation at the single-cell level. One minor bottleneck is automated microscopy, which currently restricts the analysis throughput. We analyze about 100 MGCs during a typical experiment, which we found to be a good compromise between throughput, time resolution and image analysis effort for most fast-growing microorganisms.

Previous versions of our microfluidic MGC device layout were successfully applied in several research projects (7,12,20,21,26-29). The two adjacent supply streams continuously deliver fresh medium and remove any by-products and secreted metabolites, while the MGC interior fluid volume is replenished solely by diffusion, which was confirmed experimentally by fluorescent microspheres and by CFD simulations. This configuration enables cells to be cultivated under optimal conditions (initial rate conditions) inside the MGCs under the absence of any convection or shear stress. Environmental changes can be implemented within seconds simply by infusing a different medium. The availability of (in particular low-abundance) specific medium compound (for example, N, P sources and micronutrients) and

oxygen supply is currently under investigation utilizing more advanced microfluidic setups with integrated fluid control and comprehensive modeling and simulation work.

C. glutamicum was chosen as a model organism due to its high relevance for biotechnological applications (in particular, in industrial biotechnology) and its relation to the pathogenic relative *Mycobacterium tuberculosis* (30). Several other studies on *C. glutamicum* reported cell-to-cell heterogeneity within isogenic populations, revealing differences in cellular viability, membrane potential and growth (31), amino acid productivity (12) and spontaneous prophage induction (20,32); offering a wide range of applications ideal to verify and validate our new system.

The described results and plots on *C. glutamicum* in the present report were mainly derived to demonstrate the broad analysis spectrum at the single-cell level instead of focusing on the biological phenomena themselves. We basically investigated *C. glutamicum* at four different levels of detail, namely:

i. The high spatial and temporal resolution due to monolayer cultivation in combination with image-based microscopy favors the generation of complete lineage trees, shown for two clonal colonies as an example in Figure 20. Such lineage trees give expressive impressions of evolving microcolonies but this format is limited to a few generations only. Related distribution charts then give a direct impression of the obvious population heterogeneity.

ii. We analyzed 37 microcolonies with respect to growth rate distributions enabling a closer view of the growth rate variability of clonal populations (Figure 21a). In total, 4804 cells were analyzed to investigate specific cellular parameters over the entire cultivation period or over cell generations, deriving cellular dynamics on a long time scale (Figure 21b-d). The large variance of single-cell elongation rates (Figure 21d) is currently under further investigation. One reason for this could be the influence of the increasing colony size and thus the physical effects of neighboring cells on each other.

iii. During cultivation of *C. glutamicum,* several special phenotypes were identified, as illustrated in Figure 22. These events were observed in less than 1 % of all cells. Once a specific phenotype of interest was identified, all the microcolonies can be screened systematically. One explanation for the observed dormant cells and cells with elongated morphology could be the spontaneous induction of the SOS response in the absence of any external trigger but triggered by DNA damage (20,33). Therefore, we

focused in particular on elongated cells with impaired growth and division behavior and additionally utilized a genetically encoded fluorescence reporter which transformed an intracellular signal, the SOS activity, into a detectable readout. This allowed the dynamics of intracellular parameters to be traced both on the individual cell and population level (Figure 23).

iv. All final time-lapse images were screened for SOS+ cells (Figure 24a). Due to the low numbers of SOS+ cells, 318 microcolonies were analyzed to derive reliable data. As illustrated in cell size vs. fluorescence scatter plots, our single cell data agree well with FC data. Our results revealed that 0.07–0.5 % of *C. glutamicum* cells expressed spontaneously induced SOS under standard cultivation conditions which is in good agreement with results from conventional FC analysis (SOS+ cells = 0.07–1.25 %) and shake flask cultivation (Figure 24d).These findings confirm that the MGC cultivation conditions used in the present study have no significant impact on cellular physiology. Notably, MGC cultivations allowed the identification of the growth of SOS+ cell clusters originating from a common mother cell (Figure 24a – Colony III). This crucial information remains hidden if solely flow cytometry is performed.

The investigations into dynamic single-cell division are of high interest, for example for the investigation of single-cell lag phase behavior after changes in different environmental conditions. Roostaltu et al. (34) monitored the dilution of green fluorescent protein (GFP) due to cell growth and division by flow cytometry. They found a bimodal distribution of the isogenic population of growing and non-growing cells when the cells were transferred from stationary phase to fresh medium conditions.

In a similar approach, Kotte et al. (35) used a fluorescent membrane-intercalating dye to follow the dilution of the cellular fluorescence due to cell growth over time with FC. They determined the number and growth rate of the growing cell fraction upon a shift to a new carbon source and also found a bimodal distribution of growing and non-growing cells.

These two examples applying FC and fluorescence dilution methods revealed highly interesting bet-hedging strategies as a result of stochastic switching or responsive diversification. Despite this, the more complex dynamics and lineage behavior could not be resolved solely by FC. Using our MGC with time-lapse imaging and a controlled medium switch, this bet-hedging strategy could be directly investigated without any fluorescence stains that may affect cell metabolism. In particular, the growth dynamics and lineage information would be directly accessible, allowing more accurate interpretations of the

bimodal distribution at the single-cell level and functionally at population level. Furthermore, critical cellular phenomena such as cell lysis would also be directly observable. This is not possible with FC.

In contrast, dynamic large-scale processes, such as monitoring the synthesis of a destabilized green fluorescent protein (GFP) (36) under changing environmental reactor conditions could be difficult to investigate with the current MGC setup. Whereas flow cytometry can be connected to real bioprocesses, the MGC cannot mimic complex dynamic bioprocesses yet. This needs further development, for example the possibility of performing batch cultivation, as shown by Dai et al. (37), or the implementation of integrated valves and pumps to create and control dynamic flow profiles (15).

We further want to emphasize that our method is not limited to one specific microorganism and can be applied for various other microorganisms. Currently, the limiting step for widespread use in microbiology and biotechnology is the demand for automatic image analysis tools. Most of the organisms have different specific characteristics in division behavior and cell morphology, which typically require tailor-made image analysis algorithms.

7.6 Conclusions

The presented microfluidic technology allows the systematic single-cell analysis of clonal microbial populations and screening for rare cellular events with high statistical reliability, an important prerequisite for systematic cell-to-cell heterogeneity studies.

Using conventional cultivation technology in combination with FC enables a snapshot analysis of rare events. However, the history, cell lineages and cellular dynamics cannot be investigated. The MGC has proven useful for investigating single-cell growth and dynamic behavior such as spontaneous SOS response and interestingly revealed both spontaneously induced single cells as well as spontaneously induced cell clusters. We propose that such technology will find its place in microbiology as a complimentary technique next to conventional FC. This may offer new insights into the mechanisms of rare bacterial cellular events.

Future applications of these techniques for cultivation and analysis at the single-cell level will expand our understanding of cell-to-cell heterogeneity in various biological processes, ranging from antibiotic screening (38) and adaption processes (39-41) to new insights for applied fields such as food microbiology (42). Particularly for the investigation of cellular processes in the

early exponential and lag phase (43), suitable tools are still lacking. The MGCs offer a novel technique for future investigation of these phenomena.

7.7 Publication II Supplement

7.7.1 Publication II - Supplement 1

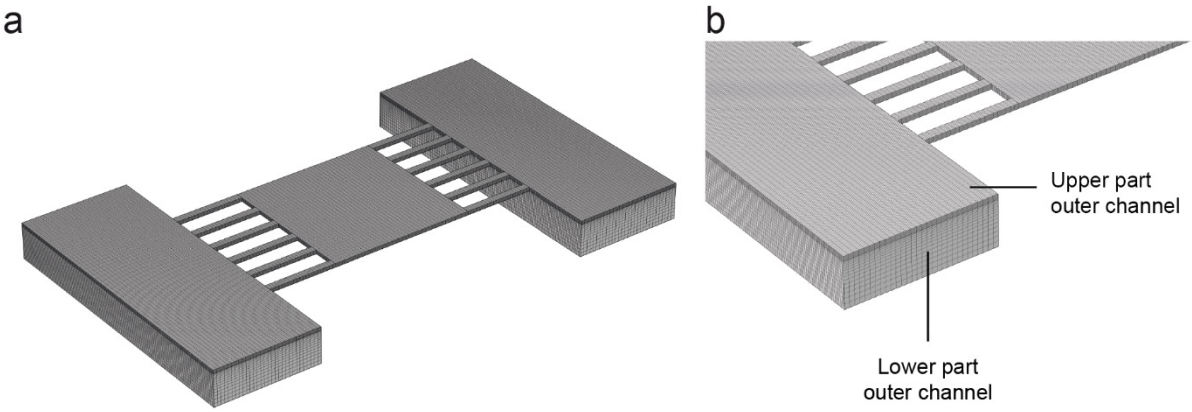

Publication II Supplement Figure 1: (a-b) Generated mesh used for CFD simulations.

Publication II Supplement Table 1: . General overview of the mesh used for CFD simulations.

Mesh	Number of Hexahedral elements	Number of Quadrilateral elements	Number of Edge elements	Number of Vertex elements	Number of Hexahedral elements in height	Number of Hexahedral elements in depth	Number of Hexahedral elements in weight	Minimumelement quality*	Average element quality*	Mesh volume in µm³	Average Hexahedral element volume in µm³
Entire geometry	613120	139184	7736	120	-	-	-	0.1198	0.2482	50060	0.0816

Element quality definition of Comsol: "The absolute value of the mesh element quality is based on the ratios of the inscribed and circumscribed circles' or spheres' radii for the simplex corresponding to each corner of the element. If the simplex cannot be clearly determined (an apex of the pyramid, for example), the corresponding corner is excluded from the consideration. The absolute value is always between 0 and 1, where 0.0 represents a degenerated element and 1.0 represents the best possible element. A negative value means a contradiction to the COMSOL Multiphysics numbering convention for mesh element vertices (see Element Numbering Conventions), and the element is then referred to as an inverted element."

Publication II Supplement Table 2: Detailed overview of the mesh parameters for individual parts of the microfluidic chip geometry, used for CFD simulations.

Mesh	Number of Hexahedral elements	Number of Hexahedral elements in x-direction	Number of Hexahedral elements in y direction	Number of Hexahedral elements in z direction	Element length in x-direction in µm	Element length in y-direction in µm	Element length in z-direction in µm	Minimum element quality*	Average element quality*	Mesh volume in µm³	Hexahedral element volume in µm³
1 of the 12 inner channels	1760	22	10	8	0.86	0.2	0.125	0.1564	0.1564	38	0.021590909
Chamber	64000	40	200	8	1	0.2	0.125	0.1198	0.1198	1600	0.025
Upper part of 1 of the 2 outer channels	96000	30	400	8	1	0.2	0.125	0.1198	0.1198	2400	0.025
Lower part of 1 of the 2 outer channels	168000	30	400	14	1	0.2	0.214-1.07	0.1972	0.3655	21600	0.0428-0.214

*Element quality definition of Comsol: "The absolute value of the mesh element quality is based on the ratios of the inscribed and circumscribed circles' or spheres' radii for the simplex corresponding to each corner of the element. If the simplex cannot be clearly determined (an apex of the pyramid, for example), the corresponding corner is excluded from the consideration. The absolute value is always between 0 and 1, where 0.0 represents a degenerated element and 1.0 represents the best possible element. A negative value means a contradiction to the COMSOL Multiphysics numbering convention for mesh element vertices (see Element Numbering Conventions), and the element is then referred to as an inverted element."

7.7.2 Publication II - Supplement 2

7.7.2.1 Frequency of spontaneously SOS+ induced cells at MGC at various gatings

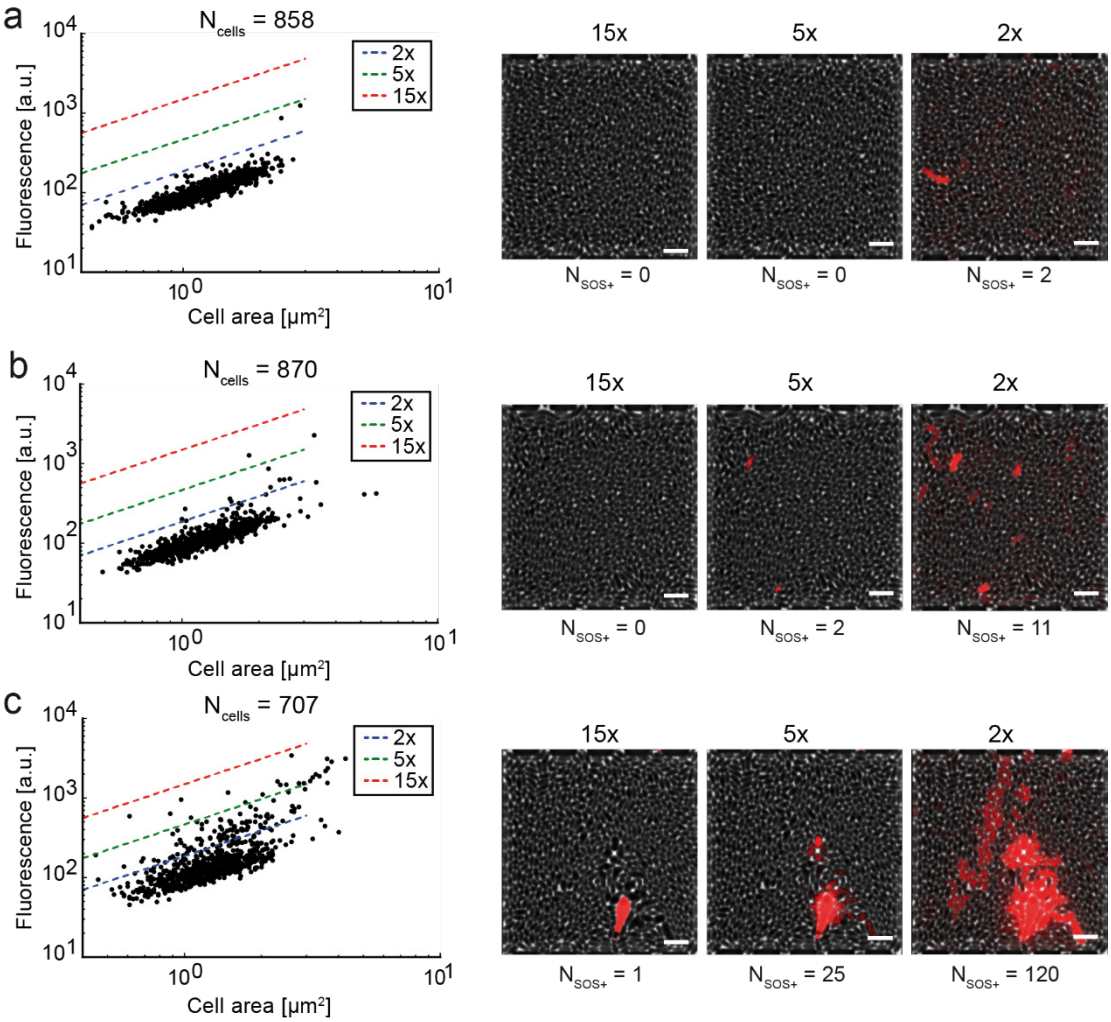

Publication II Supplement Figure 2: Occurrence of spontaneously induced cells (SOS+). Here, cells with a 2-fold (**blue**), 5-fold (**green**) and 15-fold (**red**) increased reporter signal were counted as SOS+ (scale bars 5 µm).

7.7.2.2 Occurrence of spontaneously induced cells

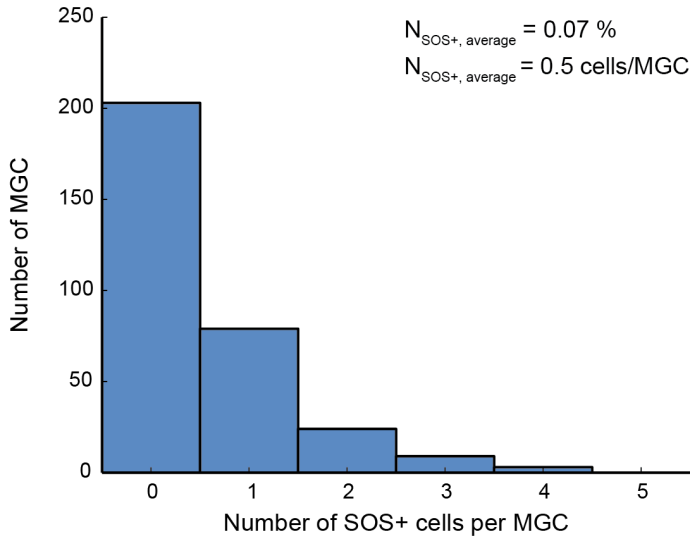

Publication II Supplement Figure 3: Frequency of spontaneous induced cells, if cells with a 15-fold increased reporter signal were considered as SOS-positive (SOS+).

7.7.3 Publication II - Supplement 3

7.7.3.1 Occurrence of spontaneously induced cells vs. total number of analyzed cells

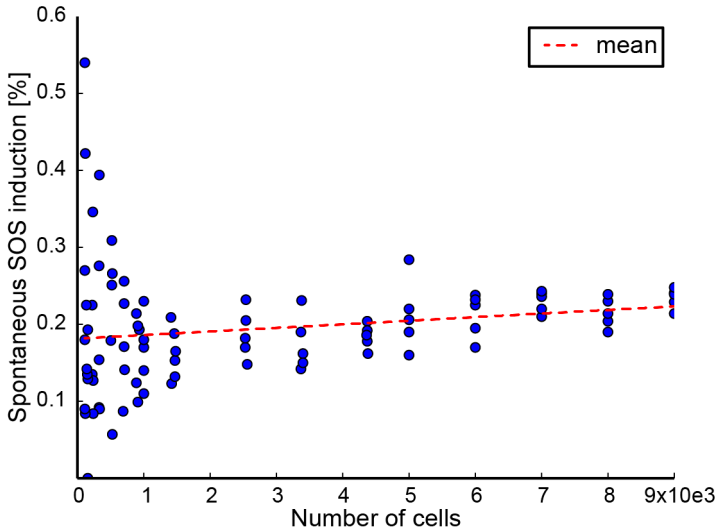

Publication II Supplement Figure 4: Occurrence of spontaneously induced SOS response in cells based on the number of cells analyzed by FC.

7.7.3.2 Determination of SOS positive cells for FC measurements

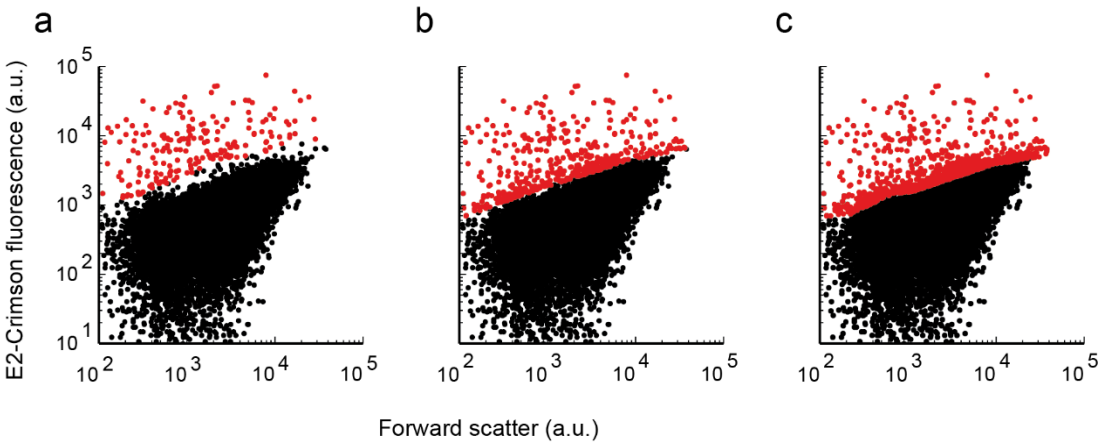

Publication II Supplement Figure 5: FC scatter plots of the strain *C. glutamicum*/pJC1-PrecA-*e2-crimson*. A total of 10e6 cells were analyzed. (a) - (c) Different gating threshold, manually selected.

8 Publication III - Rapid inoculation of single bacteria into parallel picoliter fermentation chambers

Christopher Probst, Alexander Grünberger, Nadja Braun, Stefan Helfrich, Katharina Nöh, Wolfgang Wiechert, Dietrich Kohlheyer
Analytical Methods, (2014).
DOI:10.1039/c4ay02257b

8.1 Abstract

Microfluidic single-cell cultivation devices have been successfully utilized in a variety of biological research fields. One major obstacle to the successful implementation of high throughput single-cell cultivation technology is the requirement for a simple, fast and reliable cell inoculation procedure. In the present report, an air-bubble-based cell loading methodology is described and validated for inoculating single bacteria into multiple picoliter sized growth chambers arranged in a highly parallel manner. It is shown that the application of the injected air bubble can serve as a reproducible mechanism to modify laminar flow conditions. In this way, convective flow was temporarily induced in more than 1000 cultivation chambers simultaneously, which under normal conditions operate exclusively under diffusive mass transport. Within an inoculation time of 100 s, *Corynebacterium glutamicum* cells were inoculated by convection at minimal stress level and single bacteria remain successfully trapped by cell-wall interactions. The procedure is easy, fast, gentle and requires only minimal fluidic control and equipment. The technique is well suited for microbial cell loading into commonly used microfluidic growth sites arranged in parallel intended for high throughput single-cell analysis.

8.2 Introduction

Single-cell analysis based on microfluidic cultivation systems has been successfully developed to investigate a variety of living organisms in vivo [49, 202–206]. In contrast to all other procedures, this technology facilitates exceptional environmental control as well as full spatial and temporal resolution at the single-cell level and is thus well suited to investigate cellular dynamics for microbiology and biotechnology [207, 208]. The functional microfluidic cultivation geometries utilized so far can be classified into simple cultivation wells [172], shallow growth sites restricting cellular growth to a monolayer [141, 209], growth tracks harboring single cells arranged in a straight queue [98, 100] and single-cell traps holding exclusively one cell [90]. Typically these micrometer and sub micrometer sized cultivation sites are arranged in a highly parallel manner thereby incorporating up to several thousand regions of interest in a single device. During operation, preferably a single cell is inoculated into each cultivation site facilitating spatiotemporal investigations on isogenic microcolonies, for example by automated time-lapse microscopy. One major obstacle to the successful implementation of high throughput microfluidic single-cell cultivation technology is the prerequisite for simple and fast but reliable cell inoculation from the pre-culture suspension. Inoculation procedures differ and depend to a large extent on the microfluidic cultivation geometry applied. However, the vast majority of cell seeding routines are based on random cell trapping while the cell suspension is infused into the microfluidic device. As illustrated in Figure 25 a, this is straightforward if simple trapping obstacles and barriers are directly infused with the cell suspension during loading [92, 93, 107, 192]. These barrier structures facilitate excellent medium exchange and constant cultivation conditions by continuous convective flow. However, cells may be washed out and become lost as soon as the drag force exceeds the force of the barrier structure's trapping mechanisms and convection may be undesirable for many applications. As depicted in Figure 25 b, cultivation chambers and channels have therefore been placed perpendicular to the flow and interconnected between parallel media supply channels avoiding convection and shear stress [100, 141, 186]. This latter configuration facilitates exclusively diffusion-based mass transport if the two media-supplying volume flows are equal.

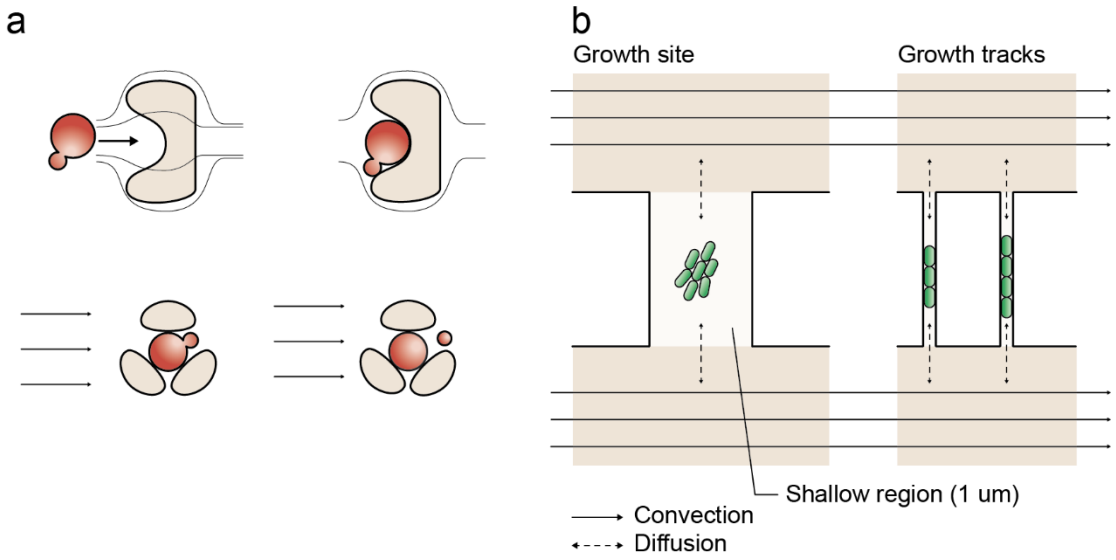

Figure 25: Examples of microfluidic single-cell cultivation geometries: (a) microfluidic barrier structures for single-cell cultivation with continuous laminar flow; (b) cultivation chambers and growth tracks facilitating exclusively diffusion-based mass transport if the two parallel media volume flows are equal.

The cultivation sites can have different geometries [100, 104, 141, 210], which have been applied for bacteria [141, 210], yeast [209] and eukaryotic cells. At short micrometer length scales, diffusive mass transport is typically very efficient thus guaranteeing stable cultivation conditions. However, cell inoculation remains a bottleneck since cells are not directly flushed into the cultivation sites (Figure 25 b). To overcome this limitation, several workarounds have been reported to load single cells into the chambers, for example, “manually applied pressure pulses to the channels to induce a momentary flow change” [106], whole-device centrifugation for inoculation by centrifugal forces [98], incorporation of additional seeding channels elaborately operated by flexible valves [211], controlled but low throughput cell seeding by optical tweezers [62] and interconnected under-pressure channels to actively draw cells into the cultivation sites [212, 213]. Clearly, there is an urgent requirement for improvement, particularly in view of the challenge of implementing a reliable, user-friendly, fast and perhaps commercially applicable procedure. In the present report, a simple, fast, gentle and reproducible method is described for microbial cell inoculation into micro-fluidic cultivation sites, in which during cultivation exclusively diffusive mass transport is present whereas convective flow occurs only inside the adjacent supply channels. Our inoculation procedure utilizes an entrapped nanoliter sized air bubble to temporarily modify the flow conditions. The bubble induces a momentary convective flow also through the cultivation

chambers, thus enabling cell transport into the chambers. In contrast to previously described procedures, the present chip device remains inside the temperature incubator the whole time and the connected tubing is not removed during operation, which is ideal for a fast and gentle cell transferal from the pre-culture to the main microfluidic chip culture. The principle is limited to gas permeable device material since the bubble removal is based on gas diffusion through the interfacing wall material. The proposed gas-bubble inoculation requires neither a complex fabrication procedure nor elaborate control equipment. Furthermore, by applying multiple bubbles it is highly parallelizable because the gas–liquid interface adapts to any channel geometry. The procedure was successfully validated with the organism *Corynebacterium glutamicum*, which subsequently exhibited normal growth behavior.

8.3 Materials and Methods

8.3.1 Chip fabrication

Single-use microfluidic cultivation devices were fabricated by standard polydimethylsiloxane (PDMS) (Sylgard 184 Silicone Elastomer, Dow Corning Corporation, Midland, USA) molding, casting a 100 mm silicon wafer carrying appropriately designed SU-8 (MicroChem Corp, USA) structures processed by cleanroom photolithography. To this end, SU-8 layers 1 µm and 10 µm in height were spin-coated and processed separately, resulting in a layered dual resist configuration. The molded PDMS chips had supply channels of 10 µm height and cultivation sites 1 µm in height. Prior to the experiments, each chip was thoroughly cleaned and permanently bonded onto 170 µm thick glass plates (SCHOTT Malaysia) after oxygen plasma treatment and manually connected to tubing (Saint Gobain; VWR International GmbH, Germany). A detailed fabrication procedure has been published previously [201].

8.3.2 Device configuration

The present PDMS-glass microfluidic device incorporates four individual perfusion channels with a single inlet and outlet respectively (Figure 26 a and b). Each inlet channel (100 µm width) branches into two separate cultivation arrays having a partly beveled air bubble entrapment zone (430 µm width) in front (Figure 26 c). By this configuration one single chip combines 1184 growth chambers in total. Growth chambers are arranged in between and perpendicular to the flow. Therefore, two opposing chamber openings are connected to the supply channels (30 µm width, 10 µm height) for continuous media supply. In the present design two different growth chamber sizes were implemented (W x L x H), namely: 40 µm x 60 µm x 1 µm and 50 µm x 60 µm x 1 µm, as depicted in Figure 26 d. An exemplary SEM image is shown in Figure 26 e.

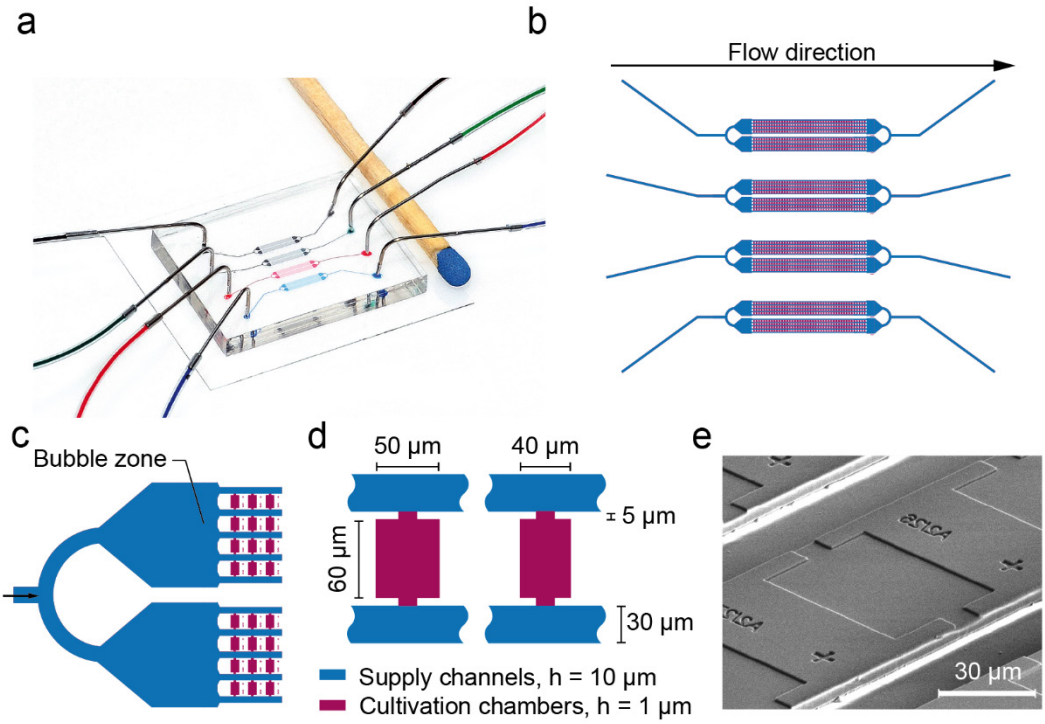

Figure 26: Microfluidic single cell cultivation device developed for air bubble based cell inoculation. (a) Microfluidic PDMS chip (h = 3 mm) bonded to a glass plate (h = 170 µm) and channels filled with differently colored dye; (b) each chip incorporates 4 separate channels for multiple analysis in parallel; (c) each channel branches into two cultivation arrays having an air bubble zone arranged in front; (d) two different cultivation chambers are arranged perpendicular to the flow interconnected between parallel supply channels; (e) SEM image of a single cultivation chamber.

8.3.3 Experimental setup

Experiments were carried out using an inverted time-lapse microscope (Nikon TI-Eclipse, Nikon, Japan), equipped with an temperature incubator (PeCon GmbH, Germany). Images were recorded with a 10x objective during air bubble removal and a 100x objective during cultivation. Prior to cell inoculation desired air bubbles were injected using a pressure-driven pumping system (MCFS, Fluigent, France) as well as 2 external electromagnetic 3/2 valves (Cetoni GmbH, Germany), as illustrated in Figure 27 a. Afterwards and during cultivation, a syringe pump (NeMESYS, Cetoni GmbH, Germany) was used instead to continuously supply the cells with fresh medium at a flow rate of 200 nl min^{-1}.

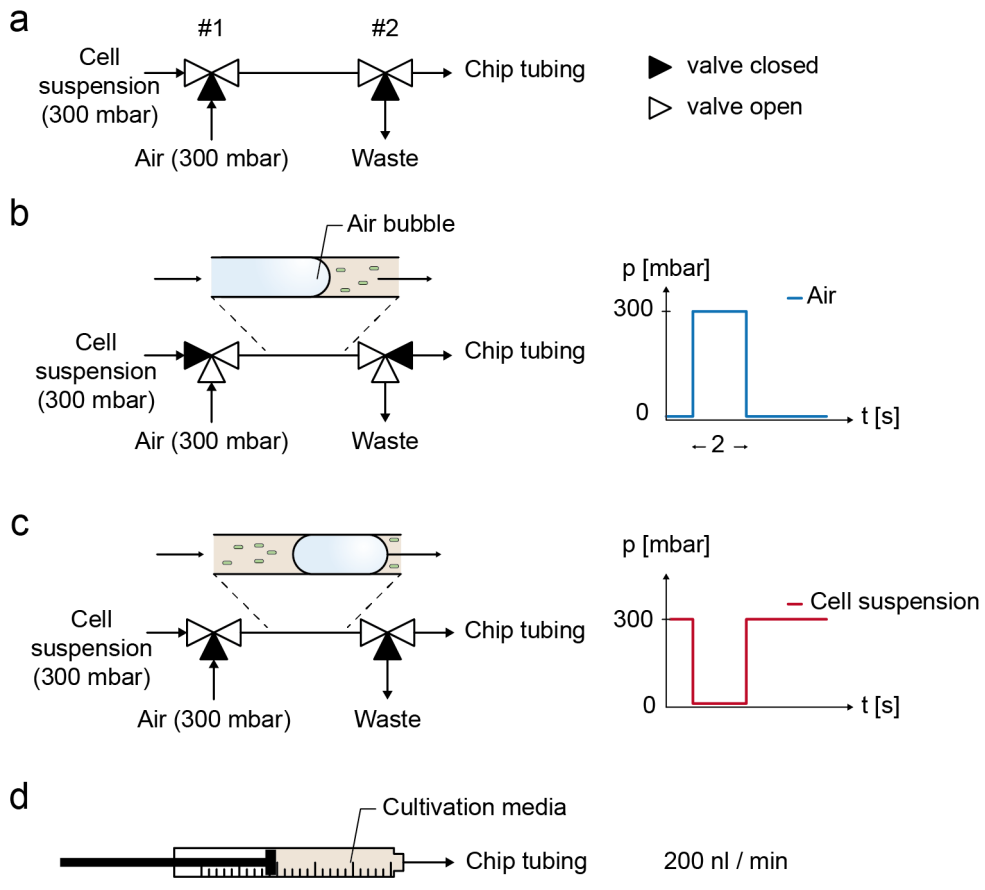

Figure 27: Air bubble injection into the microfluidic cultivation device using externally set-up electromagnetic valves. (a) Cell suspension flow, (b) air bubble injection, (c) cell suspension flow, (d) continuous cultivation media supply at 200 nl min^{-1}.

8.3.4 Bubble injection and cell inoculation procedure

Two electromagnetic 3/2 way valves connected in series were used to quickly and reproducible switch between cell suspension, pressurized air and a waste outlet. This external configuration was connected to the microfluidic chip inlets. Desired air bubbles for cell inoculation were induced by an automated valve actuation sequence to realize following procedure (Figure 27 a):

1. Cell suspension supply from a 300 mbar pressurized container (Figure 27 a).
2. Within a 2 second pulse, air is injected at 300 mbar into the tubing (Figure 27 b).
3. Cell suspension supply at 300 mbar is restored and the resulting entrapped air bubble is pushed through the tubing into the microfluidic channels (Figure 27 c).
4. After the successful inoculation procedure, cultivation medium is supplied continuously (Figure 27 d).

Once in its operational position located in front of the fivefold channel junctions, air bubbles disappeared by continuous gas diffusion through the interfacing PDMS walls under constant pressure conditions (Figure 28 and Figure 30). Several pressure levels (200, 300, 400 and 500 mbar) were experimentally characterized. Phase contrast images of shrinking air bubbles were captured every second to derive geometrical parameter information by image analysis. After cell inoculation, 1184 growth chambers were optically inspected and trapped cells were counted to derive the trapping efficiency.

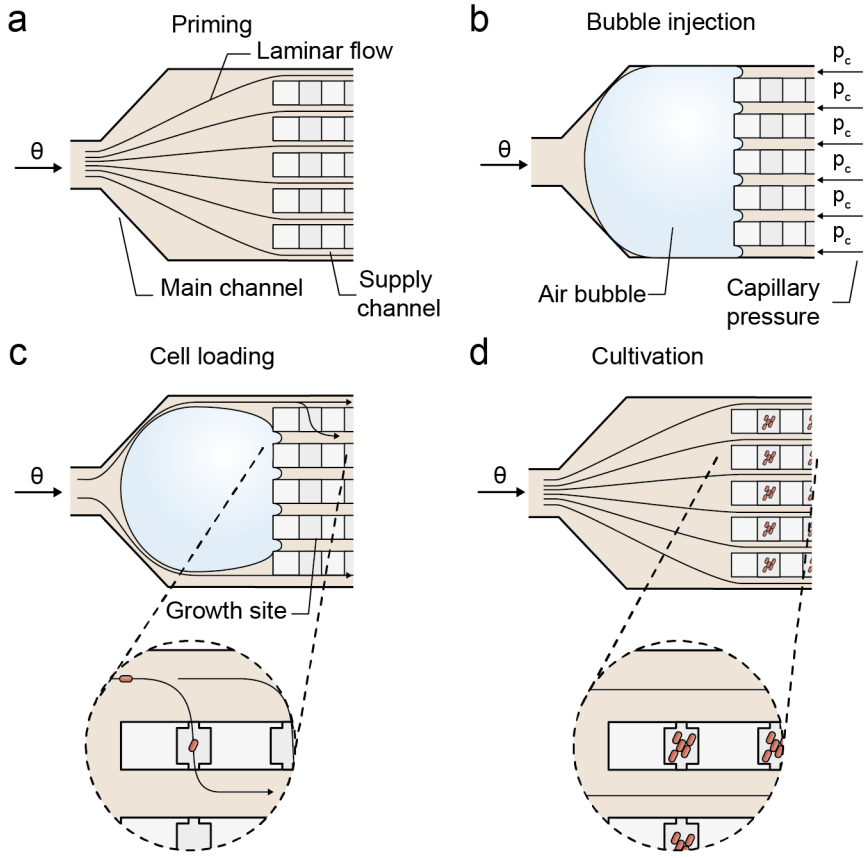

Figure 28: Air bubble based inoculation procedure for microbial single-cells: (a) priming: flow inside all supply channels is homogeneous and solely diffusion based mass transport occurs inside the growth sites. (b) Injection: air bubble is injected and blocks the multifold channel junction. The sum of capillary pressures pc counteracts the applied externally pressure keeping the air bubble at its operating position. (c) Cell inoculation: the air bubble temporary distorts the flow profile resulting in an inhomogeneous flow through the parallel supply channels and convection through the growth sites. Single cells get inoculated. (d) Cultivation: growth media is supplied continuously and mass transport inside the growth sites is based on diffusion only.

8.3.5 Fluorescent flow tracer analysis

Flow characterization was performed by infusing fluorescently labeled latex beads of 1 mm diameter (blue fluorescent 350/440) and 200 nm diameter (yellow-green fluorescent 505/515), respectively. FluoSpheres® carboxylate-modified microspheres (2 % solids) were purchased from Molecular Probes (Invitrogen, USA). 1 µm beads were applied to visualize the laminar flow profile during air-bubble-assisted cell loading thereby mimicking cell trapping. 200 nm beads were applied to track the diffusive particle behavior during subsequent normal cultivation conditions. Prior to flow visualization, the channels were primed with 0.1 % BSA solution for 60 minutes to minimize unspecific bead adhesion. All bead suspensions were diluted (5 ml in 1000 ml of 0.1 % BSA). An exposure time of 500 ms was used to record the trajectories of the 1 µm beads, whereas an exposure time of 10 s was used to track the 200 nm beads. Fluorescently labeled beads were excited using a fluorescent light source (Intensilight, Nikon, Japan) at the maximum intensity and using appropriate optical filters.

8.3.6 Cultivation of *C. glutamicum*

C. glutamicum wild type was pre-cultured in 20 ml of fresh CGXII medium [201] in 100 ml shake flasks and shaken at 30 °C at 150 rpm overnight. Prior to inoculation into the chip, 500 µl from the overnight culture was transferred to 20 ml of fresh CGXII and incubated until an optical density of 1 was reached. After successful inoculation, fresh CGXII medium was infused. Images of growth sites were recorded every 10 minutes to derive the growth rate. Growth of single-cell microcolonies was analyzed by using a customized semi-automated image analysis toolkit. Advanced image analysis methods were adapted for time-lapse image stacks and implemented as a plugin for the ImageJ platform [214].

8.4 Results and discussion

8.4.1 Single-cell inoculation procedure

The present device operates with a simple microfluidic geometry, thereby minimizing technological efforts and improving applicability. The configuration facilitates exclusively diffusion based mass transport inside the cultivation chambers if the two parallel media supplying volume flows are equal and no pressure gradient is present through the cultivation site. This is achieved by configuring the single inlet channel so that it branches into multiple parallel supply channels of identical hydrodynamic resistance (Figure 26 c). Successfully inoculated cells grow under minimal shear stress and with efficient media exchange by diffusion based mass transport. By utilizing a nanoliter sized air bubble entrapped in front the supply channels, a simple and reproducible inoculation procedure was realized as illustrated in Figure 28. The procedure follows following sequence:

1. Device priming (homogenous flow conditions inside the channels and solely diffusion based mass transport inside the cultivation chambers);
2. air bubble injection; air bubble blocks the five-fold channel junction.
3. cell suspension infusion and cell inoculation (inhomogeneous flow conditions inside the supply channels supporting convection across the chambers until bubble fully disappears); continuous medium supply and cell cultivation (homogenous flow conditions along the channels and solelydiffusion across the chambers).

To initiate single cell inoculation, air was injected during a 2 s pulse from a pressurized air supply into the external tubing by actuating two electromagnetic valves in automated sequence (Figure 27). The resulting air bubble was then pushed with the cell suspension flow downstream the tubing into the connected microfluidic chip where it blocked the multifold junction to the parallel supply channels due to the counteracting capillary force as illustrated in Figure 28 b (Publication III - Capillary force calculation). Once in its operating position at the channel junction, the bubble volume continuously decreases due to the high gas permeability of the interfacing PDMS wall material. However, the bubble must not be pushed through the entire device at higher pressure levels, since cells may be detached from the cultivation chambers by the propagating air–liquid interface. The transient blockage of several media supply channels creates an flow imbalance in the parallel supply channels, thereby inducing convection through the cultivation chambers supporting the inoculation of single microbes.

Infused cells simply remain trapped inside the shallow cultivation chambers by cell-wall interactions. During this stochastic filling process cells are distributed inside the chambers. Preferably, single cells become trapped inside sufficient number of chambers. Typically these stochastic filling processes follow a well-known Poisson distribution. However, in the present configuration the inoculation rate is not constant over time and the individual chambers, thus Poisson is not applicable. The trapping efficiency depends on various parameters, for example, the inoculation period, cell suspension density, flow velocities, cell size, and was optimized experimentally. As soon as the air bubble completely disappears, the inoculation procedure is finished and the cultivation medium is continuously pumped through the channels instead.

8.4.2 Flow tracer characterization

Fluorescently labeled beads and long exposure times during fluorescence microscopy were used to visualize the particle trajectories during normal cultivation conditions and inoculation conditions as shown in Figure 29 a and c. Under normal cultivation conditions the volume flows were equal in all supply channels as visualized by identical tracer patterns (Figure 29 a and b). Fluorescent beads entering the growth chambers exclusively revealed diffusive and random motion (Figure 29 c). As soon as the air bubble was injected (Figure 29 d and e), tracer analysis revealed unbalanced flow rates and resulting fluid convection through the cultivation chambers. The fluorescent beads then followed straight laminar flow lines through the chamber (Figure 29 f). Several beads attached to the channel walls resulting in noticeably bright sports in the image (Figure 29 d and e) not further influencing the analysis. The flow situation was completely reversed once the air bubble disappeared by diffusion in less than two minutes.

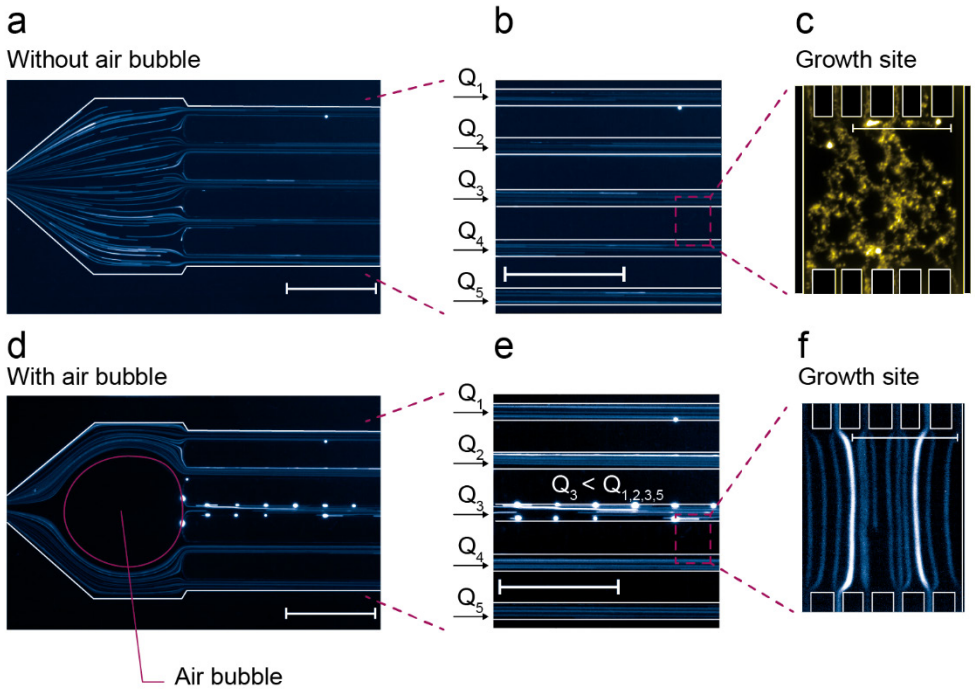

Figure 29: Fluorescent flow tracer analysis: (a–c) normal cultivation conditions with equal flow rates inside all supply channels; (c) diffusive mass transport conditions inside the cultivation chambers; (d) air bubble is deployed at the fivefold channel junction resulting in (e) a temporary inhomogeneous laminar flow profile and different volume flows ϕ_1, ϕ_2, ϕ_3, ϕ_4 and ϕ_5 and thus (f) laminar flow through the cultivation chambers (scale bar 25 µm).

8.4.3 Air bubble injection

During bubble injection the applied flow pressure should not exceed the sum of the counteracting capillary pressures to avoid loss of the functional bubble. The maximum pressure during the procedure results from the sum of the counteracting capillary pressures at the liquid air interface (Figure 28 b). For a rectangular channel with constant cross-section and width (w) height (h), the capillary pressure can be estimated from eqn (1) (more details see Publication III - Capillary force calculation). The capillary pressure (p_c) of one single supply channel with a height of h = 10 mm, a surface tension g = 0.07 N m^{-1} and a contact angle q = 111 ° results in approximately p_c = 120 mbar. Thus in the present geometry, the resulting fivefold counteracting pressure is about 600 mbar. This was in good agreement with our experimental findings, as the bubble was ineffectively pushed through the junction at an inlet pressure around 600 mbar. By adjusting the device layout, this restriction can be easily increased to specific requirements, but flow rates during inoculation were satisfactory in our experiments. At a later phase during cell inoculation and a smaller bubble size, it still remains

trapped at its position mainly due the surface tension and the flow diverging around the bubble.

8.4.4 Air bubble diffusion

The available time window for inoculation is greatly dependent on the gas permeation rate through the surrounding wall material. The procedure is limited to PDMS or other materials or device configurations supporting gas diffusion. Figure 30 a shows a time-lapse image series of an injected air bubble, which then continuously shrank due to diffusion at the applied pressure p = 300 mbar. It can be seen from Figure 30 b that a minimal pressure of 300 mbar was needed to remove the air bubble effectively. Each inoculation sequence was repeated 3 times and the measured cross-sectional bubble area plotted over time. A simple first-order decay expression was used to at the bubble removal rate [215] (details in Publication III - Fitting of experimental data).

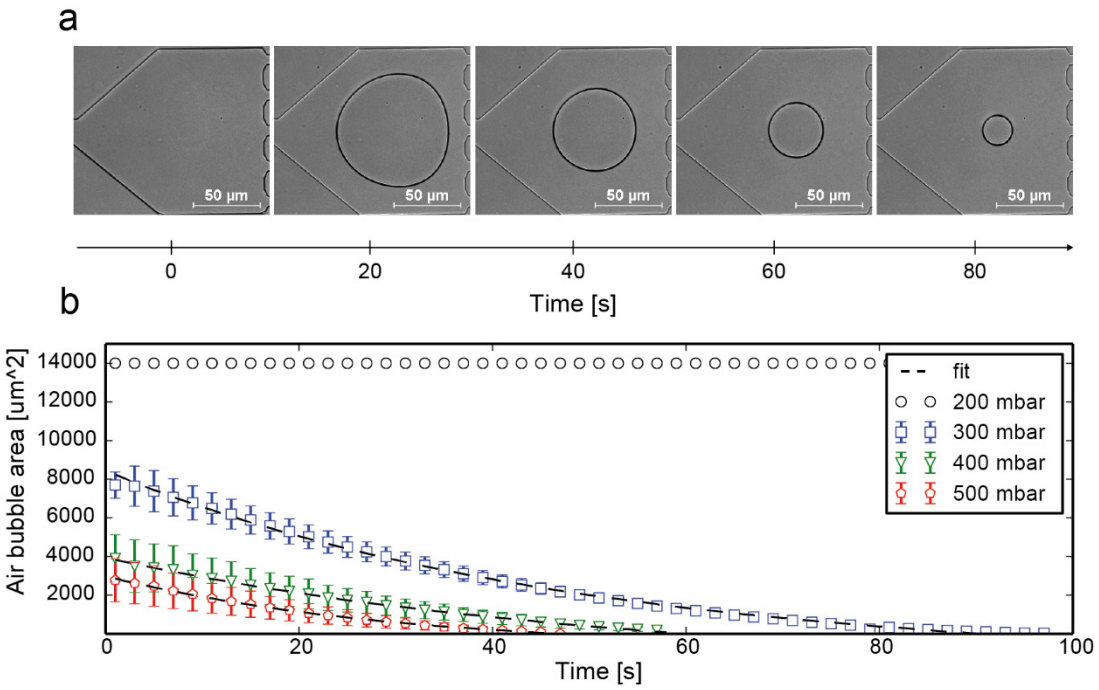

Figure 30: Experimental air bubble removal validation: (a) time-lapse images after the successful injection of the air bubble and continuous decay at 300 mbar; (b) air bubble surface area decay vs. time for various pressure settings and respective fit.

8.4.5 Cell loading performance

The presented method was validated using the microorganism *C. glutamicum*. In order to guarantee isogenic starting conditions of each microcolony, only one cell per growth side needs to be trapped during inoculation. During cell division of *C. glutamicum* two related cells often remain attached to each other [216]. These cell pairs were also considered as one cell since they obviously arise from the same lineage. The inoculation was performed at 300 mbar inoculation pressure and a cell suspension with an optical cell density of OD 0.1 and OD 1. Each cultivation chamber was inspected by microscopy afterwards and the entrapped cell number was counted. Figure 31 a and c shows the distribution of trapped cells per growth chamber (50 µm x 60 µm) for both cell suspension densities. In addition, the position distributions of all trapped cells inside the growth chamber is depicted in Figure 31 b and d.

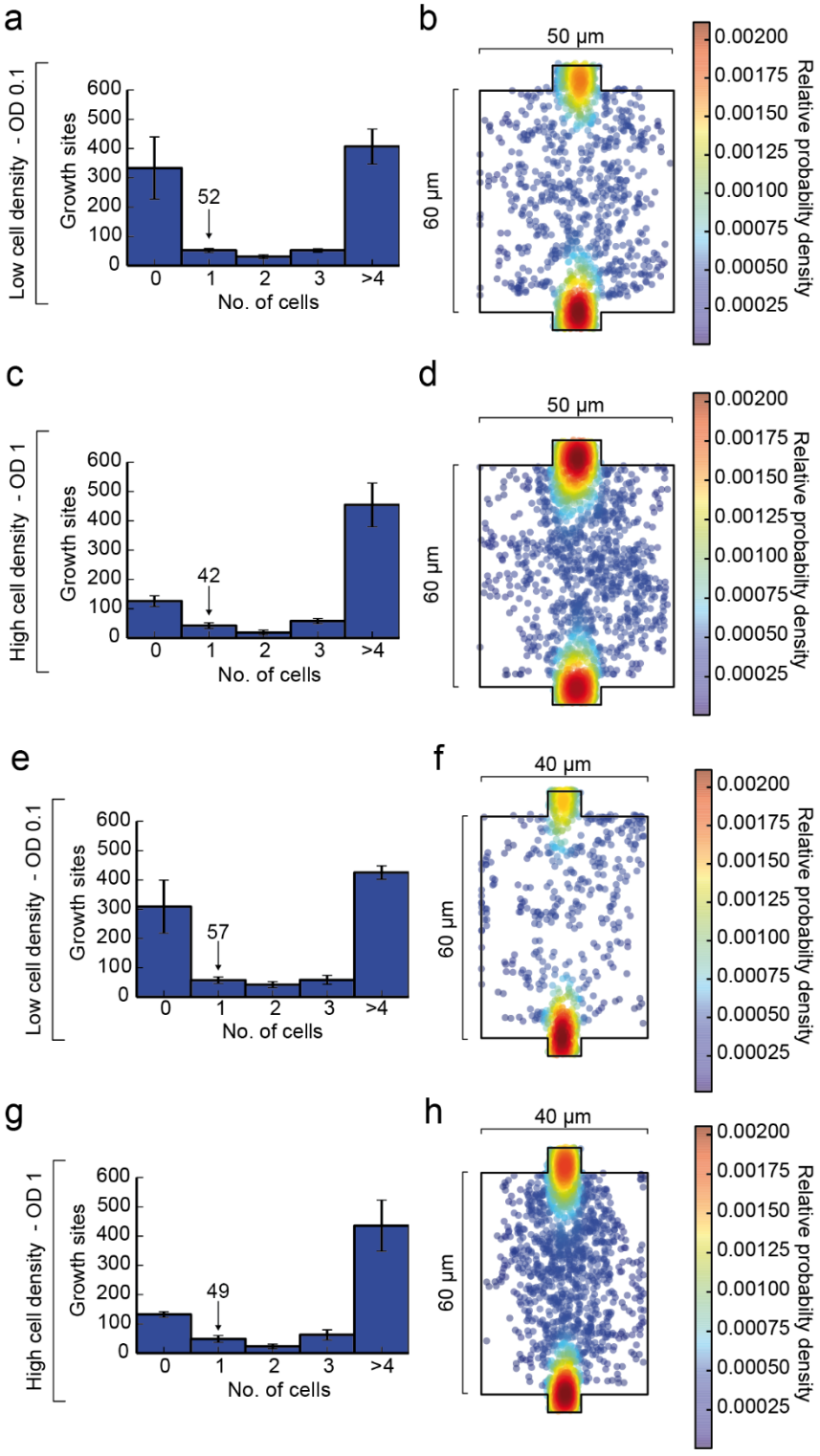

Figure 31: Cell trapping analysis (N = 3) of *C. glutamicum* at 300 mbar and different cell suspension densities for growth sites of 50 µm x 60 µm (N =592) and 40 µm x 60 µm (N = 592). (a and b, e and f) OD 0.1: inoculation efficiency distribution and single-cell location plot; (c and d, g and h) OD 1: inoculation efficiency distribution and single-cell location plot.

It is noted that a central cell positioning is most desirable to allow homogenous and radial colony growth with maximum diameter. Inoculation was performed most efficiently at a low cell density (OD 0.1). On average, 52 chambers out of 592 were successfully inoculated with one individual cell (technical replicate: N = 3). In the same device 57 out of 592 chambers (40 µm x 60 µm) were satisfactory inoculated with a single cell as shown in Figure 31 e–h. The small size difference did not significantly impact cell loading efficiency. At first sight, these numbers seem low, but typically time lapse microscopy can hardly handle more regions of interest if appropriate time resolution in the order of a few minutes is anticipated. Inoculation at 300 mbar within 100 s resulted in a trapping efficiency of around 10 %. Even higher cell density led to an increased number of chambers with more than one cell and more cells being trapped at the inlet of the growth sites rather than in the center of the chamber.

8.4.6 Viability and cell growth

Finally, the growth of *C. glutamicum* after our inoculation procedure was validated. Each colony exhibited excellent viability and showed no impact on cellular growth or morphology. Figure 32 a shows microcolony growth for 9 hours in one of the observed growth sites. As an example, 23 microcolonies were analyzed in more detail and single-cell growth rates μ_{max} were derived as shown in Figure 32 b and c. We found the maximum average growth rate μ_{max_mean} to be 0.6 ± 0.03 h^{-1}, which corresponded very well to previously published results obtained with *C. glutamicum* in microfluidic devices [184]. The shifts in time of the different growth curves can be explained by different cell cycle states of the individual mother cells.

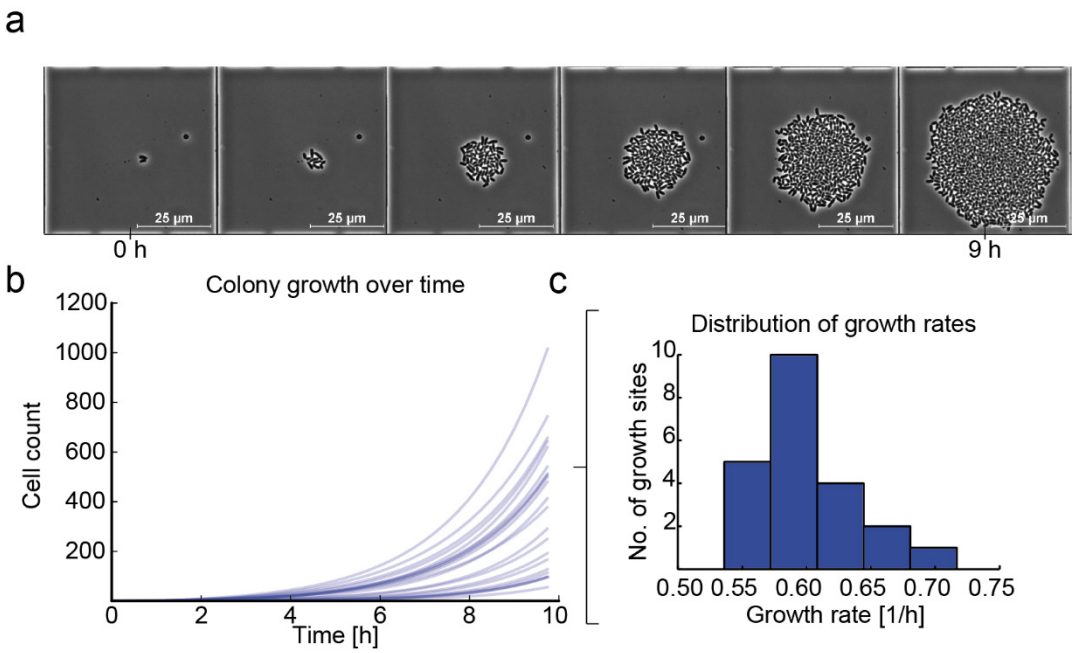

Figure 32: Viability analysis of *C. glutamicum* after the inoculation procedure: (a) time-lapse image series of *C. glutamicum* colony growing in one growth site over 9 hours. (b and c) microcolony growth curves of multiple microcolonies (N = 23) revealing an average maximum growth rate μ_{max_mean}= 0.6 ± 0.04 h^{-1}.

8.5 Conclusion

A fast, gentle and simple microbial cell inoculation procedure for microfluidic single-cell analysis is described. Air bubbles are often considered as a negative side effect in microfluidics [217]. However, we have shown that the application of an injected air bubble can serve as a reproducible mechanism to modify laminar flow conditions. In this way, convective flow is temporarily induced in more than 1000 cultivation chambers in parallel, which under normal conditions operate exclusively under diffusive mass transport. Within an inoculation time of 100 s, *C. glutamicum* cells were inoculated by convection and single bacteria remain successfully trapped by cell-wall interactions. During cell trapping, the air bubble continuously reduced in size due to gas permeation through the surrounding. Once the bubble had been removed, normal flow conditions were fully restored. The inoculation efficiency of 10 % was sufficient for our experiments but can certainly be further enhanced. The method is not restricted to the geometries presented here and can be adapted to other microfluidic single-cell analysis devices. Inoculated *C. glutamicum* cells survived the procedure well as shown by their vital growth and morphology.

8.6 Publication III Supplement

8.6.1 Publication III - Capillary force calculation

The pressure (p_c) generated by the capillary force can be expressed by Publication III Supplement Equation 1:

$$p_c = -\gamma_{lg}\left(\cos\theta \frac{dA_{sl}}{dV_1} - \frac{dA_{lg}}{dV_1}\right)$$

Publication III Supplement Equation 1

where γ_{lg} refers to the surface tension of the liquid, θ to the contact angle, A_{sl} to the solid/liquid interfacial area, A_{lg} to the liquid/gas interface interfacial area and V_1 to the liquid volume of the channel.

For a rectangular channel with constant cross-section and w >> h, the Young-Laplace equation can be obtained (Publication III Supplement Equation 2).

$$p_c = -\gamma_{lg}\cos\theta \left(\frac{2}{h}\right)$$

Publication III Supplement Equation 2

The pressure of one subchannel (p_c) with a height of 10 µm, a surface tension γ = 0.07 Nm^{-1} and a contact angle θ = 111° induced by capillary force was found to be approximately 120 mbar using Publication III Supplement Equation 2. Thus the fivefold capillary pressure of 600 mbar pushes the injected air bubble into its operational position.

8.6.2 Publication III - Fitting of experimental data

Fitting of the experimentally obtained data for the air bubble removal was done accordingly to Kang et *al.* [31] Based on the gas permeation, Publication III Supplement Equation 3 was derived for the shrinkage of the bubble cross-sectional area *A* over time.

$$A(t) = c_1 exp\left(\frac{aP(p_1 - p_2)}{hb}\,\frac{T * 76}{273 P_{atm}}\,t\right) + c_2$$

Publication III Supplement Equation 3

Appropriate values for the permeability *P*, channel height *h*, membrane thickness *b* and temperature *T* were chosen based on the material and geometry. The constants c_1, c_2 and *a* were obtained from fitting Publication III Supplement Equation 3 to the experimental values. The values derived for c_1, c_2 and *a* by Publication III Supplement Equation 3 are depicted in Table S 1 for P = 1.92 x 10^{-15} m^2 s^{-1} Pa^{-1}, h = 1 x 10^{-3} cm, b = 0.3 cm, P_{atm} = 76 cm Hg, and T = 298 K.

Publication III Supplement Table 1: Values of c_1, c_2 and *a* derived from experimental data at 300 mbar, 400 mbar and 500 mbar with P = 1.92 x 10^{-15} m^2 s^{-1} Pa^{-1}, h = 1 x 10^{-3} cm, b = 0.3 cm, P_{atm} = 76 cmHg, and T = 298 K.

p [mbar]	c_1	c_2	a
300	9.92e+03	5.73e+07	-1.49e+03
400	5.74e+03	5.29e+07	-1.80e+03
500	3.80e+03	9.09e+07	-8.15e+02

9 Publication IV - Microfluidic growth chambers with optical tweezers for full spatial single-cell control and analysis of evolving microbes

Christopher Probst, Alexander Grünberger, Wolfgang Wiechert, Dietrich Kohlheyer
Journal of Microbiological Methods **95**, 470–476 (2013).
DOI: 10.1016/j.mimet.2013.09.002

9.1 Abstract

Single-cell analysis in microfluidic systems has opened up new possibilities in biotechnological research enabling us to deal with large eukaryotic cells and even small bacteria. In particular, transient investigations in laminar flow or diffusive environments can be performed to unravel single cell behaviour. Up to now, most systems have been limited with respect to precise cell inoculation and sampling methods. Individual cell selection and manipulations have now been made possible by combining laser tweezers with microfluidic cell cultivation environments specifically tailored for micrometre-sized bacteria. Single cells were optically seeded into various micrometre-sized growth sites arranged in parallel. During cultivation, single-cell elongation, morphology and growth rates were derived from single cells and microcolonies of up to 500 cells. Growth of irradiated bacteria was not impaired by minimizing the exposed laser dosage as confirmed by exceptional growth rates. In fact, *Escherichia coli* exhibited doubling times of less than 20 min. For the first time, a filamentous *Escherichia coli* WT (MG1655) was safely relocated from its growing microcolony by laser manipulations. The cell was transferred to an empty cultivation spot allowing single-cell growth and morphology investigations. Contrary to previous discussions, the filamentous *E. coli* exhibited normal cell morphology and division after a few generations. This combination of optical tweezers and single-cell analysis in microfluidics adds a new degree of freedom to microbial single-cell analysis.

9.2 Introduction

The technology of microfluidics is steadily evolving and several promising tools for studying living cells under tight environmental control have been demonstrated. Microfluidic cell culture systems have the advantage of well-predictable and stable environmental conditions through a fast exchange of heat and mass. The potential for massive parallelization of micrometre-sized components offers ideal conditions for performing high-throughput cultivations of single cells as well as isogenic colonies [90, 98, 99, 107]. Recently, we described the cultivation and analysis of bacteria inside picoliter bioreactors for several biotechnological applications [184–186]. The device was infused with a cell suspension and single bacteria remained trapped in the shallow cultivation regions of 1 µm in height by cell–wall interactions. Although single cells and hundreds of evolving colonies were analysed, cell trapping inside the cultivation reactor was a random process. Consequently, not every cultivation site was filled with a single cell. Furthermore, striking cells, for example, exhibiting high growth rates or special morphology, could not be relocated from a colony for further single-cell analysis.

Optical tweezers (OT) have proved to be an effective manipulation tool for various cell types and particles [61, 218–224]. OT necessitate a highly focused laser beam to trap and manipulate micro-sized objects [225]. However, OT is not well suited for performing high-throughput single cell cultivation over longer time periods if used alone. This is mainly due to the negative effect on cell metabolism and viability during OT exposure. OT manipulations of living organisms may induce cell damage due to the introduction of heat aswell through oxygen radicals generated by photochemical processes [196]. We have developed a microfluidic microbial cultivation device for single cell and microcolony growth analysis. In contrast to previously reported systems, cultivation geometries were developed, allowing the cultivation under solely diffusion based medium supply. Furthermore, the integration of OT was utilized for precise and specific single cell manipulations rather than using random flow inoculations. This article describes the microfluidic device principles, growth analysis and the application of OT for single bacteria seeding and manipulation. Cultivation was conducted over many generations to analyse evolving isogenic microcolonies. In our approach, only minimal power levels and short exposure times were applied thus avoiding cell damage during OT manipulations. The cultivation setup was constantly infused with fresh medium to achieve a continuous supply of nutrients while at the same time reducing the local heat exposure by the laser beam. Isogenic microcolonies exhibited doubling times of less than 20 min although OT was applied to seed the single *E. coli* WT (MG1655) mother cells into the growth sites. In contrast to earlier systems, our approach offers a high degree of flexibility with regard to cell

inoculation and manipulations. The combination of the two technologies facilitates the cultivation of microorganisms under well-controllable environmental conditions and at the same time cell manipulations. We utilized this method to transfer a single filamentous *E. coli* cell from its original microcolony into an empty growth site for further studies. Currently, further investigations are being performed to study cell filaments in more detail. A video based description of the fabrication procedure and further details on assembly can be found in.

9.3 Materials and Methods

9.3.1 Fabrication of microfluidic growth chambers

The microfluidic cultivation device was fabricated by simple polydimethylsiloxane (PDMS) moulding using a lithography fabricated multilayer master mould. Fabrication details can be found in previous work [201].

9.3.2 Experimental microscopy setup

The assembled cultivation device was placed inside an in-house fabricated temperature incubator mounted onto an automated microscope (Nikon Ti Eclipse). The microfluidic channels were interfaced with dispensing needles inserted into the PDMS connected with tubing (Tygon S-54-HL, ID = 0.25 mm, OD = 0.76 mm, VWR International) to 1 ml disposable syringes (Omnifix-F Tuberculin 1 ml, B. Braun AG). Medium and cell suspension were perfused through the microfluidic device utilizing a high-precision syringe pump system (neMESYS, Cetoni, Germany). The microscope was equipped with a focus correction system (Perfect Focus System, Nikon), Apo TIRF 100 × Oil DIC N objective, NIKON DS-Vi1 colour camera). Additionally, an objective heater system (ALA OBJ-Heater, Ala Scientific Instruments, USA) was used to minimize heat flux through the objective. The OT system (E3300, Elliot Scientific Ltd., United Kingdom) was connected to the epi-fluorescence port of the microscope setup and equipped with a Nd:YAG laser (Lambda = 1064 nm) with a maximum power output of 5 W.

9.3.3 Cultivation of *Escherichia coli*

E. coli WT (MG1655) was pre-cultured in 20 ml of fresh LB medium (5 g yeast extract, 10 g peptone and 10 g NaCl per liter) in 100 ml shake flasks and cultivated at 37 °C and 150 rpm overnight. Next day, 25 µl was transferred to a main-culture with 20 ml of fresh LB. Cells were grown until an optical density (OD 600, BioPhotometer plus, Eppendorf AG, Germany) of 2 was reached. Afterwards 100 µl of themain-culture was diluted in 900 µl of fresh LB medium.

9.3.4 Cultivation in microfluidic chambers

Microfluidic cultivation chambers (Figure 33 a) and cultivation pockets were used to study the influence due to IR laser radiation. All experiments were performed at 37 °C. To reduce unspecific adhesion of *E. coli* to the channel walls and glass, prior to cell infusion the microfluidic channels were perfused with a 10:1 solution of bovine serum albumin (BSA, 10 mg/ml) in LB at 1000 nl/min for 30 min. After surface treatment, a small amount of the freshly diluted cell suspension was drawn directly into the tubing connected to a syringe with BSA

(10:1) in LB medium. The tubing was once more inserted into the main channel inlet and cells were infused at 400 – 700 nl/min. After infusion, pressure gradients were generated manually to perform random cell seeding simply by the fluid flow. Then, the flow was stopped for specific OT-based cell trapping and seeding. OT cell manipulations were performed simply by moving the microfluidic device mounted to the motorized microscope stage instead of sophisticated optical stirring methods as demonstrated in other publications [226]. Subsequently, cell cultivation was initiated by a continuous flow of LB medium. Time-lapse images were taken every 5 min for approximately 8 h.

9.3.5 Image analysis and data evaluation

Growth analysis was performed using the commercially available software package NIS-Elements AR (Nikon Instruments, Japan), by counting the number of cells in each growth site and image. Growth evaluation of each microcolony was done by fitting the data to an exponential curve. Consequently, the growth rate (μ) was determined from the exponent. In this way, the average time a cell inside a growing colony needed to undergo division was calculated. This is further referred to as the interdivision time (t_d), which is defined as $t_d = \ln(2)/\mu$ [1/h]. Earlier approaches used the microcolony surface area to determine growth rates instead of counting individual cells [227]. Surface area measurements are advantageous in particular when nutrient depletion occurs within the colony resulting in heterogeneous cell sizes. In our system fresh medium was provided continuously and nutrients were supplied very efficiently by diffusion. This resulted in homogeneous culture conditions throughout the entire microcolony and similar cell lengths. Therefore, precise growth rate determination by cell number is appropriate.

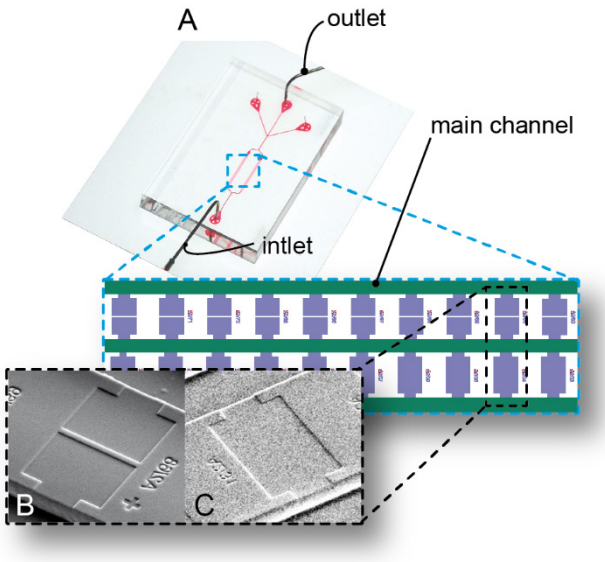

Figure 33: (a) Assembled microfluidic PDMS device bonded to a 170 µm thin glass plate and connected to tubing via steel needles. The device was filled with blue ink for the purpose of illustration. (b) SEM image of the growth pockets for OT-based cell seeding. (c) Scanning electronmicroscopy (SEM) image of fabricated growth chambers for hydrodynamical cell seeding.

9.3.6 Device principle and design

Several microfluidic structures were used in this study. Our microfluidic device of 20 mm x 30 mm x 3 mm (width x length x height) (w x l x h) is shown in Figure 33 a. Each device incorporates: 100 “growth pockets” with a single entrance (30 µm x 40 µm x 1.2 µm) (w x l x h) (Figure 33 b) allowing single-cell inoculation exclusively by OT. Mass transport inside the growth pocket is dominated by diffusion due to an 8-fold reduction in height compared to the deeper supply channel. 200 parallel “growth chambers” (30 µm x 40 µm x 1.2 µm) (w x l x h) depicted in Figure 33 c. As depicted, growth chambers are arranged between 8-fold deeper supply channels. If media supply volume flows are equal, no convective flow is present inside the growth chamber but mass transport is based solely on diffusion. However, during cell inoculation volume flows were imbalanced and the resulting convective flow was used for flow based cell inoculation. The 1.2 µm deep growth sites limit cell growth to a monolayer ideal for time-lapse imaging and cell counting. Due to low Reynolds numbers, convective media flow inside the supply channels was always laminar (Re = 0.04 at 400 nl/min).

9.4 Results and Discussion

9.4.1 Growth in microenvironments

Cell growth is the key viability indicators of organisms in microbiology. To investigate the impact of OT onto the growth behaviour of *E. coli*, different designs were utilized, as depicted in Figure 34 b and c.

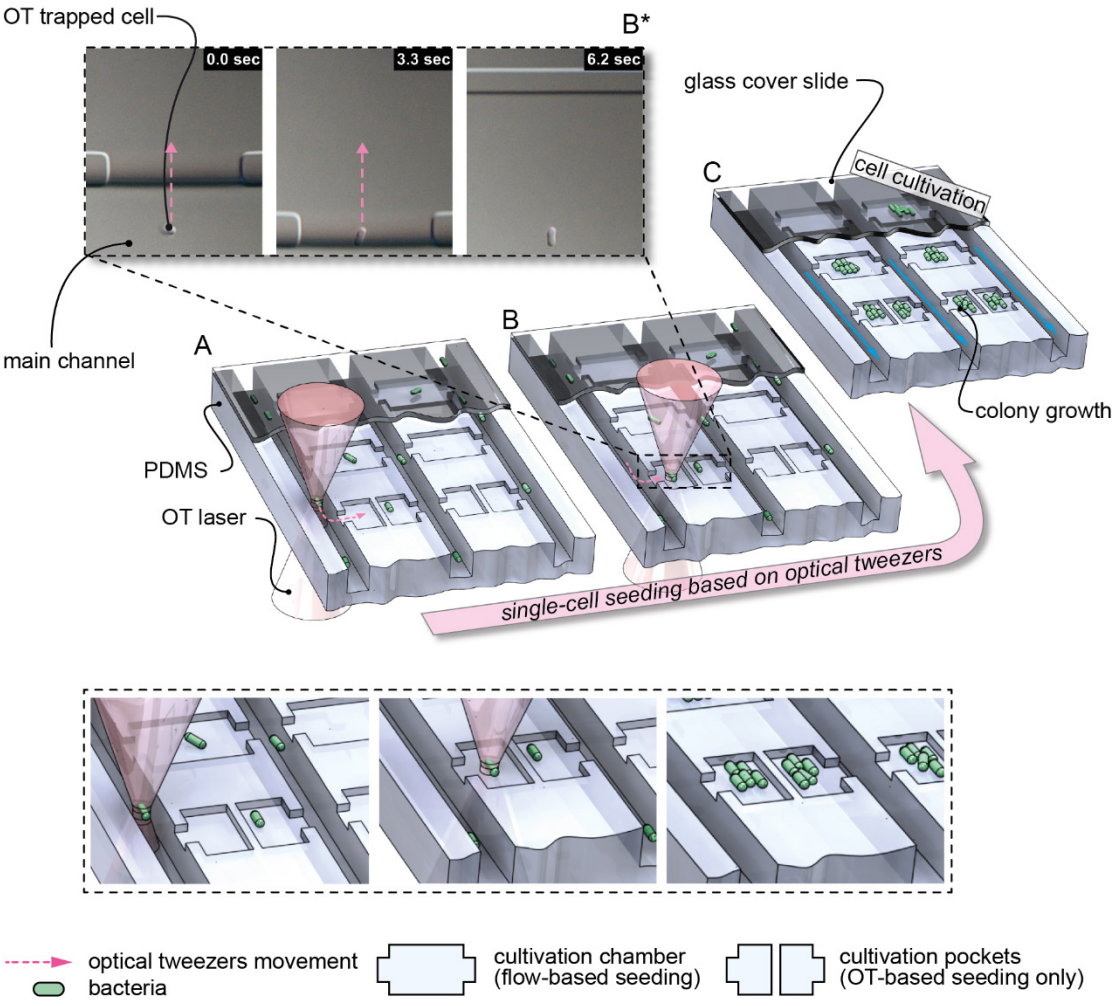

Figure 34: Filling procedure of both cultivation regions. Each channel contains cultivation chambers for hydrodynamic and pockets for OT based single-cell trapping. (a, b) Individual bacteria are inoculated into the growth pockets by means of OT. (c) Afterwards the medium is switched to growth medium to start cultivation. (b*)Microscopy image series of a single *E. coli* cell being seeded into a cultivation pocket using OT.

The viability impact is proportional to the amount of absorbed energy generated by the IR laser beam as known from [196]. The present study did not aim to provide further insights into cell damage caused by optical manipulations, but was driven by the need to confirm a minimal laser dosage that does not cause detectable cell damage. Figure 34 shows the microfluidic PDMS device and filling procedure for single-cell cultivation and analysis. OT-based inoculation is presented in Figure 34 b* by a series of live-cell microscopy images in which an individual *E. coli* cell was relocated from the main supply channel into the cultivation pocket. The cell was dragged into the shallow zone of the cultivation chamber with a height of 1.2 µm without adhering to the glass or PDMS surface. Due to the elongated rod shape of *E. coli*, a single cell orients parallel to the laser beam propagation if trapped by OT inside the 10 µm deep supply channels. As soon as the bacteria cell is dragged into the narrow cultivation region the cell is forced to orient perpendicular to the beam direction. A variety of heights for the growth pockets were tested (0.8 – 1.5 µm) and the height of 1.2 µm was well suited for seeding and cultivating single cells without unspecific cell adhesion during seeding. The OT inoculation of a single cell is shown in microscopy Supplement Video 1.

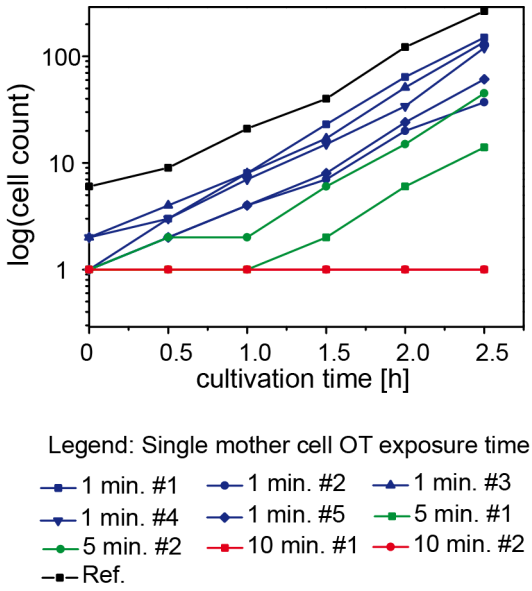

Figure 35: Growth of separate microcolonies over 2.5 h, after 1 min, 5 min and 10 min of exposing the mother cell with OT (60 mW). Exposure times below 1 min showed no effect on cell growth as indicated by normal cell growth. Above 5 min exposure cell growth was affected. Above 10 min of exposure no cell growth was observed.

Cells were irradiated by OT at 60 mW laser power below 1 min exposure time and moved into the cultivation pockets to study the possible influence due to IR laser radiation. This time was sufficient to transfer cells from the main supply channel into growth pockets as well for cell relocation from the original colony to an empty site. Cells exposed longer than 5 min showed impaired growth behaviour as shown in Figure 35. All cultivation regions were monitored by automated time-lapse imaging over a total time period of 4 h, as exemplary shown in Figure 36 a. An exemplary time-lapse microscopy recording of a growing colony can be seen in Supplement Video 2. The average growth rate of optically manipulated cells was found to be $\mu_{max,\,OT} = 2.16 \pm 0.09\ [h^{-1}]$ (N = 7), which corresponds to a maximum average doubling time of $t_{d\,max,\,OT} = 19.28 \pm 0.82$ [min] (N = 7) (Figure 36 b). The average growth rate of hydrodynamically trapped cells was found to be $\mu_{max,\,Hyd.} = 2.18 \pm 0.25\ [h^{-1}]$ (N = 7), which corresponds to a maximum average doubling time of $t_{d\,max,\,Hyd} = 19.22 \pm 1.96$ [min] (N = 7) (Figure 36 b). These results are in very good agreement and indicate that an exposure time of 1 min at 60 mW did not influence growth and is an ideal starting point for further studies applying this method. In fact, a doubling time of 20 min is known as the theoretical minimum for *E. coli* [228]. As confirmed by computational fluid dynamics (data not shown), diffusion was dominating over convective mass transport inside all growth sites. Therefore, during cultivation no or negligible convective flow occurred inside the growth sites. Due to the micrometre length scales, all growth sites were replenished with fresh medium continuously within seconds. Due to that, cultivation conditions were constant throughout the experiments and most presumably homogeneous across the growing microcolonies as indicated by homogenous cell size and equal growth rates.

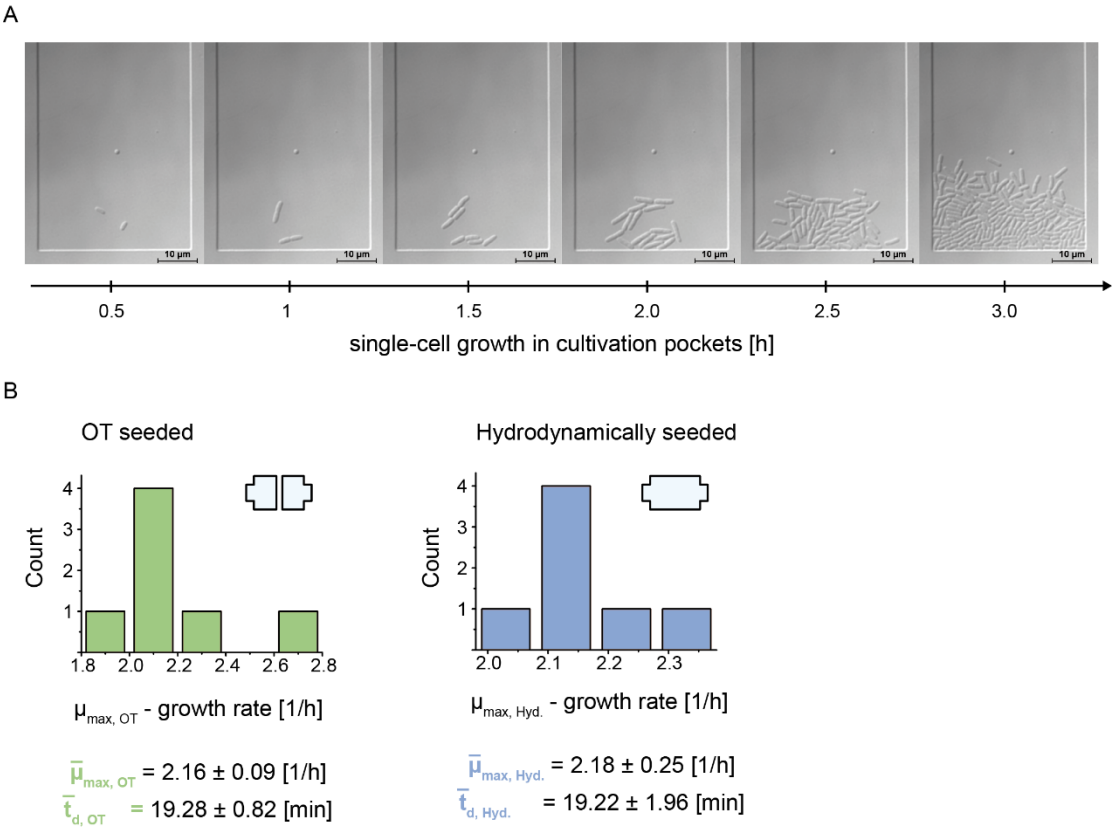

Figure 36: Single cell growth analysis: multiple cultivation pockets & chambers were inoculated with *E. coli* using OT (b1 min, b60 mW) and pressure gradients. (a) *E. coli* microcolony growing inside a cultivation pocket. (b) Growth rates of OT-manipulated cells (green bars) and growth rates of hydrodynamically seeded cells (blue bars) as reference.

9.4.2 OT control over single cells

The formation of filaments in many bacterial species has been known for a long time and is often related to external stress [9]. Metabolic changes and DNA damage (SOS response) by, for example, antibiotics, high and low temperature, ultraviolet radiation, and phage infection [229], are expected to lead to filamentation. Justice et al. further postulated that filamentation can also play an important role in the survival of bacterial populations in the presence of, for example, antibiotics [9]. However, the large variety of substances which induce filamentation make it difficult to identify specific substances. Single-cell cultivations in microfluidic environments would allow more specific investigations to unravel the origin of filamentation, e.g., by exposing bacteria to certain filamentation-forming substances in a controlled environment. Wang *et al.* were, to the best of our knowledge, the first to investigate periodically appearing cell filaments in a high-throughput manner using their microfluidic mother machine [98]. It was found that also under constant environmental conditions, *E. coli* cells formed filaments. Wang et al. related this to cell ageing affects (DNA damage/SOS response) after a mother cell had performed around 50 divisions. Unfortunately, due to their dead-end channel configuration in the mother machine, filamentous bacteria were dragged out of the growth site into the supply channel losing conspicuous cells for further analysis.

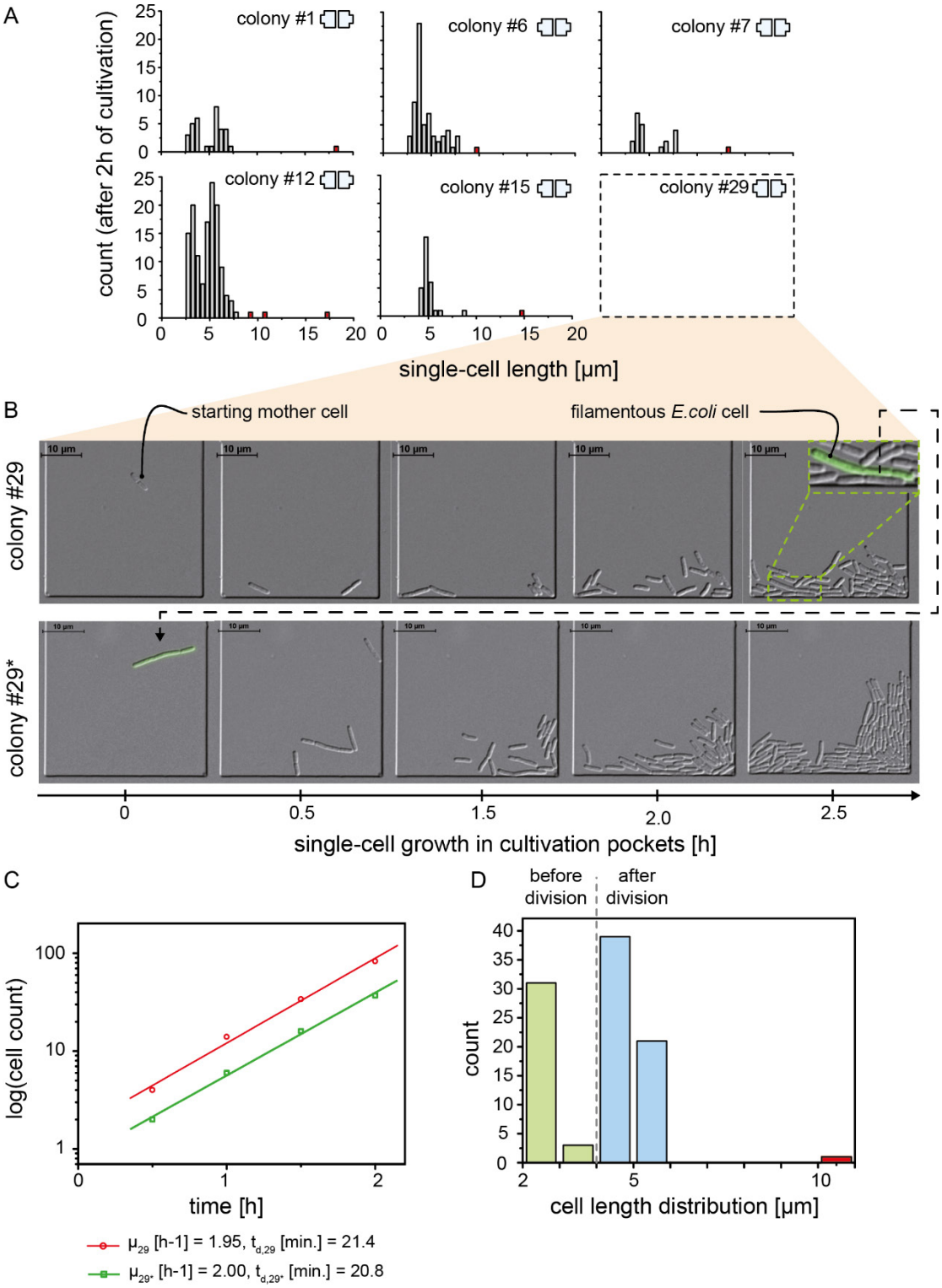

Figure 37: (a) Cell length distribution of 5 from 29 OT seeded cultivation pockets containing at least one filamentous cell. (b) Time lapse growth of a *E. coli* microcolony inside a cultivation pocket with a 10 µm long filamentous cell appearing after 2.5 h (for purpose of illustration the cell was highlighted in green by photo editing). Afterwards the filamentous cell was removed from colony #29 and placed in an empty cultivation pocket (colony #29*) using OT for further observation. (c) Growth rate analysis of colony 29 and 29* and (d) distribution of cell length of colony #29*after approximately 2 h of cultivation.

In our approach, multiple cultivation pockets were inoculated with single *E. coli* using the OT. In a first proof of principle experiment, we found that 6 of 29 filled colonies contained at least one filamentous cell with a cell length up to 18 µm as it can be seen in Figure 37 a. This is a 6-fold increase in length compared to a typical cell length of 3 µm. Since filaments typically develop after several generations, the colony can already fill the entire cultivation site before any conspicuous cell appears. Furthermore, it may become cumbersome to differentiate the descendants of the filamentous cell from the rest of the evolving microcolony. Consequently, a filamentous bacteria was identified (for purpose of illustration the cell was highlighted in green by photo editing, Figure 37 b) and this filamentous cell was transferred by OT from its original microcolony to a nearby but empty cultivation pocket (colony #29), as shown in Figure 37 b. The time-lapse microscopy recording of colony #29 can be seen in Supplement Video 3. This specific cell was observed during growth for another 2 h. In contrast to frequent speculation about cell defects in filamentous cells, this cell divided after 15 min into 4 individual cells as depicted in Figure 37 b. Presumably, four DNA replicates were present in the filamentous cell but the cell division mechanism was delayed. Further growth analysis revealed that the evolving microcolony (colony #29*) exhibited growth rates equivalent to the colony 29 (μ_{29} = 1.95 [h^{-1}] and μ_{29*} = 2.0 [h^{-1}]) (Figure 37 b). In addition, a similar cell size distribution for both populations was observed (Figure 37 b). The original filamentous cell kept dividing, but remained at a size of app. 10 µm. The method presented combines state-of-the-art microfluidics and OT and enabled us to investigate filamenting *E. coli* in more detail. In the future, this method will be applied to study the formation of filamentation through specific substances (e.g. antibiotics) or other stressful situations for an organism (e.g. nutrient depletion, temperature gradients).

9.5 Conclusion and outlook

In this article, we report on a new microfluidic device combined with optical tweezers (OT) for single-cell analysis of bacteria. The present system is used to cultivate and analyse, for example, industrially relevant microorganisms such as *E. coli* inside picoliter sized chambers. Due to the restricted channel height cells grew in a precise monolayer to be analysed by time-lapse imaging microscopy. By combining microfluidic-based cultivation and OT manipulations a new degree of freedom for performing single-cell analysis of microbes was realized. In contrast to earlier publications, we successfully applied OT to manipulate single bacteria cells without affecting cell growth. It is shown that a minimal laser dosage can be used to manipulate and seed single cells to gain more control over an evolving microcolony. Cells of interest can be individually trapped, relocated, recultivated in specific areas of the device. *E. coli* exhibited viable growth rates of around 20 min. We can therefore conclude that growth was not affected by our laser based manipulations. Small fractions of cells showed filamentous growth behaviour, a frequently observed phenomenon in general. We successfully applied OT and isolated a filamentous *E. coli* from a growing colony in order to perform further growth analysis with single-cell resolution. Our system operates with very homogeneous growth conditions so we can conclude that filamentation is unlikely to be caused by external stress factors such as nutrient depletion. The filamentous cell exhibited normal growth behaviour after isolation and cultivation contrary to previous findings. This method has great potential for selecting specific, e.g., high-performing, cells with respect to growth, productivity and ultimately performing single-cell sequencing.

10 Future Perspectives

In this thesis, different methods were established for the trapping, cultivation and analysis of single cells in a high-throughput manner. Further, the manipulation of individual cells by means of optical tweezers was realized to isolate cells of interest from a microcolony for further investigations. Additionally to the published work, also other fields of interest were pursued, which are to this date not published.

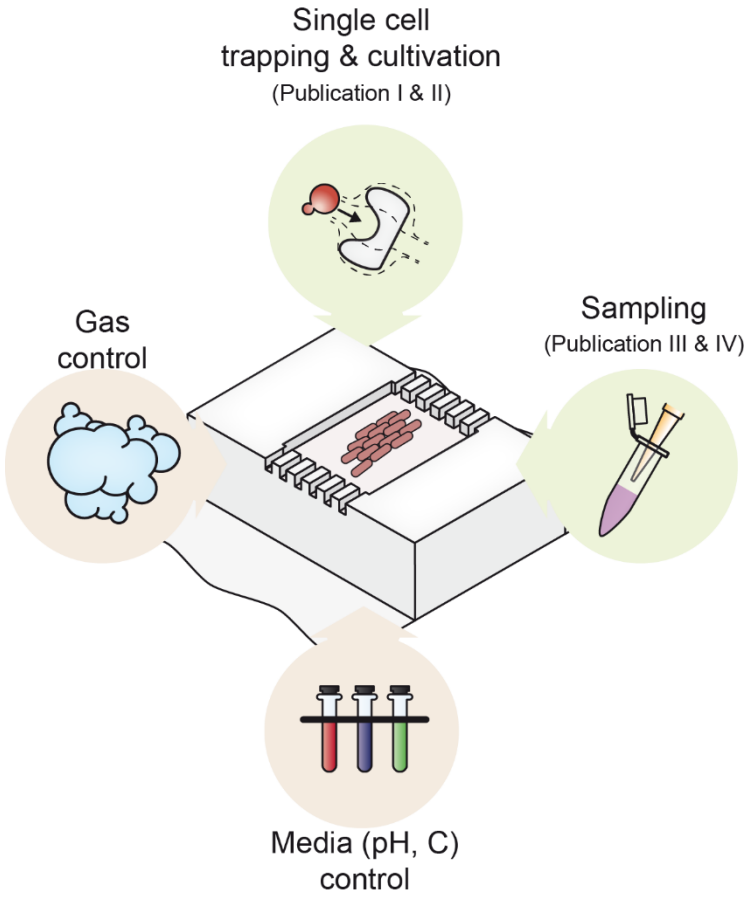

Figure 38: Overview of the different fields of interest pursed in this thesis, which were realized (single cell trapping & cultivation, sampling) and those that currently under development (media & gas control).

Figure 38 shows an overview of the additional fields of interest, which were pursued in the course of this thesis. In addition to the trapping, cultivation and manipulation of single cells, also the control of the media and oxygen concentration in microfluidic devices were investigated. These fields symbolize different aspects, which are of interest for being integrated into existing microfluidic devices for the analysis of single cells, in order to more

accurately emulate the environment in large scale bioreactors. The cultivation volume of bioreactors in industrial processes can scale up to 500 m^3 [230] and environmental conditions have found to be not entirely homogenous[3] over these large volumes. Microgradients of nutrients, oxygen, pH and temperature are still present even by constant improvement of mixing capabilities [3]. For studying bioprocesses in miniaturized cultivation system, dynamic changes of different parameters have to be achieved.

10.1 Batch cultivation in microfluidic devices

Microfluidic perfusion based cultivation systems as presented in Publication I and Publication II constantly provide fresh nutrients and remove any products/by-products, which might interact with the cells. Yet, depletion of nutrients and interaction of secreted cellular compounds is present in typical lab and industrial scaled batch cultivations.

Unger and co-workers [231] first introduced the idea of integrating small membrane valves and pumps in microfluidic PDMS devices. Here, two layers made from PDMS are sandwiched together. The bottom layer carries fluids (fluid layer), whereas the top layer (control layer) is consisting of a dead-end channel network. A valve is formed by an intersection of both channels in each of the layers. By applying pressure to a dead-channel causes the valve to seal of, stopping fluid flow immediately. Furthermore, arranging several valves along a channel and applying pressure to one after another can realize pumping of a liquid [139, 231, 232].

Dai and co-workers [124] presented a microfluidic device capable of achieving a batch cultivation by using small membrane valves at the inlet and outlet of a several cultivation chambers. Yet, cultivation chambers did not restrict growth to a monolayer not allowing high-resolution single-cell analysis.

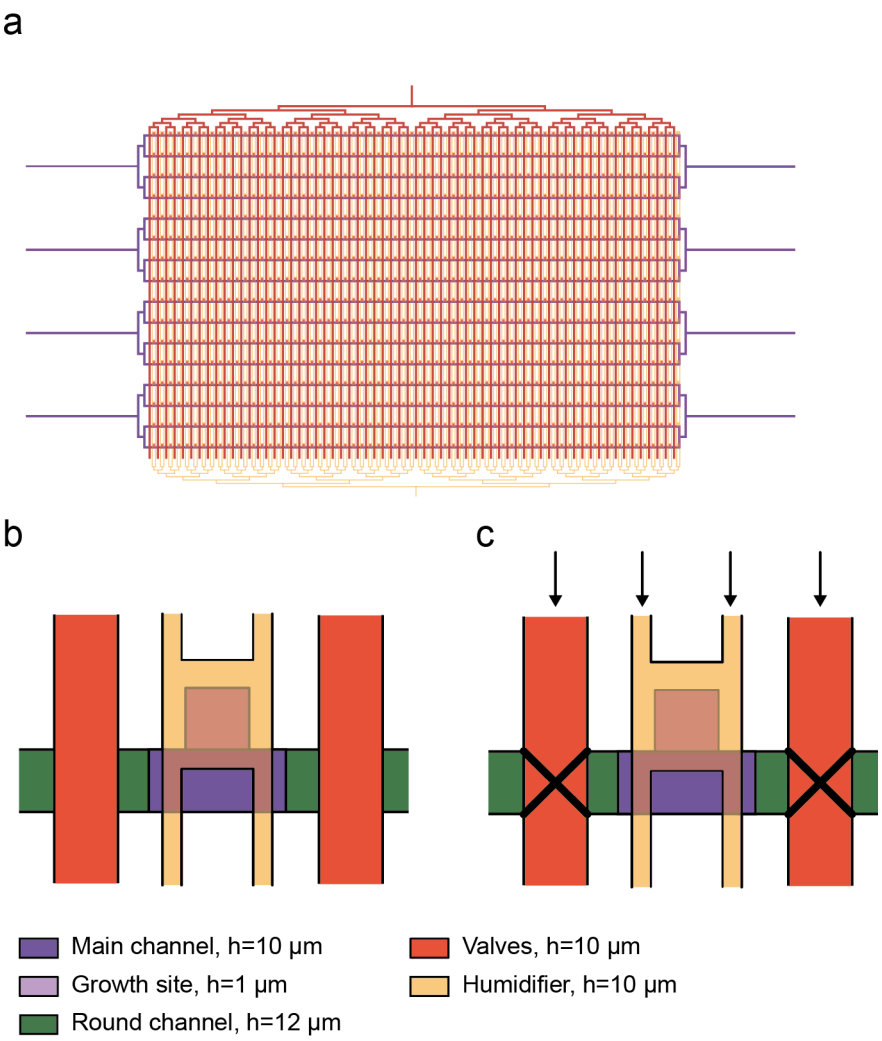

Figure 39: (a) Illustration of microfluidic device for batch cultivation consisting of several cultivation chambers. (b) Detail of cultivation chamber with a height (h) of 1 µm. Valves are arranged to the left and right of the cultivation chamber (red colored channels). (c) Applying pressure to the valve closes of the volume. A channel filled with water on top of the cultivation chamber serves as a water vapor barrier.

For analyzing single cells in a similar environment as in typical batch cultivations, micron scaled valves were integrated in existing tools for the cultivation of single cells. Figure 39 depicts the microfluidic device for batch cultivation of single cells and consists of several cultivation chambers arranged along the main channels (Figure 39 b). A cultivation chamber (height = 1 µm) is arranged between to valves (red colored channel) and by applying pressure the valves close of the volume (Figure 39 c). Detailed description of the fabrication is given in the Supplement “Master mold fabrication”.

Proof-of-principle experiments were conducted by cultivating *E. coli* with two different sugars, glucose and lactose, at present. *E. coli* is known for sequentially using one sugar after another, favoring glucose [233]. After glucose has entirely been consumed, cells switch to lactose

(diauxic shift). The switch from glucose and lactose is accompanied by a short halt in growth (lag phase) until lactose is metabolized. For monitoring the diauxic shift and start of lactose metabolization a fluorescent sensor was integrated into *E. coli* (lacZ::gfp).

First preliminary results are depicted in Figure 40. Figure 40 a shows a time-lapse image series of a cultivation chamber with a single *E. coli* cell. Growth is observed over 5 hours and batch cultivation is started after 3 hours. Growth continues solely on glucose (Figure 40 b) until approximately 4.5 hours. Afterwards, a halt in growth was observed as well as increase in fluorescence. Growth on lactose continues after a period of 1 hour and with a further increase in the fluorescence signal.

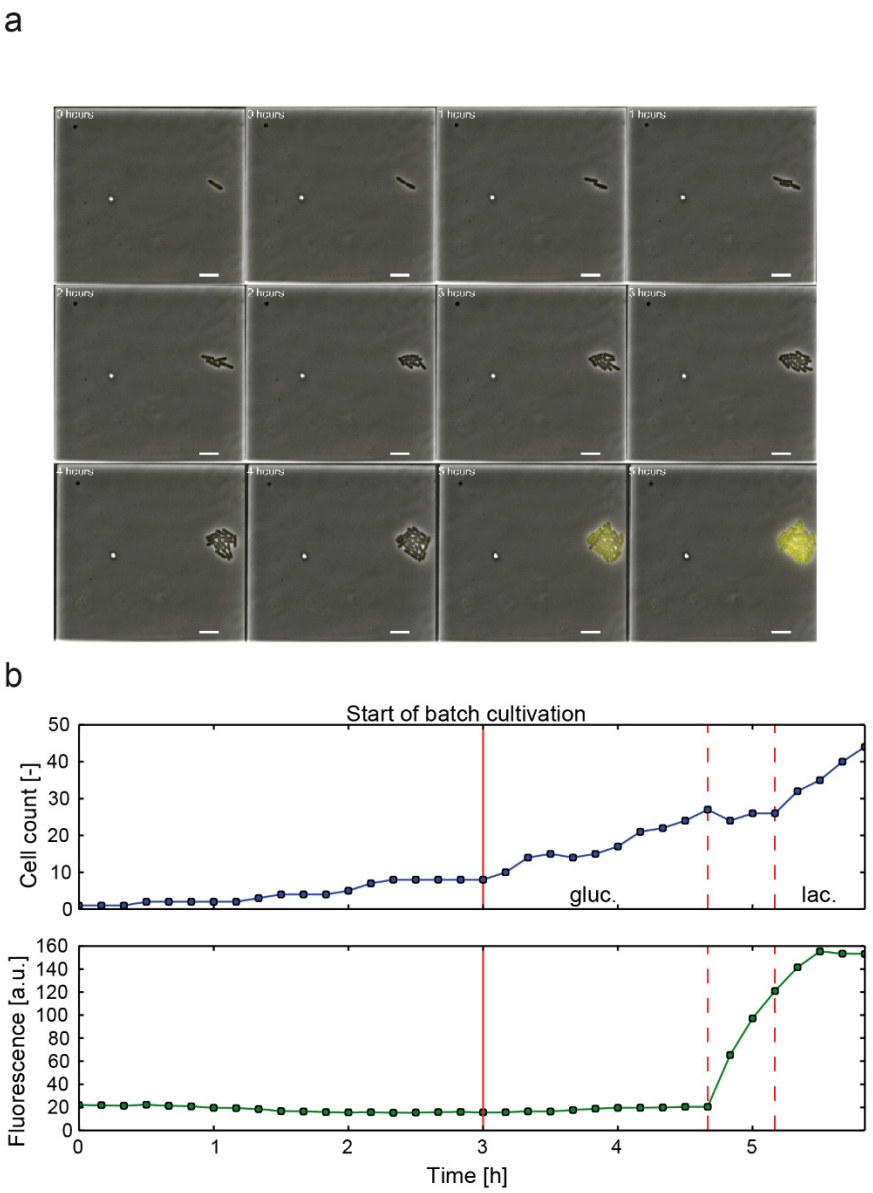

Figure 40: Proof-of-principle experiment of batch cultivation. (a) Growth of *E. coli lacZ::gfp* at 37 °C (M9CA medium) over 5 hours. (b) Cell count and fluorescence signal over time.

10.2 Flow control of liquids in microfluidic devices

Controlling and manipulating liquids in microfluidics has been one of the key elements for realizing any kind of application. Various methods can be found, which apply different physical principles for the transport and manipulation of fluids in microfluidic systems [234, 235].

These physical principles can be categorized into passive or active. Passive principles make use of capillary/surface forces [236–240], difference in gravity [241–248], or osmotic flow [238, 239, 249, 250].

Active pumping can be realized by syringe pumps [251, 252] peristaltic pumping [243, 253–260], electroosmosis [261–267] or by centrifugal forces [268–270]. The emergenceof soft lithography using elastomeric polymers, paved the way for the development of pneumatic membrane pumps [231]. Here, two layers made from polydimetyhlsiloxane are sandwiched together. The bottom layer carries fluids (fluid layer), there as the top layer (control layer) is consisting of a dead-end channel network. A valve is formed by an intersection of both one channel in each of the layers. By applying pressure to the dead-channel causes the valve to seal of, stopping fluid flow immediately. Furthermore, arranging several valves along a channel and applying pressure to one after another can realize pumping of a liquid [115, 139, 231]. Nevertheless, only few studies investigated the performance and reproducibility of microfluidic membrane pumps.

In this work, a detailed characterization of the maximum achievable flow rates as well as the reproducibility regarding the geometry, fabrication process and experimental parameters was carried out. Particle image velocimetry (PIV) was used to visualize the flow in the micro channels and for determining the flow rate, by using automated image analysis. Microfluidic devices were fabricated with different geometries, as well as various membrane thicknesses. Further, different channel shapes in the fluid layer were investigated with either rectangular or round cross-sections. It is shown that for reaching a desired flow rate certain aspects have to be taken into account to significantly reduce the variations in a series of experiments.

10.2.1 Fabrication procedure of membrane pumps

10.2.1.1 Fabrication of microfluidic master molds

Multilayer fluid master molds were fabricated using either the negative photoresist SU8 2010 (MicroChem Corp, USA) and the positive photoresist SPR-220 7.0 (Rohm and Haas, USA). Prior to resist depositing a 4" silicon wafer was cleaned with piranha solution, hydrofluoric acid and rinsed with DI water. After dry spinning, the substrate was dehydrated for 20 minutes at 200 °C.

Channels with a rectangular cross-section were fabricated by spin coating 4 ml of SU8-2010 onto a cleaned wafer, at 500 rpm with and acceleration of 100 rpm/s for 10 s and 4000 rpm with an acceleration of 300 rpm/s for 30 s. Afterwards the wafer was soft baked for 15 minutes at 65 °C and 60 minutes at 95 °C. Exposure was carried out for 12 s. The wafer was then post-baked on a hotplate for 5 minutes at 65 °C and 3 minutes for 95 °C. Development of the exposed photoresist parts was done as described for the first layer of SU8. Hard bake was carried out for 6 hours on a hotplate at 150 °C.

Channels with a ellipse shaped cross-section were fabricated by spin-coating SPR-220 7.0 onto a cleaned wafer, at 500 rpm with an acceleration of 100 RPM/s for 5 s and 2000 rpm with an acceleration of 300 rpm/s for 40 s. Prior to exposure, the substrate was baked for 4 minutes at 105 °C. Consequently, the photoresist was exposed to UV light (365 nm, 7 mW/cm²) for 60 seconds using a chromium brightfield mask. For development the substrate was immersed in developer solution (MF CD 26, micro resist technology GmbH, Germany) for approximately 2 minutes. Afterwards the substrate was placed in fresh DI water for approximately 5 minutes and eventually blow dried. To round the positive photoresist structures the substrate was placed onto a hotplate for 15 minutes at 115 °C.

Control layer master molds were fabricated using a 4" silicon wafer which was cleaned with piranha solution, hydrofluoric acid and rinsed with DI water. A cleaned substrate was dehydrated at 200 °C for 20 minutes and coated with the negative photoresist SU8 2010 at 500 rpm with an acceleration of 100 rpm/s for 10 s and 4000 rpm with an acceleration of 300 rpm/s for 30 s. After deposition the substrate was baked at 65 °C for 15 minutes and 95 °C for 60 minutes. For structuring the photoresist it was exposed to UV light (365 nm, 7 mW/cm²) for 12 s using a chromium darkfield mask. Post-exposure bake was carried out 65 °C for 5 minutes and 95 °C for 3 minutes. Consequently, the development was done as described for fluid master molds. At last the structures were hard baked for 6 hours at 150 °C. Both substrates were treated with Trichloromethylsilane (CH_3SiCl_3, Carl Roth, Germany).

10.2.1.2 PDMS multilayer chip fabrication

Multilayered microfluidic PDMS chips were fabricated from different ratios of PDMS (Sylgard 184 Silicone Elastomer, Dow Corning Corporation, Midland, USA). Two mixtures of PDMS were prepared, 15 g with a ratio of 20:1 and 15 g with a ratio of 7:1, and degased for 30 minutes. The 7:1 mixture was poured over the control layer master mould and baked for 30 minutes at 80 °C. The 20:1 mixture was spin-coated onto the fluid layer master moulds at 2750 rpm with an acceleration of 275 rpm/s for 70s. After 10 minutes of leveling the mold was baked for 20 minutes at 80 °C. Consequently, the control layer was released and cut into pieces. Inlets were punched with an outer diameter of 0.42 mm (Nordsen EFD, USA). Control layer pieces were aligned to the fluid layer and bake again at 80 °C for 1 hour. Afterwards individual chips were released from the fluid layer to punch the remaining inlets and outlets.

10.2.2 Device design and principle

Figure 41a shows an illustration of the used microfluidic chip with a membrane pump consisting of three valves with a given width w_v and distance d to each other as well as a fluid channel with a given width w_f. The different values for w_v, d and w_f used for experiments are given in Table 6.

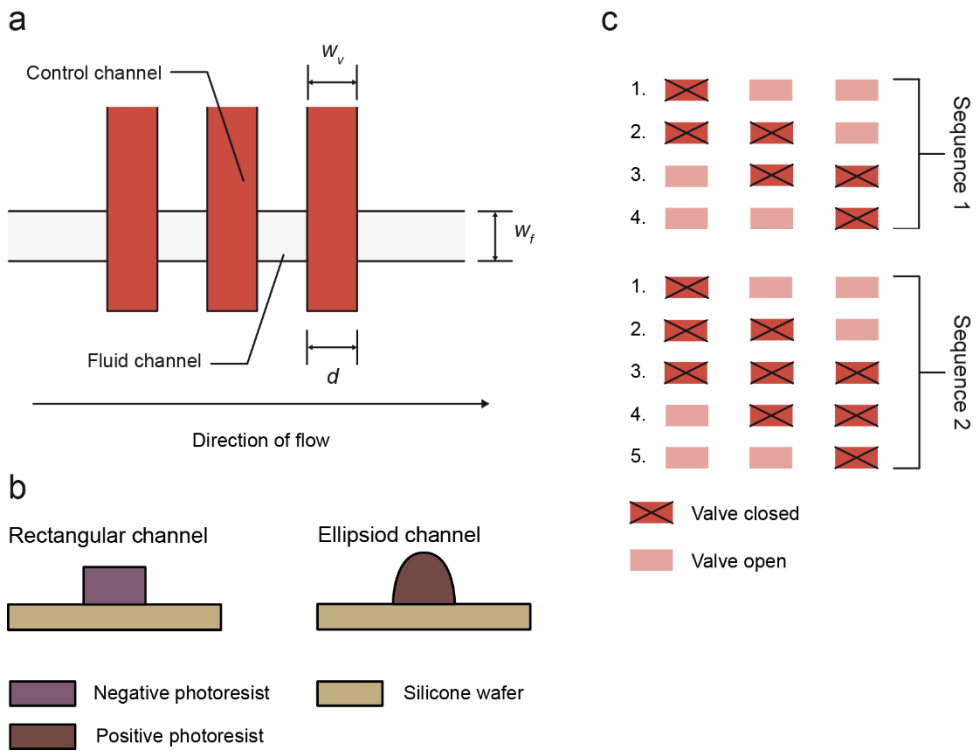

Figure 41: (a) Illustration of microfluidic membrane pump realized with three individual valves. (b) Description of pumping sequences used in all experiments for both rectangular and round shaped fluid layer channels.

Figure 41 b depicts the sequential activation of each valve over defined time steps. As shown in Figure 41 c, a 4-step sequence and a 5-step sequence were chosen, which are further referred to as sequence 1 and sequence 2. The actuation frequency between each step was kept constant for one experiment at a time but increase from starting with 3 Hz, 5 Hz, 10 Hz, 20 Hz, 50 Hz and to 100 Hz.

Table 6: Overview of all valve geometries used for experiments.

No.	w_v [µm]	d [µm]	w_v [µm]
1	100	100	100
2	100	100	200
3	200	100	100
4	200	100	200
5	100	50	100
6	150	50	200
7	150	100	200
8	200	50	200

10.2.3 Experimental setup

Control channels were supplied with compressed air by electro-magnetic valves (S070B-SDG, SMC Corporation, Japan) at a pressure of 14.5 psi. Valves were controlled using a national instruments card (BNC-2110, National Instruments, USA) at 5 V and 500 mA.

Fluorescent beads (Diameter 2 µm, FluoSpheres carboxylate-modified microspheres, Molecular Probes, USA) were suspended in DI water and bovine serum albumin (BSA, 10 %, Sigma-Aldrich, USA) in a ratio of 1:1000. Fluorescent images were recorded using an inverted microscope (Axiovert 25 CFI, Carl Zeiss, Jena, Germany) equipped with a CCD camera (AxioCAM MRC, Carl Zeiss, Jena, Germany), fluorescent light source (HBO 50, Carl Zeiss, Jena, Germany) and filter (excitation wavelength=546/12 nm, emission wavelength=590 nm) . Each image-sequence was taken at a 5x magnification Objectiv "Epiplan" 5x/0,13 HD M27, Carl Zeiss, Jena, Germany) in a 15 seconds interval with a sampling rate of 120 ms resulting in stacks of 124 images for each measurement.

10.2.4 Particle image velocimetry

Particle image velocimetry (PIV) bases on the identification of particles and tracking their path

over a sequence of images (Figure 42). Analysis of the recorded fluorescent images was carried out using the image analysis tool FIJI [271]. Pre-processing of image sequences was performed by removing background fluorescence and possible bead adhesion to the channel walls.
Next, the ImageJ plug-in „Particle Tracker 2D/3D“ [272] was used to compute the travelled distance (d) of each bead in a given image sequence. Calculation of the velocity was done using a selfwritten software in Java. The resulting mean velocity ($\underline{u}$) of the entire number of beads was correlated to the mean flow rate ($\underline{\theta}$) using the respective cross-section area (A) of the fluid channel.

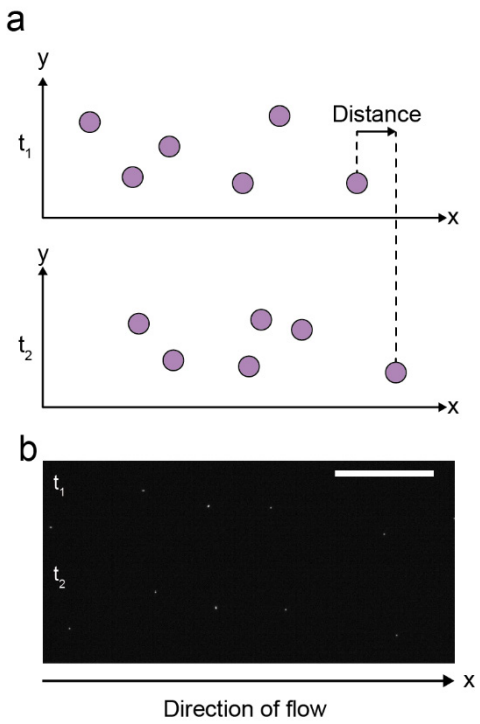

Figure 42: (a) Illustration of fluorescent labelled beads traveling along a channel and analysis of travelled path from frame to frame. (b) Original recorded fluorescent images of beads being pumped through a microfluidic channel from the right to the left side (scale bar 200 µm).

10.2.5 Characterization of flow rates

Our findings show a strong correlation between the geometry and the resulting flow rate as well as variations over repeated experiments. Additionally, the shape of the fluid channel, in this particular case rectangular or ellipsoid cross-section, alters the resulting flow rate significantly. Figure 43 - Figure 44 illustrate the obtained flow rates and variations for different valve widths (w_v) *a*nd the distance to each valve (d), as well as the fluid channel width (w_f) for rectangular and ellipsoid shaped fluid channels. A pressure of 14.5 psi was applied in varying

frequencies starting from 3 Hz, 5 Hz, 10 Hz, 20 Hz, 40 Hz to 100 Hz and with two different actuation sequences (Figure 41 c).

Distribution of flow rates in rectangular shaped fluid channels over frequency for different valve geometries (Table 6) are shown in Figure 43 a. The maximum flow rate was reached at a frequency 40 Hz except for no. 7 & 8, where a further increase was possible at a frequency of 20 Hz. It can be seen that the flow rate drastically decreases for frequencies above 10 Hz as well as the standard deviation over repeated experiments.

Comparison of the two sequences, revealed only minor differences in the flow rate and standard deviation. Greater variations in mean flow rate were found for geometry no. 3, 4 and 5 with frequencies over 20 Hz, which showed either an increase or decrease in achieved flow rate compared to the other sequence. Variations due to a change of sequence depleted for frequencies above 10 Hz.

Mean flow rates of each geometry for a particular frequency in Figure 43 b, show that the highest flow rate of ≈ 21 nl/min was achieved for geometry no. 7 at a frequency of 100 Hz and sequence 1. The minmal flow rate of ≈ 1.7 nl/min was found at a frequency 3 Hz for geometry no. 1 and both sequences. The maximum flow rates at a particular frequency strongly vary for each valve geometry. Especially, at high frequencies this clearly can be seen, but similar maximal flow rates are found at lower frequencies.

Repeated measurements showed strong variations in the resulting flow rate for certain values of w_v and w_f (Figure 43 c). High variations were found for geometry no. 2 at the entire investigated frequencies from 3 Hz to 100 Hz and with both sequences. This can also be seen for geometry no. 6 there the variations are neither influenced by the frequency nor the used sequence. Nevertheless, most of valve geometries show small variations at both sequences. Lower values of variations in the flow rate, where found for no geometry 1, 6 and 7 which also showed no influence due to change in frequency or sequence.

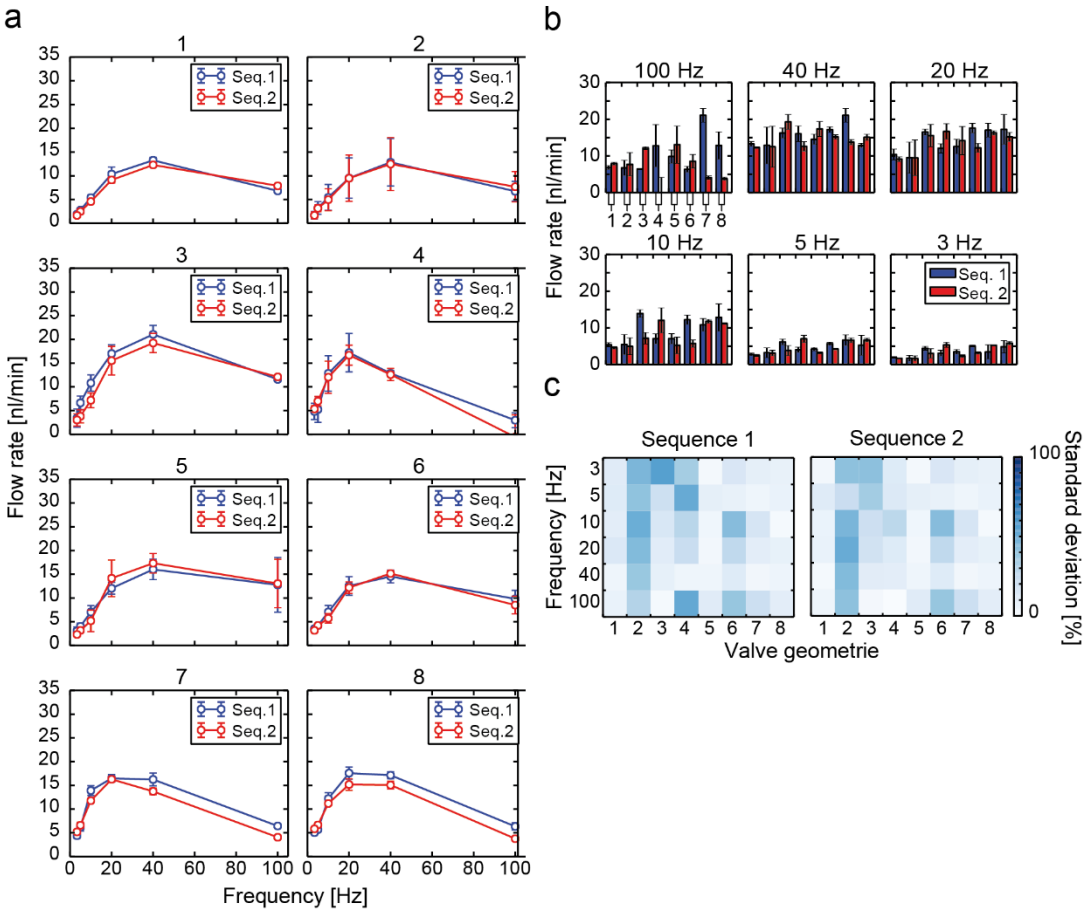

Figure 43: Characterization of achievable flow rates and variations in rectangular shaped fluid channels. (a) Mean flow-rates [nl/min] and standard deviations for different geometries and sequences 1 & 2, over frequency [Hz]. (b) Mean flow rates and standard deviation at 3 Hz, 5 Hz, 10 Hz, 20 Hz, 50 Hz and 100 Hz for sequences 1 & 2. (c) Comparison of standard deviations for different geometries, frequencies and sequences 1 & 2.

Distribution of flow rates in ellipsoid shaped fluid channels over frequency for different valve geometries (Table 6) are shown in Figure 44 a. Equal to the results from the rectangular shaped fluid channels, the flow rate reaches its maximum for all valve geometries at an actuation time of 40 Hz. Consequently the flow rate drops after decreasing the frequency any further (Figure 44 a). Similar to the previous shown results, variations between the different sequences can be found at a frequency of 20 Hz for no. 3 and 4, which decrease at lower frequencies.

The maximum flow rate of 21.6 nl/min was found for geometry no. 1* at a frequency of 100 Hz, with sequence 1. The minimal flow rate of 0.5 nl/min was found for geometry no. 4 at a frequency of 100 Hz, for sequence 2 (Figure 44 b). Differences in the maximum achievable flow rate at a particular frequency were also found here at a frequency of 100 Hz. Especially values of valve geometries no. 3 and no. 4, revealed drastically low flow rates at 100 Hz and

40 Hz.

Variations over repeated experiments with ellipsoid fluid channels showed a similar behaviour as with rectangular shaped ones (Figure 44 c). Geometry no. 1 shows a low variation, independent from the used frequency and sequence. For valve geometries no. 3 and 4 the relative variations are as high as the mean flow rate itself, at a frequency of 40 Hz and 100 Hz for both sequences.

For rectangular shaped fluid channels, valve geometry no. 1 & 2 achieved high flow-rates with low variations (in % or nl/min,). Here, w_v and w_f are identical, whereas other geometries also have an irregular combination of these two values. Reducing d also resulted in higher mean flow rates and low variations for unequal w_v and w_f, as it can be seen for no. 7, but shifted the frequency for highest achievable mean flow rate to 20 Hz. Increasing w_v and w_f in a 2 x ratio, gave slightly higher flow-rates, but lead to higher variations. By reducing d to 50 um a higher flow rate could be maintained for w_v = 200 um and w_f = 200 (no. 8) with variations similar to geometry no. 1 & 7.

Stable flow rates for ellipsoid shaped fluid channels could only be achieved if both w_v and w_f were equal, at high frequencies. By increasing w_v and w_f to 2x of the original size (no. 4), a similar effect as for the rectangular shaped fluid channel (no. 4) could be seen.

In conclusion, whether rectangular or ellipsoid fluid channels are applied variations over repeated experiments can be avoided by keeping w_v and w_f identical.

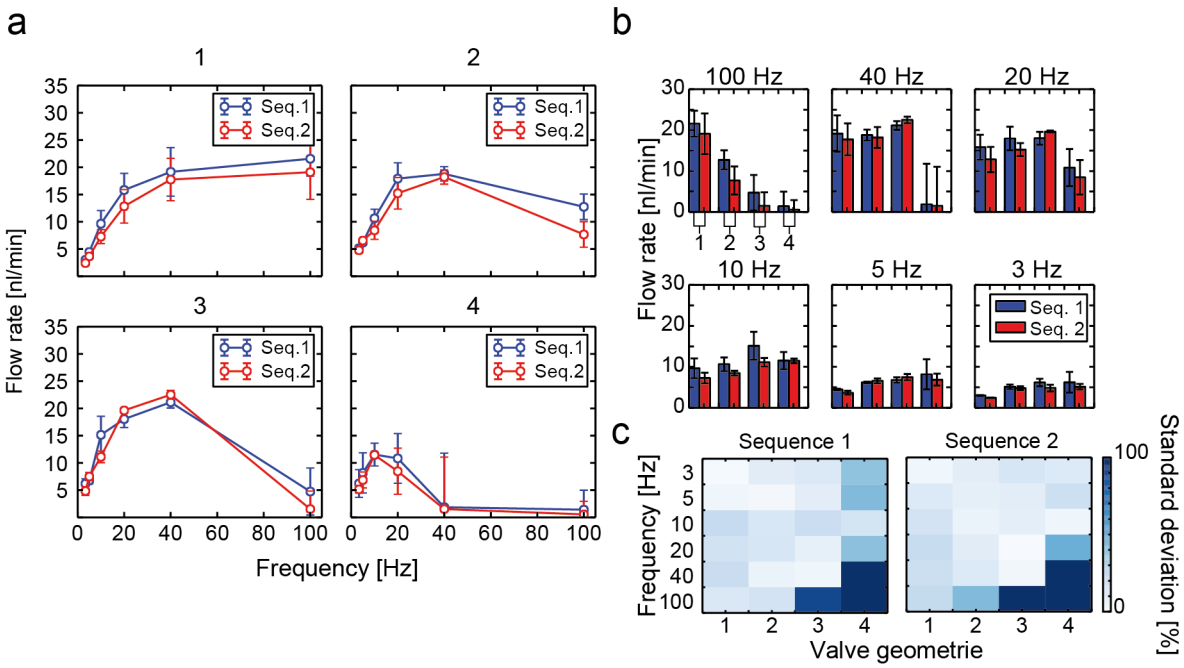

Figure 44: Characterization of achievable flow rates and variations in ellipsoid shaped fluid channels. (a) Mean flow-rates [nl/min] and standard deviations for different geometries and sequences 1 & 2, over frequency [Hz]. (b) Mean flow rates and standard deviation at 3 Hz, 5 Hz, 10 Hz, 20 Hz, 50 Hz and 100 Hz for sequences 1 & 2. (c) Comparison of standard deviations for different geometries, frequencies and sequences 1 & 2.

10.2.6 Pulsation in flow

Pulsation or the oscillation of liquid in microfluidic channels is a common problem when handling small volumes below in range of µL to nl. Distortion in the flow by pulsation causes inhomogeneities. Especially in the field of biology, where microfluidics is more and more applied, gradients caused by such inhomogeneities have to be avoided[107]. Here, the use of syringe pumps is critical, since pulsation are more likely to occur[234]. Subsequently, pressure driven pumps do not cause pulsations, but are bulky and have rather high dosage volumes as their predecessors.

Microfluidic membrane pumps allow to dosage volumes in the range of nl and below, per minute. Yet, our work showed that the effects of pulsation cannot be neglected when using microfluidic membrane pumps.

The rate of pulsation was quantified by calculating the total travelled path of each particle and its reached distance over a certain time using PIV (Figure 45 a). By plotting the distribution for each geometry and frequency, both values should show a linear correlation if no pulsation occurs. Fitting a linear curve through each, the coefficient of determination R^2 is retrieved, where values of $R^2 = 0 \ldots 1$ correspond to the quality of fit with $R^2 = 1$ representing a perfect fit and no pulsation. Detailed information regarding the linear fitting can be found in

Supplement “Rectangular shaped cross-section” and “Ellipsoid shaped cross-section”.

Values of R^2 were determined for every geometry, frequency and sequence for rectangular as well as ellipsoid shaped fluid channels in are shown in Figure 45 b, c**.** Detailed coefficients of determination can be found in Supplement “Coefficient of determination”. For rectangular shaped fluid channels almost no pulsation was found for all geometries at a frequency of 100 Hz and both actuation sequences. Furthermore, geometry no. 1 showed no pulsation at almost the entire used frequencies from 5 Hz to 100 Hz at sequence 1, at 3 Hz minor increase in pulsation was observed. With sequence 2, slight higher rates of pulsation for no. 1 could be seen. Pulsations occurred more often after decreasing the frequency further for the other geometries. The highest rate of pulsation was found for no. 2 at sequence 2 and a frequency of 20 Hz.

In ellipsoid shaped fluid channels pulsation occurred at most geometries, frequencies and sequences. The highest rate of pulsation was found for no. 4 with sequence 2 at 20 Hz. No direct correlation between the rate of pulsation and the decrease in frequency could be found here, as for rectangular shaped channels.

Geometry no. 1 shows only minor changes over entire range of used actuation time and sequence, making it preferable for applications where inhomogeneities in the flow pattern have to be avoided.

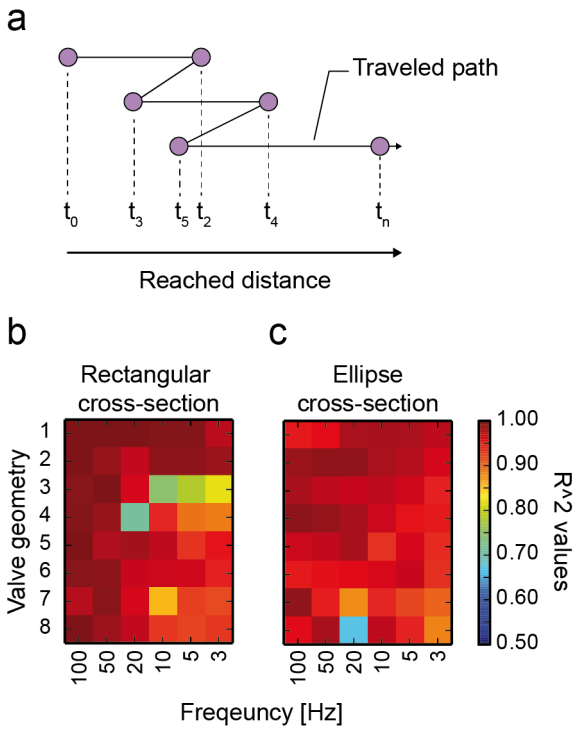

Figure 45: **Characterization of pulsation rate by membrane pumps. (a) Illustration of pulsation described on a single particle being flushed through the channel. (b - c) Rate of pulsation expressed by coefficient of determination R^2, for rectangular (b) and ellipsoid (c) fluid channels.**

10.2.7 Conclusion and outlook

A detailed characterization of microfluidic membrane pumps regarding achievable flow rate and reproducibility was achieved. Different geometries of the valves, making up a pump, as well as actuation frequency and shape of the fluid channel were investigated. Fabrication of multilayered microfluidic PDMS devices was realized by establishing an additional process to the existing creation of microfluidic master molds in a clean room. Replica molding by means of softlitography was extended by introducing the concept of fluid layers and control layers to create membrane valves and peristaltic pumps in microfluidic chips for single-cell analysis.

Further, an experimental setup was established consisting of electromagnetic valves and electronics to control microfluidic membrane valves and pumps respectively. Visualization of fluid flow in the microfluidic channels was done by PIV, recording with an inverted fluorescence microscope. Analysis of recorded fluorescent particle movements was done using automated image analysis and in-house developed software tools.

Analysis of PIV data revealed significant differences in the achievable flow rates as well as reproducibility for different microfluidic membrane pump designs. It can be concluded that rectangular and ellipsoid shaped microfluidic channel achieved comparable flow rates, but reproducibility is significantly lower for ellipsoid shaped ones. Further, the chosen geometry drastically influences the achievable flow rate and reproducibility. It was found, that the width of a valve w_v and the width of the fluid channel w_f have to be the same in order to avoid high variations over repeated experiments.

In addition to the achievable flow rates and reproducibility, the rate of pulsation was investigated for different geometries, frequencies and channel shapes. Pulsations in the fluid flow have to be avoided for microfluidic single cell analysis, since it can be the cause of inhomogeneity. It could be demonstrated that the rate of pulsation is rather affected by the frequency which is used to actuate the valves of a pumps, rather than the geometry or the channel shape.

Integration of microfluidic membrane pumps in applications for single-cell analysis has the advantage to dose small volumes in the range of pL to nL. Further, external devices such as syringe pumps, which may cause pulsations, can be avoided. Still, certain aspects have to be taken into account regarding the design of individual valves in a membrane pump as well as the desired flow rate and what rate of fluctuations can be tolerated.

10.3 Control of oxygen levels in microfluidic devices

Cultivation of a variety of industrial relevant microorganisms, e.g. *Escherichia coli,* takes place in an environment where oxygen is present (aerobic conditions) and needed for enabling growth. Yet, organisms such as *Clostridia* cannot tolerate the presence of oxygen (anaerobic conditions). Strains of *Clostridia*, such as *Clostridium acetobutylicum* (*C. acetobutylicum*) have been used for the production of organic solvents like acetone and butanol (bio-fuels), as an alternative to oil based refinery [273].

Cultivation requires the creation of a special environment with no oxygen in media and the gas phase. Conventionally, this is achieved using air tied cultivation containers filled with medium and removing oxygen by flushing the container with nitrogen or carbon dioxide for a certain period of time. Additional, oxygen scavenger agents can be added to the medium. Measurement of oxygen levels is realized by using a color indicator such as Resazurin[a] for optical control.

Microfluidic PDMS based system offer the advantage of being gas-permeable [274]. Several microfluidic systems have been presented over the last years that allow controlling the level of oxygen in microfluidic devices as depicted in Table 7. Most of these studies focus on the investigating the effects of hyperoxia (oxygen above physiological levels) or hypoxia (oxygen below physiological levels) on a population of cells. Yet, only a few microfluidic systems focus in reducing the concentration of oxygen that far that it would allow the growth of organisms that cannot tolerate the presence of oxygen [275].

[a] 7-Hydroxy-3H-phenoxazin-3-one 10-oxide

Table 7: Overview of concepts regarding the control of dissolved oxygen levels in microfluidic devices. *Use of chemical oxygen scavenger *e.g.* pyrogallol $C_6H_3(OH)_3$.

	Organism	Oxygen indicator	Oxygen control	Application	Ref
Chen *et al.*	Mammalian	DAF-FM[b]	Chemical*	Nitric oxide gradients	[276]
Li *et al.*	Bacteria	RTDP[c]	Gas exchange	Cell migration	[277]
Oppegard *et al.*	Mammalian	PtOEPK[d]	Gas exchange	Oxygen gradients	[278]
Thomas *et al.*	-	PtTFPP	Gas exchange	Proof-of-concept	[279]
Wang *et al.*	Mammalian	PtOEP[e]	Gas exchange	Oxygen gradients	[280]
Chang *et al.*	Mammalian	RTDP	Chemical*	Oxygen gradients	[281]
Chen *et al.*	Mammalian	RTDP	Chemical*	Oxygen gradients	[282]
Funamoto *et al.*	Mammalian	RTDP	Gas exchange	Cell migration	[283]
Peng *et al.*	Mammalian	RTDP	Chemical*	Oxygen gradients	[284]
Adler *et al.*	-	RTDP	Gas exchange	Proof-of-concept	[285]
Lo *et al.*	Mammalian	PtOEPK	Gas exchange	Oxygen gradients	[286]
Forry *et al.*	Mammalian	[f]	Gas exchange	Cell culture	[287]
Lou *et al.*	Mammalian	RTDP	Gas exchange	Oxygen gradients	[288]
Cui *et al.*	Bacteria	PtOEPK	Gas exchange	Oxygen gradients	[275]

[b] 4,5-diaminofluorescein 4-amino-5-methylamino-20,70-difluorofluorescein

[c] Ruthenium tris (2,20 - bipyridil) dichloride hexahydrate

[d] Platinum(II) octaethylporphine ketone

[e] Platinum octaethylporphyrin

[f] 5-(and-6)-carboxy SNARF-1

In course of this thesis, the foundation was laid out for the development, fabrication and characterization of microfluidic devices in order to cultivate obligate anaerobic organisms such as *C. acetobutylicum*.

For measuring the dissolved oxygen (DO) concentration, a sensor layer was integrated consisting of two different fluorescent indicators (MFY[g], PtTFPP[h]), as previously described by Ungerböck and co-workers [289]. The working principle of the oxygen sensor is illustrated in Figure 46. The oxygen sensitive indicator PtTFPP (red channel) is quenched in the presence of oxygen leading to a reduction in the fluorescence signal. In contrast, the signal of MFY (green channel) stays constant and is used to cancel out any inhomogeneity, created by e.g. the fabrication. Hence, the ratio (red channel/green channel) of both signals is formed dividing the signal of PtTFPP by the one of MFY.

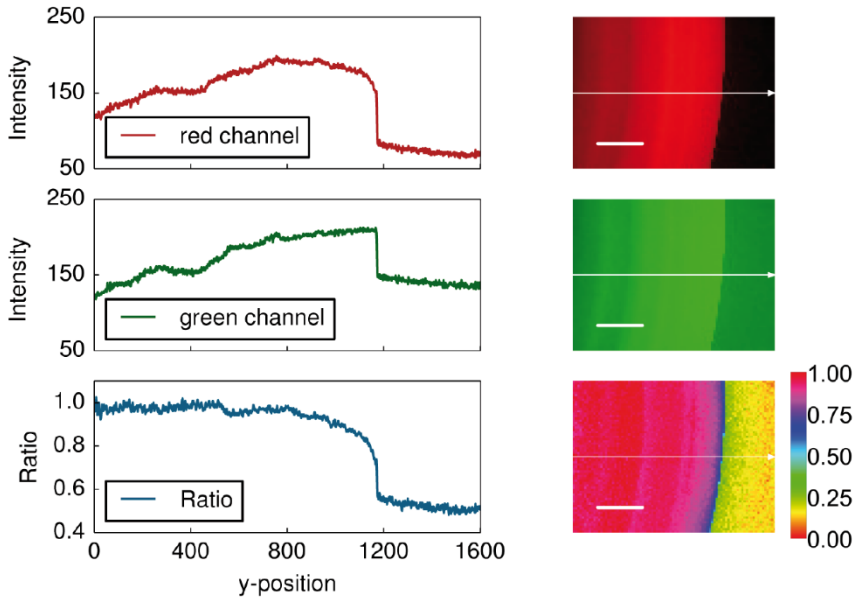

Figure 46: Fluorescence intensity for the red and green channel along the y-position (white arrow) and ratio of red/green channel (Scale bar 200 µm).

[g] Macrolex Fluorescent Yellow

[h] Platinum(II)-5,10,15,20-tetrakis-(2,3,4,5,6-pentafluorphenyl)-porphyrin

Characterization of the oxygen sensor layer was realized with a simple microfluidic device consisting of a liquid channel (Figure 47 a), which is supplied with water at a certain pressure. Gas channels are arranged to each side of the liquid channel for gas exchange. Pure nitrogen (100 %) was flushed through the gas channels, whereas the pressure was increased step wise in the liquid channel. Imaging of the entire device, as depicted in Figure 47 b, allows visualizing the change of DO over the length of the liquid channel. Additionally the increase in the ratio value over the length of the channel is shown in Figure 47 c. Overview of the ratio profiles at different flow velocities is given in Supplement 12.2. In the future, the concept shall be applied for the cultivation of anaerobic organisms.

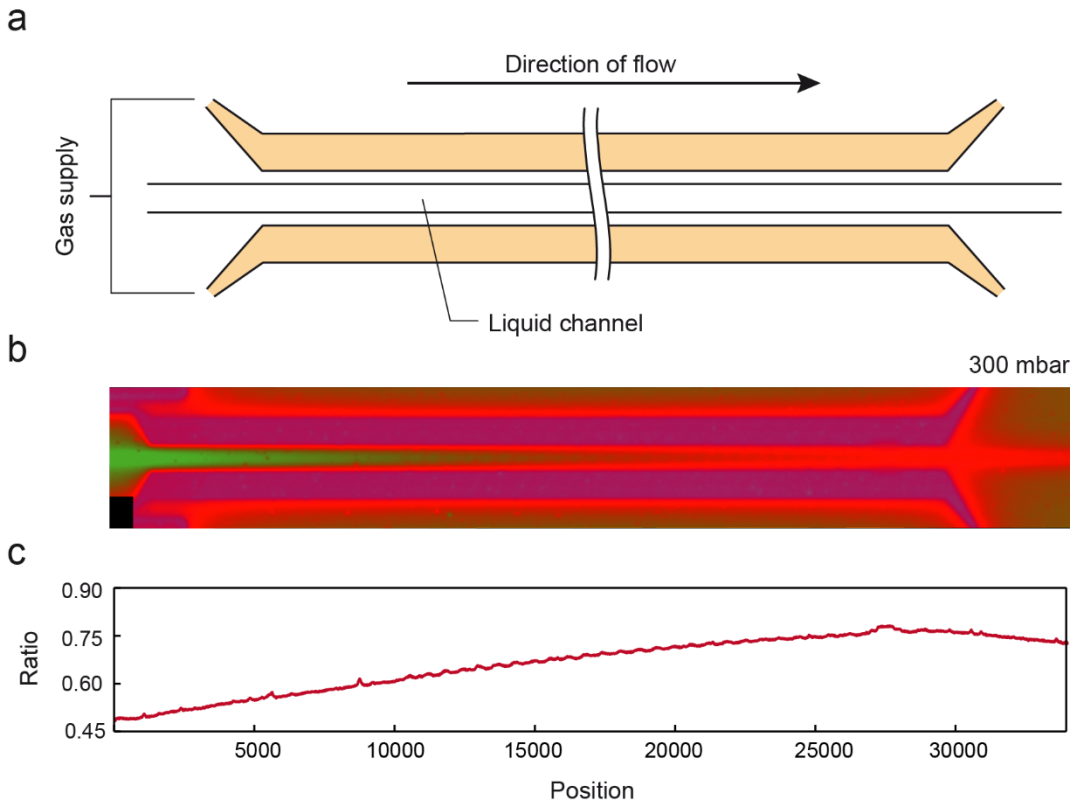

Figure 47: Calibration of oxygen sensor layer. (a) Microfluidic device consisting of a liquid channel and two gas channels arranged in parallel. (b) Ratio image of microfluidic device with water flowing through the liquid channel at 300 mbar and the gas channel filled with 100% nitrogen. (c) Ratio values measured along the liquid channel.

11 References

1. BMBF (2012) The German biotechnology sector 2012.
2. BMBF (2010) Nationale Forschungsstrategie BioÖkonomie 2030 (National Research Strategy BioEconomy 2030).
3. Delvigne F, Zune Q, Lara AR, et al (2014) Metabolic variability in bioprocessing: Implications of microbial phenotypic heterogeneity. Trends Biotechnol 32:608–616. doi: 10.1016/j.tibtech.2014.10.002
4. Lidstrom ME, Konopka MC (2010) The role of physiological heterogeneity in microbial population behavior. Nat Chem Biol 6:705–12. doi: 10.1038/nchembio.436
5. Sanchez A, Golding I (2013) Genetic Determinants and Cellular. Science (80-) 342 :1188–1193. doi: 0.1126/science.1242975
6. Stewart EJ, Madden R, Paul G, Taddei F (2005) Aging and death in an organism that reproduces by morphologically symmetric division. PLoS Biol 3:0295–0300. doi: 10.1371/journal.pbio.0030045
7. Bigger J (1944) Treatment of Staphylococcal Infections With Penicillin By Intermittent Sterilisation. Lancet 244:497–500. doi: 10.1016/S0140-6736(00)74210-3
8. Maisonneuve E, Gerdes K (2014) Review Molecular Mechanisms Underlying Bacterial Persisters. Cell 157:539–548. doi: 10.1016/j.cell.2014.02.050
9. Justice SS, Hunstad D a, Cegelski L, Hultgren SJ (2008) Morphological plasticity as a bacterial survival strategy. Nat Rev Microbiol 6:162–168. doi: 10.1038/nrmicro1820
10. Wa B, Hr H, Rg S, La H (1972) Fluorescence activated cell sorting. Rev Sci Instrum 43:404–9.
11. Binder S, Schendzielorz G, Stabler N, et al (2012) A high-throughput approach to identify genomic variants of bacterial metabolite producers at the single-cell level. Genome Biol 13:R40. doi: 10.1186/gb-2012-13-5-r40
12. Barnett D, Walker B, Landay A, Denny TN (2008) CD4 immunophenotyping in HIV infection. Nat Rev Microbiol 6:7–15. doi: 10.1038/nrmicro1998.CD4
13. Young JW, Locke JCW, Altinok A, et al (2012) Measuring single-cell gene expression dynamics in bacteria using fluorescence time-lapse microscopy. Nat Protoc 7:80–8. doi: 10.1038/nprot.2011.432
14. Elowitz MB (2002) Stochastic Gene Expression in a Single Cell. Science (80-) 297:1183–1186. doi: 10.1126/science.1070919
15. McDonald JC, Chabinyc ML, Metallo SJ, et al (2002) Prototyping of microfluidic devices in poly(dimethylsiloxane) using solid-object printing. Anal Chem 74:1537–1545. doi: 10.1021/ac010938q
16. Martinez AW, Phillips ST, Whitesides GM (2008) Three-dimensional microfluidic devices fabricated in layered paper and tape. Proc Natl Acad Sci U S A 105:19606–19611. doi: 10.1073/pnas.0810903105
17. Díaz-González M, Baldi A (2012) Fabrication of biofunctionalized microfluidic structures by low-temperature wax bonding. Anal Chem 84:7838–7844. doi: 10.1021/ac301512f
18. Weibel DB, Diluzio WR, Whitesides GM (2007) Microfabrication meets microbiology. Nat Rev Microbiol 5:209–18. doi: 10.1038/nrmicro1616

19. Sia SK, Whitesides GM (2003) Microfluidic devices fabricated in poly(dimethylsiloxane) for biological studies. Electrophoresis 24:3563–3576. doi: 10.1002/elps.200305584

20. Wilson ME, Kota N, Kim Y, et al (2011) Fabrication of circular microfluidic channels by combining mechanical micromilling and soft lithography. Lab Chip 11:1550–1555. doi: 10.1039/c0lc00561d

21. Zhao DS, Roy B, McCormick MT, et al (2003) Rapid fabrication of a poly(dimethylsiloxane) microfluidic capillary gel electrophoresis system utilizing high precision machining. Lab Chip 3:93–99. doi: 10.1039/b300577a

22. Bartholomeusz DA, Boutté RW, Andrade JD (2005) Xurography: Rapid prototyping of microstructures using a cutting plotter. J Microelectromechanical Syst 14:1364–1374. doi: 10.1109/JMEMS.2005.859087

23. Li C-W, Cheung CN, Yang J, et al (2003) PDMS-based microfluidic device with multi-height structures fabricated by single-step photolithography using printed circuit board as masters. Analyst 128:1137–1142. doi: 10.1039/b304354a

24. Li CW, Yang J, Tzang CH, et al (2006) Using thermally printed transparency as photomasks to generate microfluidic structures in PDMS material. Sensors Actuators, A Phys 126:463–468. doi: 10.1016/j.sna.2005.10.046

25. Abdelgawad M, Watson MWL, Young EWK, et al (2008) Soft lithography: masters on demand. Lab Chip 8:1379–1385. doi: 10.1039/b804050h

26. Sudarsan AP, Ugaz VM (2004) Printed circuit technology for fabrication of plastic-based microfluidic devices. Anal Chem 76:3229–3235. doi: 10.1021/ac035411n

27. Stephan K, Pittet P, Renaud L, et al (2007) Fast prototyping using a dry film photoresist: microfabrication of soft-lithography masters for microfluidic structures. J Micromechanics Microengineering 17:N69–N74. doi: 10.1088/0960-1317/17/10/N01

28. Yue W, Li CW, Xu T, Yang M (2013) Screen printing of solder resist as master substrates for fabrication of multi-level microfluidic channels and flask-shaped microstructures for cell-based applications. Biosens Bioelectron 41:675–683. doi: 10.1016/j.bios.2012.09.046

29. Tan a, Rodgers K, Murrihy J, et al (2001) Rapid fabrication of microfluidic devices in poly(dimethylsiloxane) by photocopying. Lab Chip 1:7–9. doi: 10.1039/b102905n

30. Nguyen D, McLane J, Lew V, et al (2011) Shrink-film microfluidic education modules: Complete devices within minutes. Biomicrofluidics 5:-. doi: 10.1063/1.3576930

31. Kaigala G V, Ho S, Penterman R, Backhouse CJ (2007) Rapid prototyping of microfluidic devices with a wax printer. Lab Chip 7:384–7. doi: 10.1039/b617764f

32. Li Z, Hou L, Zhang W, Zhu L (2014) Preparation of PDMS microfluidic devices based on drop-on-demand generation of wax molds. Anal Methods 6:4716. doi: 10.1039/c4ay00798k

33. Chuang H-S, Wereley ST (2009) Rapid patterning of slurry-like elastomer composites using a laser-cut tape. J Micromechanics Microengineering 19:097001. doi: 10.1088/0960-1317/19/9/097001

34. Comina G, Suska A, Filippini D (2014) PDMS lab-on-a-chip fabrication using 3D printed templates. Lab Chip 14:424–30. doi: 10.1039/c3lc50956g

35. Liu H-B, Gong H-Q (2009) Templateless prototyping of polydimethylsiloxane microfluidic structures using a pulsed CO2 laser. J Micromechanics Microengineering 19:037002. doi: 10.1088/0960-1317/19/3/037002

36. Bao N, Zhang Q, Xu JJ, Chen HY (2005) Fabrication of poly(dimethylsiloxane) microfluidic system based on masters directly printed with an office laser printer. J Chromatogr A 1089:270–275. doi: 10.1016/j.chroma.2005.07.001

37. Wang L, Kodzius R, Yi X, et al (2012) Prototyping chips in minutes: Direct Laser Plotting (DLP) of functional microfluidic structures. Sensors Actuators, B Chem 168:214–222. doi: 10.1016/j.snb.2012.04.011

38. Chen A, Pan T (2011) Three-dimensional fit-to-flow microfluidic assembly. Biomicrofluidics 5:46505–465059. doi: 10.1063/1.3670368

39. Comina G, Suska A, Filippini D (2014) Low cost lab-on-a-chip prototyping with a consumer grade 3D printer. Lab Chip 14:2978–82. doi: 10.1039/c4lc00394b

40. Yuen PK, Goral VN (2010) Low-cost rapid prototyping of flexible microfluidic devices using a desktop digital craft cutter. Lab Chip 10:384–7. doi: 10.1039/b918089c

41. Wang W, Zhao S, Pan T (2009) Lab-on-a-print: from a single polymer film to three-dimensional integrated microfluidics. Lab Chip 9:1133–7. doi: 10.1039/b816287e

42. Vulto P, Glade N, Altomare L, et al (2005) Microfluidic channel fabrication in dry film resist for production and prototyping of hybrid chips. Lab Chip 5:158–62. doi: 10.1039/b411885e

43. Zhao S, Cong H, Pan T (2009) Direct projection on dry-film photoresist (DP(2)): do-it-yourself three-dimensional polymer microfluidics. Lab Chip 9:1128–32. doi: 10.1039/b817925e

44. Zhao S, Chen A, Revzin A, Pan T (2011) Stereomask lithography (SML): a universal multi-object micro-patterning technique for biological applications. Lab Chip 11:224–30. doi: 10.1039/c0lc00275e

45. Garland SP, Jr TMM, Pan T (2014) Print-to-pattern dry film photoresist lithography. J Micromechanics Microengineering 24:057002. doi: 10.1088/0960-1317/24/5/057002

46. Liao Y, Cheng Y, Liu C, et al (2013) Direct laser writing of sub-50 nm nanofluidic channels buried in glass for three-dimensional micro-nanofluidic integration. Lab Chip 13:1626–31. doi: 10.1039/c3lc41171k

47. Sugioka K, Xu J, Wu D, et al (2014) Femtosecond laser 3D micromachining: a powerful tool for the fabrication of microfluidic, optofluidic, and electrofluidic devices based on glass. Lab Chip 14:3447–58. doi: 10.1039/c4lc00548a

48. Berry SM, Lavanway AJ, Pezzi HM, et al (2014) HIV viral RNA extraction in wax immiscible filtration assisted by surface tension (IFAST) devices. J Mol Diagnostics 16:297–304. doi: 10.1016/j.jmoldx.2014.01.004

49. Yin H, Marshall D (2012) Microfluidics for single cell analysis. Curr Opin Biotechnol 23:110–119. doi: 10.1016/j.copbio.2011.11.002

50. Lee LM, Liu AP (2015) A microfluidic pipette array for mechanophenotyping of cancer cells and mechanical gating of mechanosensitive channels. Lab Chip 15:264–273. doi: 10.1039/C4LC01218F

51. Kim HS, Weiss TL, Thapa HR, et al (2014) A microfluidic photobioreactor array demonstrating high-throughput screening for microalgal oil production. Lab Chip 14:1415–25. doi: 10.1039/c3lc51396c

52. Black J Microbiology_ Principles and Explorations, 8th Edition - Jacquelyn G. Black.pdf, 9th ed. Wiley-Blackwell

53. Reece JB (2012) Campbell biology : concepts & connections, 8th ed. Benjamin Cummings

54. Fritzsch FSO, Rosenthal K, Kampert A, et al (2012) Picoliter nDEP traps enable time-resolved contactless single bacterial cell analysis in controlled microenvironments. Lab Chip 13:397–408. doi: 10.1039/c2lc41092c

55. Eriksson E, Sott K, Lundqvist F, et al (2010) A microfluidic device for reversible environmental changes around single cells using optical tweezers for cell selection and positioning. Lab Chip 10:617–625. doi: 10.1039/b913587a

56. Ding X, Lin S-CS, Kiraly B, et al (2012) On-chip manipulation of single microparticles, cells, and organisms using surface acoustic waves. Proc Natl Acad Sci 109:11105–11109. doi: 10.1073/pnas.1209288109

57. Shi J, Ahmed D, Mao X, et al (2009) Acoustic tweezers: patterning cells and microparticles using standing surface acoustic waves (SSAW). Lab Chip 9:2890–5. doi: 10.1039/b910595f

58. Mazutis L, Gilbert J, Ung WL, et al (2013) Single-cell analysis and sorting using droplet-based microfluidics. Nat Protoc 8:870–891. doi: 10.1038/nprot.2013.046

59. Brouzes E, Medkova M, Savenelli N, et al (2009) Droplet microfluidic technology for single-cell high-throughput screening. Proc Natl Acad Sci U S A 106:14195–200. doi: 10.1073/pnas.0903542106

60. Ashkin A, Dziedzic JM (1987) Optical trapping and manipulation of viruses and bacteria. Science 235:1517–1520. doi: 10.1126/science.3547653

61. Eriksson E, Enger J, Nordlander B, et al (2007) A microfluidic system in combination with optical tweezers for analyzing rapid and reversible cytological alterations in single cells upon environmental changes. Lab Chip 7:71–76. doi: 10.1039/b613650h

62. Probst C, Grünberger A, Wiechert W, Kohlheyer D (2013) Microfluidic growth chambers with optical tweezers for full spatial single-cell control and analysis of evolving microbes. J Microbiol Methods 95:470–476. doi: 10.1016/j.mimet.2013.09.002

63. Robert D, Pamme N, Conjeaud H, et al (2011) Cell sorting by endocytotic capacity in a microfluidic magnetophoresis device. Lab Chip 11:1902–1910. doi: 10.1039/C0LC00656D

64. Osman O, Zanini LF, Frenea-Robin M, et al (2012) Monitoring the endocytosis of magnetic nanoparticles by cells using permanent micro-flux sources. Biomed Microdevices 14:947–954. doi: 10.1007/s10544-012-9673-4

65. Eun YJ, Utada AS, Copeland MF, et al (2011) Encapsulating bacteria in agarose microparticles using microfluidics for high-throughput cell analysis and isolation. ACS Chem Biol 6:260–266. doi: 10.1021/cb100336p

66. Weitz M, Mueckl A, Kapsner K, et al (2014) Communication and computation by bacteria compartmentalized within microemulsion droplets. J Am Chem Soc 136:72–75. doi: 10.1021/ja411132w

67. Leung K, Zahn H, Leaver T, et al (2012) A programmable droplet-based microfluidic device applied to multiparameter analysis of single microbes and microbial communities. Proc Natl Acad Sci 109:7665–7670. doi: 10.1073/pnas.1106752109

68. Tanyeri M, Ranka M, Sittipolkul N, Schroeder CM (2011) A microfluidic-based hydrodynamic trap: design and implementation. Lab Chip 11:1786–1794. doi: 10.1039/c0lc00709a

69. Johnson-Chavarria EM, Agrawal U, Tanyeri M, et al (2014) Automated single cell microbioreactor for monitoring intracellular dynamics and cell growth in free solution. Lab Chip 14:1–10. doi: 10.1039/c4lc00057a

70. Wang X, Gou X, Chen S, et al (2013) Cell manipulation tool with combined microwell array and optical tweezers for cell isolation and deposition. J Micromechanics Microengineering 23:075006. doi: 10.1088/0960-1317/23/7/075006

71. Wang X, Chen S, Chow YT, et al (2013) A microengineered cell fusion approach with combined optical tweezers and microwell array technologies. RSC Adv 3:23589. doi: 10.1039/c3ra44108c

72. Landenberger B, Hofemann H, Wadle S, Rohrbach A (2012) Microfluidic sorting of arbitrary cells with dynamic optical tweezers. Lab Chip 12:3177–3183. doi: 10.1039/C2LC21099A

73. Evander M, Johansson L, Lilliehorn T, et al (2007) Noninvasive acoustic cell trapping in a microfluidic perfusion system for online bioassays. Anal Chem 79:2984–2991. doi: 10.1021/ac061576v

74. Chen A, Byvank T, Chang W-J, et al (2013) On-chip magnetic separation and encapsulation of cells in droplets. Lab Chip 13:1172–1181. doi: 10.1039/C2LC41201B

75. Baret J-C, Miller OJ, Taly V, et al (2009) Fluorescence-activated droplet sorting (FADS): efficient microfluidic cell sorting based on enzymatic activity. Lab Chip 9:1850–8. doi: 10.1039/b902504a

76. Gregory C, Veeman M (2013) 3D-printed microwell arrays for Ciona microinjection and timelapse imaging. PLoS One 8:e82307. doi: 10.1371/journal.pone.0082307

77. Wood DK, Weingeist DM, Bhatia SN, Engelward BP (2010) Single cell trapping and DNA damage analysis using microwell arrays. Proc Natl Acad Sci 107:10008–10013. doi: 10.1073/pnas.1004056107

78. Woodruff K, Fidalgo LM, Gobaa S, et al (2013) Live mammalian cell arrays. Nat Methods 10:1–5. doi: 10.1038/nmeth.2473

79. Zaban B, Liu W, Jiang X, Nick P (2014) Plant cells use auxin efflux to explore geometry. Sci Rep 4:5852. doi: 10.1038/srep05852

80. Park MC, Hur JY, Kwon KW, et al (2006) Single-cell level array of yeast cells in pumpless microfluidic channels induced by receding meniscus. Proc IEEE Sensors 6:638–641. doi: 10.1109/ICSENS.2007.355549

81. Yu J, Liu Z, Liu Q, et al (2009) A polyethylene glycol (PEG) microfluidic chip with nanostructures for bacteria rapid patterning and detection. Sensors Actuators, A Phys 154:288–294. doi: 10.1016/j.sna.2008.07.005

82. Ingham CJ, Sprenkels A, Bomer J, et al (2007) The micro-Petri dish, a million-well growth chip for the culture and high-throughput screening of microorganisms. Proc Natl Acad Sci U S A 104:18217–18222. doi: 10.1073/pnas.0701693104

83. Shen C, Xu P, Huang Z, et al (2014) Bacterial chemotaxis on SlipChip. Lab Chip 14:3074–80. doi: 10.1039/c4lc00213j

84. Jiang X, Hu J, Petersen ER, et al (2013) Probing single- to multi-cell level charge transport in Geobacter sulfurreducens DL-1. Nat Commun 4:2751. doi: 10.1038/ncomms3751

85. Kim HJ, Boedicker JQ, Choi JW, Ismagilov RF (2008) Defined spatial structure stabilizes a synthetic multispecies bacterial community. Proc Natl Acad Sci U S A 105:18188–18193. doi: 10.1073/pnas.0807935105

86. Renner LD, Weibel DB (2011) Cardiolipin microdomains localize to negatively curved regions of Escherichia coli membranes. Proc Natl Acad Sci U S A 108:6264–6269. doi: 10.1073/pnas.1015757108

87. Tan W-H, Takeuchi S (2007) A trap-and-release integrated microfluidic system for dynamic microarray applications. Proc Natl Acad Sci USA 104:1146–51. doi: 10.1073/pnas.0606625104

88. Kobel S, Valero A, Latt J, et al (2010) Optimization of microfluidic single cell trapping for long-term on-chip culture. Lab Chip 10:857–863. doi: 10.1039/b918055a

89. Di Carlo D, Aghdam N, Lee LP (2006) Single-cell enzyme concentrations, kinetics, and inhibition analysis using high-density hydrodynamic cell isolation arrays. Anal Chem 78:4925–4930. doi: 10.1021/ac060541s

90. Di Carlo D, Wu LY, Lee LP (2006) Dynamic single cell culture array. Lab Chip 6:1445–1449. doi: 10.1039/b605937f

91. Ryu W, Huang Z, Sun Park J, et al (2008) Open micro-fluidic system for atomic force microscopy-guided in situ electrochemical probing of a single cell. Lab Chip 8:1460–1467. doi: 10.1039/b803450h

92. Ryley J, Pereira-Smith OM (2006) Microfluidics device for single cell gene expression analysis in Saccharomyces cerevisiae. Yeast 23:1065–1073. doi: 10.1002/yea.1412

93. Lee SS, Avalos Vizcarra I, Huberts DHEW, et al (2012) Whole lifespan microscopic observation of budding yeast aging through a microfluidic dissection platform. Proc Natl Acad Sci U S A 109:4916–20. doi: 10.1073/pnas.1113505109

94. Probst C, Grünberger A, Wiechert W, Kohlheyer D (2013) Polydimethylsiloxane (PDMS) sub-micron traps for single-cell analysis of bacteria. Micromachines 4:357–369. doi: 10.3390/mi4040357

95. Stratz S, Eyer K, Kurth F, Dittrich PS (2014) On-chip enzyme quantification of single Escherichia coli bacteria by immunoassay-based analysis. Anal Chem 86:12375–12381. doi: 10.1021/ac503766d

96. Kim M-C, Isenberg BC, Sutin J, et al (2011) Programmed trapping of individual bacteria using micrometre-size sieves. Lab Chip 11:1089–1095. doi: 10.1039/c0lc00362j

97. Balaban NQ, Merrin J, Chait R, et al (2004) Bacterial persistence as a phenotypic switch. Science 305:1622–1625. doi: 10.1126/science.1099390

98. Wang P, Robert L, Pelletier J, et al (2010) Robust Growth of Escherichia coli. Curr Biol 20:1099–1103. doi: DOI 10.1016/j.cub.2010.04.045

99. Moffitt JR, Lee JB, Cluzel P (2012) The single-cell chemostat: an agarose-based, microfluidic device for high-throughput, single-cell studies of bacteria and bacterial communities. Lab Chip 12:1487. doi: 10.1039/c2lc00009a

100. Long Z, Nugent E, Javer A, et al (2013) Microfluidic chemostat for measuring single cell dynamics in bacteria. Lab Chip 13:947–954. doi: 10.1039/c2lc41196b

101. Long Z, Olliver A, Brambilla E, et al (2014) Measuring bacterial adaptation dynamics at the single-cell level using a microfluidic chemostat and time-lapse fluorescence microscopy. Analyst 139:5254–62. doi: 10.1039/c4an00877d

102. Javer A, Kuwada NJ, Long Z, et al (2014) Persistent super-diffusive motion of Escherichia coli chromosomal loci. Nat Commun 5:3854. doi: 10.1038/ncomms4854

103. Amir A, Babaeipour F, McIntosh DB, et al (2014) Bending forces plastically deform growing bacterial cell walls. Proc Natl Acad Sci U S A 111:5778–83. doi: 10.1073/pnas.1317497111

104. Groisman A, Lobo C, Cho H, et al (2005) A microfluidic chemostat for experiments with bacterial and yeast cells. Nat Methods 2:685–9. doi: 10.1038/nmeth784

105. Dénervaud N, Becker J, Delgado-Gonzalo R, et al (2013) A chemostat array enables the spatio-temporal analysis of the yeast proteome. TL - 110. Proc Natl Acad Sci U S A 110 VN - :15842–15847. doi: 10.1073/pnas.1308265110

106. Prindle A, Samayoa P, Razinkov I, et al (2012) A sensing array of radically coupled genetic "biopixels". Nature 481:39–44. doi: 10.1038/nature10722

107. Grünberger A, Paczia N, Probst C, et al (2012) A disposable picolitre bioreactor for cultivation and investigation of industrially relevant bacteria on the single cell level. Lab Chip 12:2060–2068. doi: 10.1039/c2lc40156h

108. Braschler T, Johann R, Heule M, et al (2005) Gentle cell trapping and release on a microfluidic chip by in situ alginate hydrogel formation. Lab Chip 5:553–9. doi: 10.1039/b417604a

109. Krajniak J, Lu H (2010) Long-term high-resolution imaging and culture of C. elegans in chip-gel hybrid microfluidic device for developmental studies. Lab Chip 10:1862–8. doi: 10.1039/c001986k

110. Braschler T, Valero A, Colella L, et al (2010) Fluidic microstructuring of alginate hydrogels for the single cell niche. Lab Chip 10:2771–2777. doi: 10.1039/c004988c

111. Kim MS, Yeon JH, Park JK (2007) A microfluidic platform for 3-dimensional cell culture and cell-based assays. Biomed Microdevices 9:25–34. doi: 10.1007/s10544-006-9016-4

112. Chen MCW, Gupta M, Cheung KC (2010) Alginate-based microfluidic system for tumor spheroid formation and anticancer agent screening. Biomed Microdevices 12:647–654. doi: 10.1007/s10544-010-9417-2

113. Frisk T, Rydholm S, Liebmann T, et al (2007) A microfluidic device for parallel 3-D cell cultures in asymmetric environments. Electrophoresis 28:4705–4712. doi: 10.1002/elps.200700342

114. Timp W, Mirsaidov U, Matsudaira P, Timp G (2009) Jamming prokaryotic cell-to-cell communications in a model biofilm. Lab Chip 9:925–34. doi: 10.1039/b810157d

115. Balagaddé FK (2014) Long-Term Monitoring of Bacteria Undergoing Programmed Population Control in a Microchemostat Long-Term Monitoring of Bacteria Undergoing Programmed Population Control in a Microchemostat. Science (80-) 137:137–140. doi: 10.1126/science.1109173

116. Austin RH, Tung C, Lambert G, et al (2010) An introduction to micro-ecology patches. Chem Soc Rev 39:1049–1059. doi: 10.1039/B911230H

117. Männik J, Driessen R, Galajda P, et al (2009) Bacterial growth and motility in sub-micron constrictions. Proc Natl Acad Sci U S A 106:14861–14866. doi: 10.1073/pnas.0907542106

118. Männik J, Wu F, Hol FJH, et al (2012) Robustness and accuracy of cell division in Escherichia coli in diverse cell shapes. Proc Natl Acad Sci U S A 109:6957–62. doi: 10.1073/pnas.1120854109

119. Keymer JE, Galajda P, Muldoon C, et al (2006) Bacterial metapopulations in nanofabricated landscapes. Proc Natl Acad Sci U S A 103:17290–17295. doi: 10.1073/pnas.0607971103

120. Hol FJH, Galajda P, Nagy K, et al (2013) Spatial Structure Facilitates Cooperation in a Social Dilemma: Empirical Evidence from a Bacterial Community. PLoS One 8:e77042. doi: 10.1371/journal.pone.0077042

121. Hol FJH, Voges MJ, Dekker C, Keymer JE (2014) Nutrient-responsive regulation determines biodiversity in a colicin-mediated bacterial community. BMC Biol 12:68. doi: 10.1186/s12915-014-0068-2

122. van Vliet S, Hol FJH, Weenink T, et al (2014) The effects of chemical interactions and culture history on the colonization of structured habitats by competing bacterial populations. BMC Microbiol 14:116. doi: 10.1186/1471-2180-14-116

123. Tsimring L, Hasty J, Danino T, et al (2010) A synchronized quorum of genetic clocks. Nature 463:326–330. doi: 10.1038/nature08753

124. Dai J, Yoon SH, Sim HY, et al (2013) Charting microbial phenotypes in multiplex nanoliter batch bioreactors. Anal Chem 85:5892–5899. doi: 10.1021/ac400648z

125. Park J, Wu J, Polymenis M, Han A (2013) Microchemostat array with small-volume fraction replenishment for steady-state microbial culture. Lab Chip 13:4217–24. doi: 10.1039/c3lc50665g

126. Taylor RJ, Falconnet D, Niemistö A, et al (2009) Dynamic analysis of MAPK signaling using a high-throughput microfluidic single-cell imaging platform. Proc Natl Acad Sci U S A 106:3758–63. doi: 10.1073/pnas.0813416106

127. Baumgartner BL, Bennett MR, Ferry M, et al (2011) Antagonistic gene transcripts regulate adaptation to new growth environments. Proc Natl Acad Sci 108:21087–21092. doi: 10.1073/pnas.1111408109

128. Cookson S, Ostroff N, Pang WL, et al (2005) Monitoring dynamics of single-cell gene expression over multiple cell cycles. Mol Syst Biol 1:2005.0024. doi: 10.1038/msb4100032

129. Nobs J-B, Maerkl SJ (2014) Long-term single cell analysis of S. pombe on a microfluidic microchemostat array. PLoS One 9:e93466. doi: 10.1371/journal.pone.0093466

130. Paliwal S, Iglesias P a, Campbell K, et al (2007) MAPK-mediated bimodal gene expression and adaptive gradient sensing in yeast. Nature 446:46–51. doi: 10.1038/nature05561

131. Cheong R, Wang CJ, Levchenko A (2009) High content cell screening in a microfluidic device. Mol Cell Proteomics 8:433–42. doi: 10.1074/mcp.M800291-MCP200

132. Liu W, Li L, Wang X, et al (2010) An integrated microfluidic system for studying cell-microenvironmental interactions versatilely and dynamically. Lab Chip 10:1717–1724. doi: 10.1039/c001049a

133. Albrecht DR, Underhill GH, Resnikoff J, et al (2010) Microfluidics-integrated time-lapse imaging for analysis of cellular dynamics. Integr Biol (Camb) 2:278–287. doi: 10.1039/b923699f

134. Hung PJ, Lee PJ, Sabounchi P, et al (2005) Continuous perfusion microfluidic cell culture array for high-throughput cell-based assays. Biotechnol Bioeng 89:1–8. doi: 10.1002/bit.20289

135. Wang H, Kim J, Jayaraman A, Han A (2014) Microfluidic geometric metering-based multi-reagent mixture generator for robust live cell screening array. Biomed Microdevices 16:887–896. doi: 10.1007/s10544-014-9893-x

136. Chung K, Zhan M, Srinivasan J, et al (2011) Microfluidic chamber arrays for whole-organism behavior-based chemical screening. Lab Chip 11:3689–97. doi: 10.1039/c1lc20400a

137. Yang J, Chen Z, Ching P, et al (2013) An integrated microfluidic platform for evaluating in vivo antimicrobial activity of natural compounds using a whole-animal infection model. Lab Chip 13:3373–82. doi: 10.1039/c3lc50264c

138. Chung J, Ingram PN, Bersano-Begey T, Yoon E (2014) Traceable clonal culture and chemodrug assay of heterogeneous prostate carcinoma PC3 cells in microfluidic single cell array chips. Biomicrofluidics 8:064103. doi: 10.1063/1.4900823

139. Gómez-Sjöberg R, Leyrat AA, Pirone DM, et al (2007) Versatile, fully automated, microfluidic cell culture system. Anal Chem 79:8557–8563. doi: 10.1021/ac071311w

140. Kellogg RA, berg RG oacute mez-S ouml, Leyrat AA, Tay S scedil (2014) High-throughput microfluidic single-cell analysis pipeline for studies of signaling dynamics. Nat Protoc 9:1713–1726. doi: 10.1038/nprot.2014.120

141. Mather W, Mondragón-Palomino O, Danino T, et al (2010) Streaming instability in growing cell populations. Phys Rev Lett. doi: 10.1103/PhysRevLett.104.208101

142. Norman TM, Lord ND, Paulsson J, Losick R (2013) Memory and modularity in cell-fate decision making. Nature 503:481–6. doi: 10.1038/nature12804

143. Caspi Y (2014) Deformation of filamentous Escherichia coli cells in a microfluidic device: A new technique to study cell mechanics. PLoS One 9:e83775. doi: 10.1371/journal.pone.0083775

144. Moolman MC, Huang Z, Krishnan ST, et al (2013) Electron beam fabrication of a microfluidic device for studying submicron-scale bacteria. J Nanobiotechnology 11:12. doi: 10.1186/1477-3155-11-12

145. Chen P, Xu L, Liu J, et al (2014) Nanoscale probing the kinetics of oriented bacterial cell growth using atomic force microscopy. Small 10:3018–3025. doi: 10.1002/smll.201303724

146. Pelletier J, Halvorsen K, Ha B-Y, et al (2012) Physical manipulation of the Escherichia coli chromosome reveals its soft nature. Proc Natl Acad Sci 109:E2649–E2656. doi: 10.1073/pnas.1208689109

147. Lee H, Kim SA, Coakley S, et al (2014) A multi-channel device for high-density target-selective stimulation and long-term monitoring of cells and subcellular features in *C. elegans*. Lab Chip 14:4513–22. doi: 10.1039/c4lc00789a

148. Teng S-W, Mukherji S, Moffitt JR, et al (2013) Robust circadian oscillations in growing cyanobacteria require transcriptional feedback. Science 340:737–40. doi: 10.1126/science.1230996

149. Wang P, Robert L, Pelletier J, et al (2010) Robust growth of escherichia coli. Curr Biol 20:1099–1103. doi: 10.1016/j.cub.2010.04.045

150. Wlodkowic D, Faley S, Zagnoni M, et al (2009) Microfluidic single-cell array cytometry for the analysis of tumor apoptosis. Anal Chem 81:5517–5523. doi: 10.1021/ac9008463

151. Eyer K, Stratz S, Kuhn P, et al (2013) Implementing enzyme-linked immunosorbent assays on a microfluidic chip to quantify intracellular molecules in single cells. Anal Chem 85:3280–3287. doi: 10.1021/ac303628j

152. Eyer K, Kuhn P, Hanke C, Dittrich PS (2012) A microchamber array for single cell isolation and analysis of intracellular biomolecules. Lab Chip 12:765–72. doi: 10.1039/c2lc20876h

153. Syme CD, Sirimuthu NMS, Faley SL, Cooper JM (2010) SERS mapping of nanoparticle labels in single cells using a microfluidic chip. Chem Commun (Camb) 46:7921–3. doi: 10.1039/c0cc02209h

154. Skelley AM, Kirak O, Suh H, et al (2009) Micro uidic control of cell pairing and fusion. Nat Methods 6:147–152. doi: 10.1038/NMETH.1290

155. White AK, VanInsberghe M, Petriv OI, et al (2011) High-throughput microfluidic single-cell RT-qPCR. Proc Natl Acad Sci 108:13999–14004. doi: 10.1073/pnas.1019446108

156. Chingozha L, Zhan M, Zhu C, Lu H (2014) A generalizable, tunable microfluidic platform for delivering fast temporally varying chemical signals to probe single-cell response dynamics. Anal Chem 86:10138–10147. doi: 10.1021/ac5019843

157. Lin L, Chu Y-S, Thiery JP, et al (2013) Microfluidic cell trap array for controlled positioning of single cells on adhesive micropatterns. Lab Chip 13:714–21. doi: 10.1039/c2lc41070b

158. Wheeler AR, Throndset WR, Whelan RJ, et al (2003) Microfluidic device for single-cell analysis. Anal Chem 75:3581–3586. doi: 10.1021/ac0340758

159. Banaeiyan AA, Ahmadpour D, Adiels CB, Goksör M (2013) Hydrodynamic cell trapping for high throughput single-cell applications. Micromachines 4:414–430. doi: 10.3390/mi4040414

160. Lu Y, Gao J, Zhang DD, et al (2013) Single cell antimicrobial susceptibility testing by confined microchannels and electrokinetic loading. Anal Chem 85:3971–3976. doi: 10.1021/ac4004248

161. Hong S, Pan Q, Lee LP (2012) Single-cell level co-culture platform for intercellular communication. Integr Biol 4:374. doi: 10.1039/c2ib00166g

162. Frimat J-P, Becker M, Chiang Y-Y, et al (2011) A microfluidic array with cellular valving for single cell co-culture. Lab Chip 11:231–237. doi: 10.1039/C0LC00172D

163. Kobel SA, Burri O, Griffa A, et al (2012) Automated analysis of single stem cells in microfluidic traps. Lab Chip 12:2843–2849. doi: 10.1039/c2lc40317j

164. Terao K, Gel M, Okonogi A, et al (2014) Subcellular glucose exposure biases the spatial distribution of insulin granules in single pancreatic beta cells. Sci Rep 4:4123. doi: 10.1038/srep04123

165. Chung K, Kim Y, Kanodia JS, et al (2011) A microfluidic array for large-scale ordering and orientation of embryos. Nat Methods 8:171–176. doi: 10.1038/nmeth.1548

166. Teshima T, Ishihara H, Iwai K, et al (2010) A dynamic microarray device for paired bead-based analysis. Lab Chip 10:2443–8. doi: 10.1039/c004986g

167. Rowat AC, Bird JC, Agresti JJ, et al (2009) Tracking Lineages of Single Cells in Lines Using a Microfluidic Device. Proc Natl Acad Sci 106:18149–18154. doi: 10.1073/pnas.0903163106

168. Boedicker JQ, Vincent ME, Ismagilov RF (2009) Microfluidic confinement of single cells of bacteria in small volumes initiates high-density behavior of quorum sensing and growth and reveals its variability. Angew Chemie - Int Ed 48:5908–5911. doi: 10.1002/anie.200901550

169. Quadri SMS (2015) Single-cell western blotting. West Blotting Methods Protoc 11:455–464. doi: 10.1007/978-1-4939-2694-7_46

170. Guldevall K, Vanherberghen B, Frisk T, et al (2010) Imaging immune surveillance of individual natural killer cells confined in microwell arrays. PLoS One 5:e15453. doi: 10.1371/journal.pone.0015453

171. Han Q, Bagheri N, Bradshaw EM, et al (2012) From the Cover: Polyfunctional responses by human T cells result from sequential release of cytokines. Proc Natl Acad Sci 109:1607–1612. doi: 10.1073/pnas.1117194109

172. Lecault V, VanInsberghe M, Sekulovic S, et al (2011) High-throughput analysis of single hematopoietic stem cell proliferation in microfluidic cell culture arrays. Nat Methods 8:581–586. doi: 10.1038/nmeth.1614

173. Rettig JR, Folch A (2005) Large-scale single-cell trapping and imaging using microwell arrays. Anal Chem 77:5628–5634. doi: 10.1021/ac0505977

174. Kang E, Choi YY, Jun Y, et al (2010) Development of a multi-layer microfluidic array chip to culture and replate uniform-sized embryoid bodies without manual cell retrieval. Lab Chip 10:2651–4. doi: 10.1039/c0lc00005a

175. Wang T, Zhang M, Dreher DD, Zeng Y (2013) Ultrasensitive microfluidic solid-phase ELISA using an actuatable microwell-patterned PDMS chip. Lab Chip 13:4190–7. doi: 10.1039/c3lc50783a

176. Khademhosseini A, Yeh J, Eng G, et al (2005) Cell docking inside microwells within reversibly sealed microfluidic channels for fabricating multiphenotype cell arrays. Lab Chip 5:1380. doi: 10.1039/b508096g

177. Han C, Zhang Q, Ma R, et al (2010) Integration of single oocyte trapping, in vitro fertilization and embryo culture in a microwell-structured microfluidic device. Lab Chip 10:2848–2854. doi: 10.1039/c005296e

178. Lee H, Crane MM, Zhang Y, Lu H (2013) Quantitative screening of genes regulating tryptophan hydroxylase transcription in Caenorhabditis elegans using microfluidics and an adaptive algorithm. Integr Biol (Camb) 5:372–80. doi: 10.1039/c2ib20078c

179. Jen CP, Hsiao JH, Maslov NA (2012) Single-cell chemical lysis on microfluidic chips with arrays of microwells. Sensors 12:347–358. doi: 10.3390/s120100347

180. Henley WH, Dennis PJ, Ramsey JM (2012) Fabrication of microfluidic devices containing patterned microwell arrays. Anal Chem 84:1776–1780. doi: 10.1021/ac202445g

181. Song K, Jeong H-H, Jin SH, et al (2014) Optimization of microwell-based cell docking in microvalve integrated microfluidic device. BioChip J 8:227–233. doi: 10.1007/s13206-014-8309-6

182. Lindström S, Eriksson M, Vazin T, et al (2009) High-density microwell chip for culture and analysis of stem cells. PLoS One 4:e6997. doi: 10.1371/journal.pone.0006997

183. Tan W-H, Takeuchi S (2008) Dynamic microarray system with gentle retrieval mechanism for cell-encapsulating hydrogel beads. Lab Chip 8:259–266. doi: 10.1039/b714573j

184. Grünberger A, van Ooyen J, Paczia N, et al (2013) Beyond growth rate 0.6: Corynebacterium glutamicum cultivated in highly diluted environments. Biotechnol Bioeng 110:220–228. doi: 10.1002/bit.24616

185. Mustafi N, Grünberger A, Kohlheyer D, et al (2012) The development and application of a single-cell biosensor for the detection of l-methionine and branched-chain amino acids. Metab Eng 14:449–457. doi: 10.1016/j.ymben.2012.02.002

186. Schendzielorz G, Dippong M, Gruenberger A, et al (2014) Taking control over control: Use of product sensing in single cells to remove flux control at key enzymes in biosynthesis pathways. ACS Synth Biol 3:21–29. doi: 10.1021/sb400059y

187. Miesenböck G, De Angelis D a, Rothman JE (1998) Visualizing secretion and synaptic transmission with pH-sensitive green fluorescent proteins. Nature 394:192–5. doi: 10.1038/28190

188. Choi K, Ng AHC, Fobel R, Wheeler AR (2012) Digital Microfluidics. Annu Rev Anal Chem 5:413–440. doi: doi:10.1146/annurev-anchem-062011-143028

189. Pei Yu C, Ohta AT, Wu MC (2005) Massively parallel manipulation of single cells and microparticles using optical images. Nature 436:370–372. doi: 10.1038/nature03831

190. Dusny C, Fritzsch FSO, Frick O, Schmid A (2012) Isolated microbial single cells and resulting micropopulations grow: Faster in controlled environments. Appl Environ Microbiol 78:7132–7136. doi: 10.1128/AEM.01624-12

191. Hsu H, Ohta AT, Chiou P-Y, et al (2010) Phototransistor-based optoelectronic tweezers for dynamic cell manipulation in cell culture media. Lab Chip 10:165–172. doi: 10.1039/b906593h

192. Kortmann H, Chasanis P, Blank LM, et al (2009) The Envirostat - a new bioreactor concept. Lab Chip 9:576–585. doi: 10.1039/b809150a

193. Kim SH, Yamamoto T, Fourmy D, Fujii T (2011) Electroactive microwell arrays for highly efficient single-cell trapping and analysis. Small 7:3239–3247. doi: 10.1002/smll.201101028

194. Ramser K, Hanstorp D (2010) Optical manipulation for single-cell studies. J Biophotonics 3:187–206. doi: 10.1002/jbio.200910050

195. Johann RM (2006) Cell trapping in microfluidic chips. Anal Bioanal Chem 385:408–412. doi: 10.1007/s00216-006-0369-6

196. Svoboda K, Block SM (1994) Biological applications of optical forces. Ann Rev Biophys Biomol Str 23:247–285. doi: doi:10.1146/annurev.bb.23.060194.001335

197. Khine M, Lau A, Ionescu-Zanetti C, et al (2005) A single cell electroporation chip. Lab Chip 5:38–43. doi: 10.1039/b408352k

198. Lee PJ, Hung PJ, Shaw R, et al (2005) Microfluidic application-specific integrated device for monitoring direct cell-cell communication via gap junctions between individual cell pairs. Appl Phys Lett 86:1–3. doi: 10.1063/1.1938253

199. Valero A, Post JN, van Nieuwkasteele JW, et al (2008) Gene transfer and protein dynamics in stem cells using single cell electroporation in a microfluidic device. Lab Chip 8:62–67. doi: 10.1039/b713420g

200. Zhu Z, Frey O, Ottoz DS, et al (2012) Microfluidic single-cell cultivation chip with controllable immobilization and selective release of yeast cells. Lab Chip 12:906. doi: 10.1039/c2lc20911j

201. Gruenberger A, Probst C, Heyer A, et al (2013) Microfluidic picoliter bioreactor for microbial single-cell analysis: fabrication, system setup, and operation. J Vis Exp 82:50560. doi: 10.3791/50560

202. Lecault V, White AK, Singhal A, Hansen CL (2012) Microfluidic single cell analysis: From promise to practice. Curr Opin Chem Biol 16:381–390. doi: 10.1016/j.cbpa.2012.03.022

203. Fritzsch FSO, Dusny C, Frick O, Schmid A (2012) Single-cell analysis in biotechnology, systems biology, and biocatalysis. Annu Rev Chem Biomol Eng 3:129–55. doi: 10.1146/annurev-chembioeng-062011-081056

204. Klepárník K (2013) Analytica Chimica Acta Recent advances in the development of single cell analysis — A review. Anal Chim Acta 800:12–21. doi: 10.1016/j.aca.2013.09.004

205. Love KR, Bagh S, Choi J, Love JC (2013) Microtools for single-cell analysis in biopharmaceutical development and manufacturing. Trends Biotechnol 31:280–286. doi: 10.1016/j.tibtech.2013.03.001

206. Okumus B, Yildiz S, Toprak E (2014) Fluidic and microfluidic tools for quantitative systems biology. Curr Opin Biotechnol 25:30–38. doi: 10.1016/j.copbio.2013.08.016

207. Schmid A, Kortmann H, Dittrich PS, Blank LM (2010) Chemical and biological single cell analysis. Curr Opin Biotechnol 21:12–20. doi: 10.1016/j.copbio.2010.01.007

208. Gruenberger A, Wiechert W, Kohlheyer D (2014) Single-cell microfluidics: Opportunity for bioprocess development. Curr Opin Biotechnol 29:15–23. doi: 10.1016/j.copbio.2014.02.008

209. Uhlendorf J, Miermont A, Delaveau T, et al (2012) Long-term model predictive control of gene expression at the population and single-cell levels. Proc Natl Acad Sci U S A 109:14271–6. doi: 10.1073/pnas.1206810109

210. Ullman G, Wallden M, Marklund EG, et al (2013) High-throughput gene expression analysis at the level of single proteins using a microfluidic turbidostat and automated cell tracking. Philos Trans R Soc Lond B Biol Sci 368:20120025. doi: 10.1098/rstb.2012.0025

211. Falconnet D, Niemistö a, Taylor RJ, et al (2011) High-throughput tracking of single yeast cells in a microfluidic imaging matrix. Lab Chip 11:466–473. doi: 10.1039/c0lc00228c

212. Kolnik M, Tsimring LS, Hasty J (2012) Vacuum-assisted cell loading enables shear-free mammalian microfluidic culture. Lab Chip 12:4732. doi: 10.1039/c2lc40569e

213. Wang L, Ni XF, Luo CX, et al (2009) Self-loading and cell culture in one layer microfluidic devices. Biomed Microdevices 11:679–684. doi: 10.1007/s10544-008-9278-0

214. Schneider C a, Rasband WS, Eliceiri KW (2012) NIH Image to ImageJ: 25 years of image analysis. Nat Methods 9:671–675. doi: 10.1038/nmeth.2089

215. Kang JH, Kim YC, Park J-K (2008) Analysis of pressure-driven air bubble elimination in a microfluidic device. Lab Chip 8:176–178. doi: 10.1039/b712672g

216. Letek M, Fiuza M, Ordóñez E, et al (2008) Cell growth and cell division in the rod-shaped actinomycete Corynebacterium glutamicum. Antonie Van Leeuwenhoek 94:99–109. doi: 10.1007/s10482-008-9224-4

217. Kim L, Toh Y-C, Voldman J, Yu H (2007) A practical guide to microfluidic perfusion culture of adherent mammalian cells. Lab Chip 7:681–694. doi: 10.1039/b704602b

218. Dochow S, Krafft C, Neugebauer U, et al (2011) Tumour cell identification by means of Raman spectroscopy in combination with optical traps and microfluidic environments. Lab Chip 11:1484–1490. doi: 10.1039/c0lc00612b

219. Honarmandi P, Lee H, Lang MJ, Kamm RD (2011) A microfluidic system with optical laser tweezers to study mechanotransduction and focal adhesion recruitment. Lab Chip 11:684–694. doi: 10.1039/c0lc00487a

220. Kovac JR, Voldman J (2007) Intuitive, image-based cell sorting using optofluidic cell sorting. Anal Chem 79:9321–9330. doi: 10.1021/ac071366y

221. Maruyama H, Kotani K, Masuda T, et al (2011) Nanomanipulation of single influenza virus using dielectrophoretic concentration and optical tweezers for single virus infection to a specific cell on a microfluidic chip. Microfluid Nanofluidics 10:1109–1117. doi: 10.1007/s10404-010-0739-4

222. Matsumura K, Yagi T, Hattori A, et al (2010) Using single cell cultivation system for on-chip monitoring of the interdivision timer in Chlamydomonas reinhardtii cell cycle. J Nanobiotechnology 8:23. doi: 10.1186/1477-3155-8-23

223. Salehi-Reyhani A, Kaplinsky J, Burgin E, et al (2011) A first step towards practical single cell proteomics: a microfluidic antibody capture chip with TIRF detection. Lab Chip 11:1256–1261. doi: 10.1039/c0lc00613k

224. Wang T, Oehrlein S, Somoza MM, et al (2011) Optical tweezers directed one-bead one-sequence synthesis of oligonucleotides. Lab Chip 11:1629–37. doi: 10.1039/c0lc00577k

225. Neuman KC, Block SM (2004) Optical trapping. Rev Sci Instrum 75:2787–2809. doi: Doi 10.1063/1.1785844

226. Chen H, Wang C, Lou Y (2013) Flocking multiple microparticles with automatically controlled optical tweezers: Solutions and experiments. IEEE Trans Biomed Eng 60:1518–1527. doi: 10.1109/TBME.2013.2238538

227. Lawrence J, Korber D, Caldwell D (1992) Behavioral analysis of Vibrio parahaemolyticus variants in high-and low-viscosity microenvironments by use of digital image processing. J Bacteriol 174 :5732–5739.

228. Creutziger M, Schmidt M, Lenz P (2012) Theoretical models for the regulation of DNA replication in fast-growing bacteria. New J Phys 14:95016. doi: 10.1088/1367-2630/14/9/095016

229. Slater M, Schaechter M (1974) Control of cell division in bacteria. Microbiol Mol Biol Rev 38:199–221.

230. Hermann T (2002) Industrial Production of Amino Acids. Amino Acids 104:495. doi: http://dx.doi.org/10.1016/S0168-1656(03)00149-4

231. Unger MA (2000) Monolithic Microfabricated Valves and Pumps by Multilayer Soft Lithography. Science (80-) 288:113–116. doi: 10.1126/science.288.5463.113

232. Balagaddé FK, Song H, Ozaki J, et al (2008) A synthetic Escherichia coli predator-prey ecosystem. Mol Syst Biol 4:187. doi: 10.1038/msb.2008.24

233. Monod J (1949) The Growth of Bacterial Cultures. Annu Rev Microbiol 3:371–394. doi: 10.1146/annurev.mi.03.100149.002103

234. Abhari F, Jaafar H, Md Yunus NA (2012) A comprehensive study of micropumps technologies. Int J Electrochem Sci 7:9765–9780. doi: 10.3390/mi2020179

235. Byun CK, Abi-Samra K, Cho Y-K, Takayama S (2013) Pumps for microfluidic cell culture. Electrophoresis 35:245–257. doi: 10.1002/elps.201300205

236. Juncker D, Schmid H, Drechsler U, et al (2002) Autonomous microfluidic capillary system. Anal Chem 74:6139–6144. doi: 10.1021/ac0261449

237. Walker GM, Beebe DJ (2002) A passive pumping method for microfluidic devices. Lab Chip 2:131–134. doi: 10.1039/b204381e

238. Ju J, Park JY, Kim KC, et al (2008) Backward flow in a surface tension driven micropump. J Micromechanics Microengineering 18:087002. doi: 10.1088/0960-1317/18/8/087002

239. Ju J, Ko J-M, Cha H-C, et al (2009) An electrofusion chip with a cell delivery system driven by surface tension. J Micromechanics Microengineering 19:15004. doi: 10.1088/0960-1317/19/1/015004

240. Meyvantsson I, Warrick JW, Hayes S, et al (2008) Automated cell culture in high density tubeless microfluidic device arrays. Lab Chip 8:717–24. doi: 10.1039/b715375a

241. Takayama S, McDonald JC, Ostuni E, et al (1999) Patterning cells and their environments using multiple laminar fluid flows in capillary networks. Proc Natl Acad Sci U S A 96:5545–5548. doi: 10.1073/pnas.96.10.5545

242. Cho BS, Schuster TG, Zhu X, et al (2003) Passively driven integrated microfluidic system for separation of motile sperm. Anal Chem 75:1671–1675. doi: 10.1021/ac020579e

243. Zhu X, Yi Chu L, Chueh B, et al (2004) Arrays of horizontally-oriented mini-reservoirs generate steady microfluidic flows for continuous perfusion cell culture and gradient generation. Analyst 129:1026–1031. doi: 10.1039/b407623k

244. Huh D, Bahng JH, Ling Y, et al (2007) Gravity-driven microfluidic particle sorting device with hydrodynamic separation amplification. Anal Chem 79:1369–1376. doi: 10.1021/ac061542n

245. Sung JH, Kam C, Shuler ML (2010) A microfluidic device for a pharmacokinetic-pharmacodynamic (PK-PD) model on a chip. Lab Chip 10:446–455. doi: 10.1039/B917763A

246. Lee K, Kim C, Young Yang J, et al (2012) Gravity-oriented microfluidic device for uniform and massive cell spheroid formation. Biomicrofluidics 6:-. doi: 10.1063/1.3687409

247. Goral VN, Zhou C, Lai F, Yuen PK (2013) A continuous perfusion microplate for cell culture. ｓ ｌ. Lab Chip 13:1039–43. doi: 10.1039/c2lc41102d

248. Marimuthu M, Kim S (2013) Pumpless steady-flow microfluidic chip for cell culture. Anal Biochem 437:161–163. doi: 10.1016/j.ab.2013.02.007

249. Park JY, Hwang CM, Lee SH, Lee S-H (2007) Gradient generation by an osmotic pump and the behavior of human mesenchymal stem cells under the fetal bovine serum concentration gradient. Lab Chip 7:1673–80. doi: 10.1039/b710777c

250. Park JY, Kim SK, Woo DH, et al (2009) Differentiation of neural progenitor cells in a microfluidic chip-generated cytokine gradient. Stem Cells 27:2646–2654. doi: 10.1002/stem.202

251. Hung PJ, Lee PJ, Sabounchi P, et al (2005) A novel high aspect ratio microfluidic design to provide a stable and uniform microenvironment for cell growth in a high throughput mammalian cell culture array. Lab Chip 5:44–8. doi: 10.1039/b410743h

252. Stocker R, Seymour JR, Samadani A, et al (2008) Rapid chemotactic response enables marine bacteria to exploit ephemeral microscale nutrient patches. Proc Natl Acad Sci U S A 105:4209–4214. doi: 10.1073/pnas.0709765105

253. Song JW, Gu W, Futai N, et al (2005) Computer-controlled microcirculatory support system for endothelial cell culture and shearing. Anal Chem 77:3993–3999. doi: 10.1021/ac050131o

254. Futai N, Gu W, Song JW, Takayama S (2006) Handheld recirculation system and customized media for microfluidic cell culture. Lab Chip 6:149–154. doi: 10.1039/b510901a

255. Tung Y-C, Torisawa Y, Futai N, Takayama S (2007) Small volume low mechanical stress cytometry using computer-controlled Braille display microfluidics. Lab Chip 7:1497–503. doi: 10.1039/b708187a

256. Yun SH, Cabrera LM, Song JW, et al (2007) Characterization and resolution of evaporation-mediated osmolality shifts that constrain microfluidic cell culture in poly(dimethylsiloxane) devices. Anal Chem 79:1126–1134. doi: 10.1021/ac061990v

257. Mehta G, Mehta K, Sud D, et al (2007) Quantitative measurement and control of oxygen levels in microfluidic poly(dimethylsiloxane) bioreactors during cell culture. Biomed Microdevices 9:123–134. doi: 10.1007/s10544-006-9005-7

258. Sung JH, Shuler ML (2009) A micro cell culture analog (microCCA) with 3-D hydrogel culture of multiple cell lines to assess metabolism-dependent cytotoxicity of anti-cancer drugs. Lab Chip 9:1385–1394. doi: 10.1039/b901377f

259. Ota H, Yamamoto R, Deguchi K, et al (2010) Three-dimensional spheroid-forming lab-on-a-chip using micro-rotational flow. Sensors Actuators B 147:359–365. doi: 10.1016/j.snb.2009.11.061

260. Wang J, Heo J, Hua SZ (2010) Spatially resolved shear distribution in microfluidic chip for studying force transduction mechanisms in cells. Lab Chip 10:235–9. doi: 10.1039/b914874d

261. Li PC, Harrison DJ (1997) Transport, manipulation, and reaction of biological cells on-chip using electrokinetic effects. Anal Chem 69:1564–1568. doi: 10.1021/ac9606564

262. Zeng S, Chen C-H, Mikkelsen JC, Santiago JG (2001) Fabrication and characterization of electroosmotic micropumps. Sensors Actuators B Chem 79:107–114. doi: 10.1016/S0925-4005(01)00855-3

263. Emmelkamp J, Wolbers F, Andersson H, et al (2004) The potential of autofluorescence for the detection of single living cells for label-free cell sorting in microfluidic systems. Electrophoresis 25:3740–3745. doi: 10.1002/elps.200406070

264. Xuan X, Li D (2005) Focused electrophoretic motion and selected electrokinetic dispensing of particles and cells in cross-microchannels. Electrophoresis 26:3552–3560. doi: 10.1002/elps.200500298

265. Wang X, Cheng C, Wang S, Liu S (2009) Electroosmotic pumps and their applications in microfluidic systems. Microfluid Nanofluidics 6:145–162. doi: 10.1007/s10404-008-0399-9

266. Glawdel T, Elbuken C, Lee LEJ, Ren CL (2009) Microfluidic system with integrated electroosmotic pumps, concentration gradient generator and fish cell line (RTgill-W1)--towards water toxicity testing. Lab Chip 9:3243–3250. doi: 10.1039/b911412m

267. Glawdel T, Ren CL (2009) Electro-osmotic flow control for living cell analysis in microfluidic PDMS chips. Mech Res Commun 36:75–81. doi: 10.1016/j.mechrescom.2008.06.015

268. Madou M, Zoval J, Jia G, et al (2006) Lab on a Cd. Annu Rev Biomed Eng 8:601–628. doi: 10.1146/annurev.bioeng.8.061505.095758

269. Rhee SW, Taylor AM, Cribbs DH, et al (2007) External force-assisted cell positioning inside microfluidic devices. Biomed Microdevices 9:15–23. doi: 10.1007/s10544-006-9002-x

270. Ren Y, Chow LMC, Leung WWF (2013) Cell culture using centrifugal microfluidic platform with demonstration on Pichia pastoris. Biomed Microdevices 15:321–337. doi: 10.1007/s10544-012-9735-7

271. Schindelin J, Arganda-Carreras I, Frise E, et al (2012) Fiji: an open-source platform for biological-image analysis. Nat Methods 9:676–682. doi: 10.1038/nmeth.2019

272. Jaqaman K, Loerke D, Mettlen M, et al (2008) Robust single-particle tracking in live-cell time-lapse sequences. Nat Methods 5:695–702. doi: 10.1038/nmeth.1237

273. Alper H, Stephanopoulos G (2009) Engineering for biofuels: exploiting innate microbial capacity or importing biosynthetic potential? Nat Rev Microbiol 7:715–723. doi: 10.1038/nrmicro2186

274. Brennan MD, Rexius-Hall ML, Elgass LJ, Eddington DT (2014) Oxygen control with microfluidics. Lab Chip 14:4305–18. doi: 10.1039/c4lc00853g

275. Cui X, Yip HM, Zhu Q, et al (2014) Microfluidic long-term differential oxygenation for bacterial growth characteristics analyses. RSC Adv 4:16662–16673. doi: 10.1039/C4RA01577K

276. Chen Y-A, King AD, Shih H-C, et al (2011) Generation of oxygen gradients in microfluidic devices for cell culture using spatially confined chemical reactions. Lab Chip 11:3626–33. doi: 10.1039/c1lc20325h

277. Li N, Luo C, Zhu X, et al (2011) Microfluidic generation and dynamically switching of oxygen gradients applied to the observation of cell aerotactic behaviour. Microelectron Eng 88:1698–1701. doi: 10.1016/j.mee.2011.01.003

278. Oppegard SC, Eddington DT (2013) A microfabricated platform for establishing oxygen gradients in 3-D constructs. Biomed Microdevices 15:407–414. doi: 10.1007/s10544-013-9737-0

279. Thomas PC, Raghavan SR, Forry SP (2011) Regulating oxygen levels in a microfluidic device. Anal Chem 83:8821–8824. doi: 10.1021/ac202300g

280. Wang L, Liu W, Wang Y, et al (2013) Construction of oxygen and chemical concentration gradients in a single microfluidic device for studying tumor cell-drug interactions in a dynamic hypoxia microenvironment. Lab Chip 13:695–705. doi: 10.1039/c2lc40661f

281. Chang C-W, Cheng Y-J, Tu M, et al (2014) A polydimethylsiloxane-polycarbonate hybrid microfluidic device capable of generating perpendicular chemical and oxygen gradients for cell culture studies. Lab Chip 14:3762–72. doi: 10.1039/c4lc00732h

282. Chen YH, Peng CC, Cheng YJ, et al (2013) Generation of nitric oxide gradients in microfluidic devices for cell culture using spatially controlled chemical reactions. Biomicrofluidics 7:3626–3633. doi: 10.1063/1.4829775

283. Funamoto K, Zervantonakis IK, Liu Y, et al (2012) A novel microfluidic platform for high-resolution imaging of a three-dimensional cell culture under a controlled hypoxic environment. Lab Chip 12:4855–63. doi: 10.1039/c2lc40306d

284. Peng C-C, Liao W-H, Chen Y-H, et al (2013) A microfluidic cell culture array with various oxygen tensions. Lab Chip 13:3239–45. doi: 10.1039/c3lc50388g

285. Adler M, Polinkovsky M, Gutierrez E, Groisman A (2010) Generation of oxygen gradients with arbitrary shapes in a microfluidic device. Lab Chip 10:388–91. doi: 10.1039/b920401f

286. Lo JF, Sinkala E, Eddington DT (2010) Oxygen gradients for open well cellular cultures via microfluidic substrates. Lab Chip 10:2394. doi: 10.1039/c004660d

287. Forry SP, Locascio LE (2011) On-chip CO2 control for microfluidic cell culture. Lab Chip 11:4041. doi: 10.1039/c1lc20505

288. Lou X, Kim G, Yoon HK, et al (2014) A high-throughput photodynamic therapy screening platform with on-chip control of multiple microenvironmental factors. Lab Chip 14:892–901. doi: 10.1039/c3lc51077h

289. Ungerbock B, Charwat V, Ertl P, Mayr T (2013) Microfluidic oxygen imaging using integrated optical sensor layers and a color camera. Lab Chip 13:1593–1601. doi: 10.1039/C3LC41315B

12 Supplemental information

12.1 Fabrication of multilayered microfluidic devices

12.1.1 Master mold fabrication

Fluid layer master mold

1. Clean wafer
2. Dehydrate, 20 min at 200°C

First layer (Fluid master mold)

3. Coating, SU8 2000.5 aim, 0.8µm, dispense 4ml resist, spin 10s v=500 rpm, a=100 rpm/s, spin 30s v=1000 rpm, a=300 rpm/s
4. Soft bake, 1.5 min 65 °C, 1.5 min 95 °C, 1 min 65 °C
5. Exposure, MA (>350nm), Vacuum contact, 64 mJ/cm², t=3s (I=7mW/cm²)
6. Post-Exposure Bake, 1 min 65 °C, 1 min 95 °C, 1 min 65 °C
7. Development
    a. SU8 Developer I (DEV600), immerse 45 s
    b. SU8 Developer II, immerse 60 s
8. Rinse & dry, IPA, 20 seconds dry spinning, or pressurized nitrogen
9. Hard bake, 10 min 150°C

Second layer (Fluid master mold)

10. Coating, SU8 2010, aim: 9µm, dispense 4ml resist, spin 10s v=500 rpm, a=100rpm/s, spin 30s @ v=4000 rpm, a=300rpm/s
11. Soft bake, 15 min 65 °C, 45 min 95°C
12. Exposure, MA (>350nm), Hard contact, Align, 123 mJ/cm², t=10-12 s(I=7mW/cm²)
13. Post-Exposure Bake, 5 min 65°C, 3min 30s 95°C

14. Development
    a. SU8 Developer I (DEV600), immerse 45 s
    b. SU8 Developer II, immerse 60 s
15. Rinse & dry, IPA, 20 seconds dry spinning, or pressurized nitrogen
16. Hard bake, 7 h at 150°C

Third layer (Fluid master mold)

17. Coating, SPR 220-7 spin 10 s v = 500 rpm, a = 100 rpm/s, spin 40s v = 2000 rpm, a = 300 rpm/s
18. Soft bake, 4 min. 105 °C
19. Exposure, MA (>350nm), Soft contact, 420 mJ/cm², t=60 s (I=7mW/cm²)
20. Development, MF-CD 26, immerse 3 min.
21. Rinse & dry, DI-water immerse, blow dry
22. Reflow, 15 min. 120°C

Control layer master mold

23. Clean wafer
24. Dehydrate, 20 min at 200°C

First layer (Fluid master mold)

25. Coating, SU8 2010, aim: 9µm, dispense 4ml resist, spin 10s v=500 rpm, a=100rpm/s, spin 30s @ v=4000 rpm, a=300rpm/s
26. Soft bake, 15 min 65 °C, 45 min 95°C
27. Exposure, MA (>350nm), Hard contact, Align, 123 mJ/cm², t=10-12 s(I=7mW/cm²)
28. Post-Exposure Bake, 5 min 65°C, 3min 30s 95°C

29. Development
    a. SU8 Developer I (DEV600), immerse 45 s
    b. SU8 Developer II, immerse 60 s
30. Rinse & dry, IPA, 20 seconds dry spinning, or pressurized nitrogen
31. Hard bake, 7 h at 150°C

12.1.2 PDMS replica molding

1. PDMS mixing 15 g 20:1, 15 g 7:1, 15 g 10:1
2. Degas PDMS
3. Pour 7:1 PDMS mixture over control layer master mold
4. Bake 30 minutes at 80 °C.
5. Spin coat 20:1 PDMS onto fluid layer master mold
6. Levelling 10 minutes
7. Bake 20 minutes at 80 °C.
8. Punch holes in control layer (wait 1 min. so that PDMS can cool down)
9. Align control layer to fluid layer
10. Bake for 40 minutes at 80 °C
11. Release chips
12. Punch holes (wait 1 min. so that PDMS can cool down)
13. Pour 10:1 mixture over fluid layer and bake to remove residues.

12.2 Determination of pulsation rate

12.2.1 Rectangular shaped cross-section

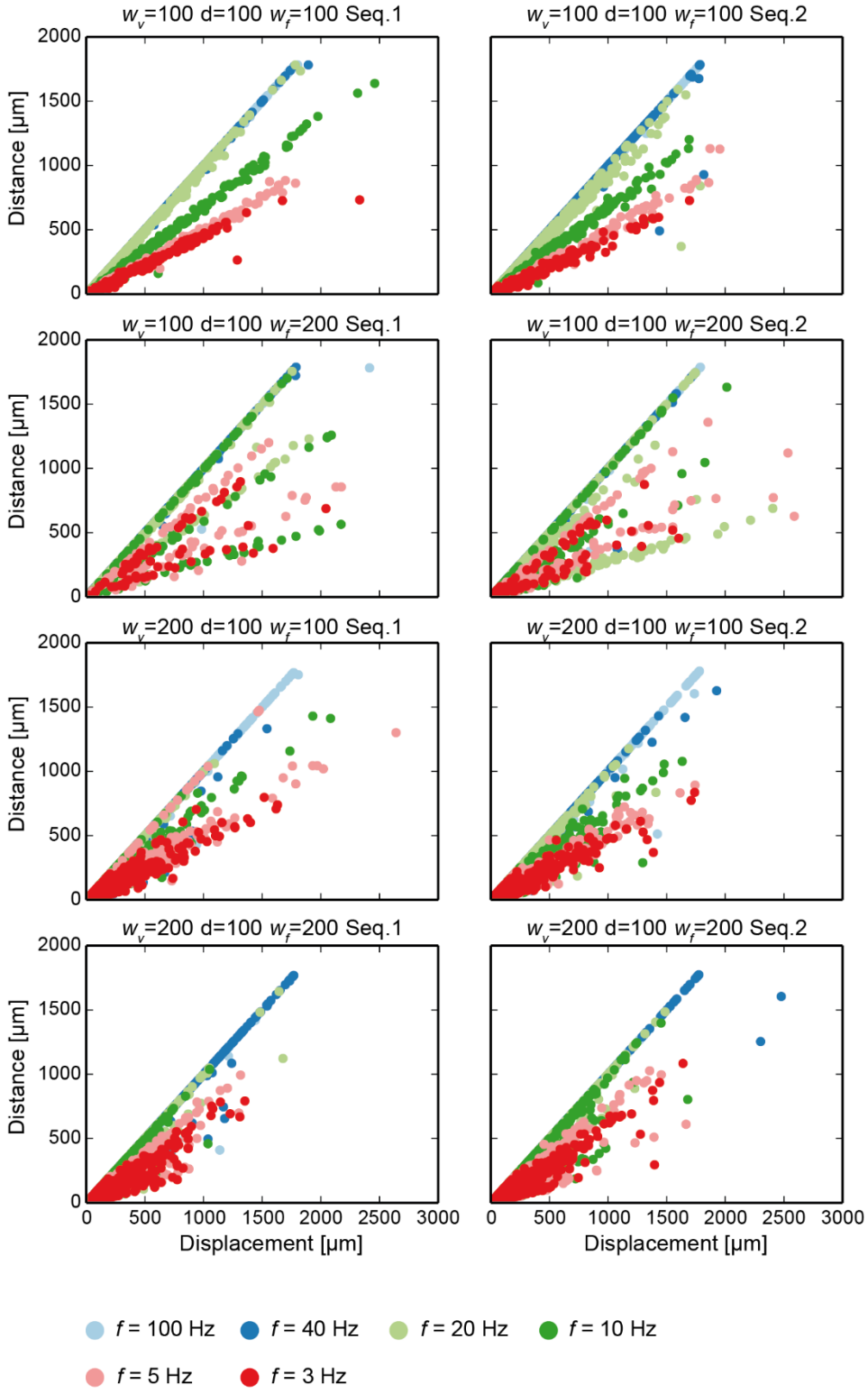

Supplement Figure 1: Correlation of particles reached distance and travelled path at different frequencies (100 Hz, 40 Hz, 20 Hz, 10 Hz, 5 Hz, 3 Hz) for rectangular shaped channel cross-section.

12.2.2 Ellipsoid shaped cross-section

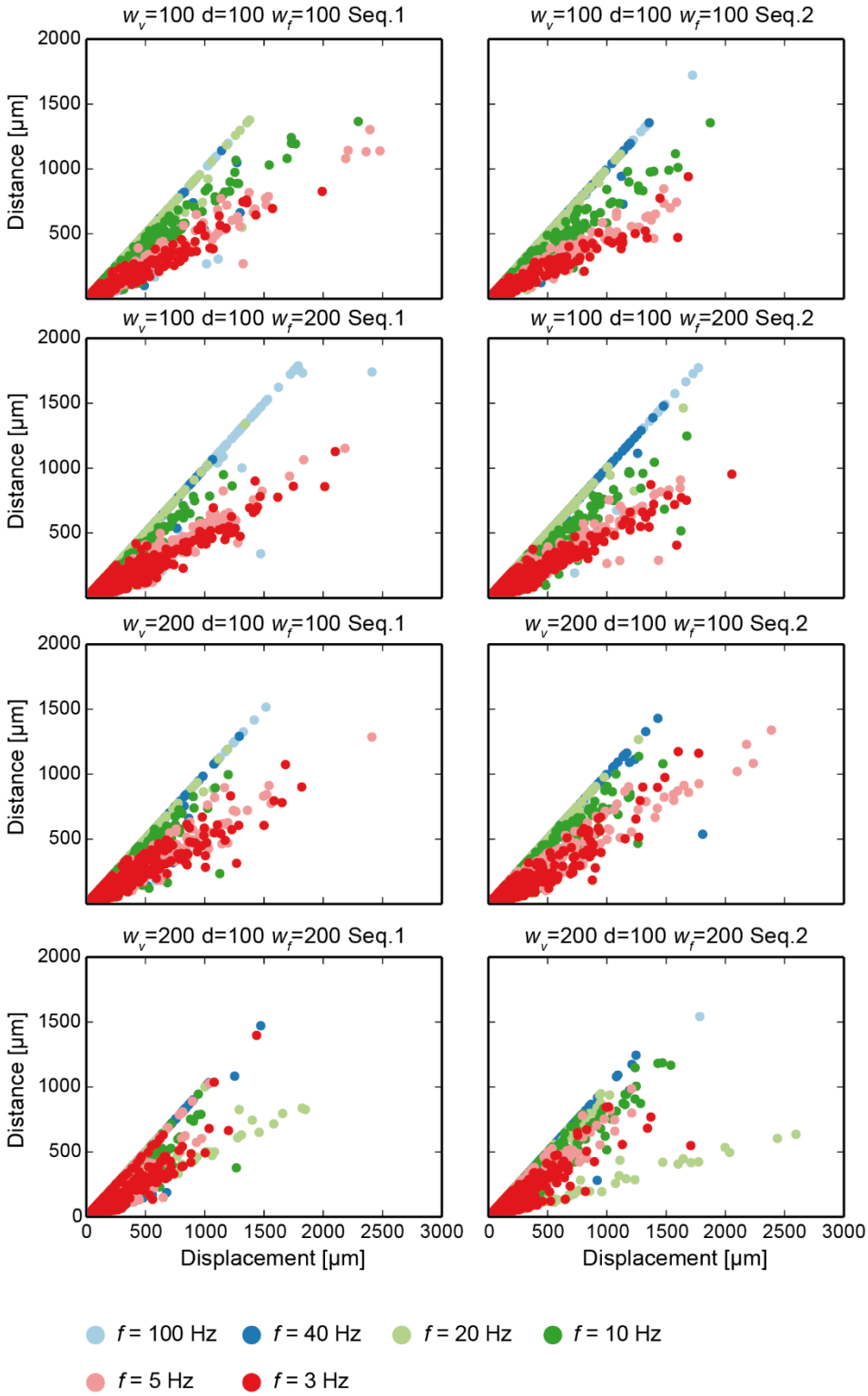

Supplement Figure 2: Correlation of particles reached distance and travelled path at different frequencies (100 Hz, 40 Hz, 20 Hz, 10 Hz, 5 Hz, 3 Hz) for ellipse shaped channel cross-section.

12.2.3 Coefficient of determination

Supplement Table 1: R^2 values for non-reflowed.

	100 Hz	40 Hz	20 Hz	10 Hz	5 Hz	3 Hz
1	1.00E+00	1.00E+00	9.99E-01	9.97E-01	9.96E-01	9.73E-01
2	1.00E+00	9.88E-01	9.70E-01	9.93E-01	9.93E-01	9.88E-01
3	9.94E-01	9.99E-01	9.62E-01	7.45E-01	7.81E-01	8.22E-01
4	9.97E-01	9.90E-01	7.14E-01	9.39E-01	8.93E-01	8.89E-01
5	9.98E-01	9.77E-01	9.83E-01	9.72E-01	9.31E-01	9.49E-01
6	9.94E-01	9.92E-01	9.68E-01	9.65E-01	9.64E-01	9.44E-01
7	9.75E-01	9.94E-01	9.62E-01	8.57E-01	9.25E-01	9.18E-01
8	9.99E-01	9.86E-01	9.70E-01	9.28E-01	9.21E-01	9.29E-01

Supplement Table 2: R2 values for reflowed.

	100 Hz	40 Hz	20 Hz	10 Hz	5 Hz	3 Hz
1	9.49E-01	9.54E-01	9.79E-01	9.81E-01	9.79E-01	9.72E-01
2	9.88E-01	9.92E-01	9.92E-01	9.79E-01	9.75E-01	9.61E-01
3	9.81E-01	9.71E-01	9.68E-01	9.71E-01	9.63E-01	9.45E-01
4	9.93E-01	9.89E-01	9.82E-01	9.65E-01	9.50E-01	9.48E-01
5	9.67E-01	9.69E-01	9.82E-01	9.31E-01	9.61E-01	9.36E-01
6	9.49E-01	9.52E-01	9.57E-01	9.60E-01	9.67E-01	9.32E-01
7	9.91E-01	9.46E-01	8.78E-01	9.39E-01	9.20E-01	9.02E-01
8	9.57E-01	9.81E-01	6.70E-01	9.72E-01	9.42E-01	8.84E-01

12.3 Changing oxygen concentrations vs. flow rate

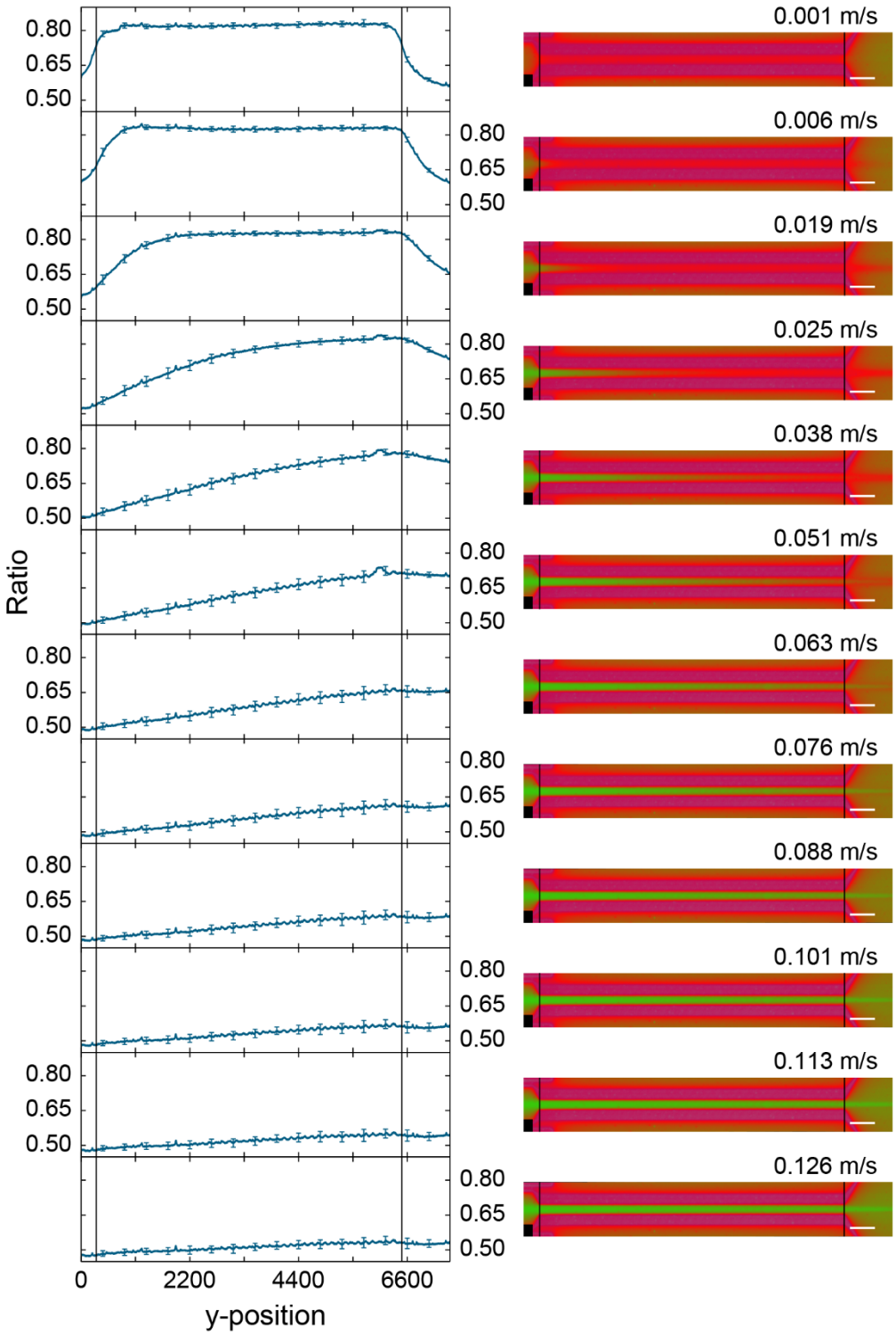

Supplement Figure 3: Changing oxygen concentration at increasing flow rates over the channel length. Graphs on the left depict the ratio value, the images on the right show the corresponding ratio image. The black vertical lines indicate beginning and ending of channel. (scale bar 700 µm).